Journal of Computational and Theoretical Transport

ISSN: 2332-4309 (Print) 2332-4325 (Online) Journal homepage: www.tandfonline.com/journals/ltty21

A Parallel, Energy-Stable Low-Rank Integrator for Nonlinear Multi-Scale Thermal Radiative Transfer

Chinmay Patwardhan & Jonas Kusch

To cite this article: Chinmay Patwardhan & Jonas Kusch (04 Feb 2026): A Parallel, Energy-Stable Low-Rank Integrator for Nonlinear Multi-Scale Thermal Radiative Transfer, Journal of Computational and Theoretical Transport, DOI: 10.1080/23324309.2026.2618786

To link to this article: https://doi.org/10.1080/23324309.2026.2618786

Published online: 04 Feb 2026.

JOURNAL OF COMPUTATIONAL AND THEORETICAL TRANSPORT
https://doi.org/10.1080/23324309.2026.2618786

A Parallel, Energy-Stable Low-Rank Integrator for Nonlinear Multi-Scale Thermal Radiative Transfer

Chinmay Patwardhan[a] and Jonas Kusch[b]

[a]Department of Mathematics, Karlsruhe Institute of Technology, Karlsruhe, Germany;
[b]Department of Data Science, Norwegian University of Life Sciences, Ås, Norway

ABSTRACT

Thermal radiative transfer (TRT) governs phenomena ranging from supernovas in astrophysics to laser-driven fusion experiments in plasma physics. The interaction of radiation and matter involves prohibitively small time scales, nonlinear coupling, and high-dimensional particle dynamics, making conventional numerical methods prohibitively expensive. Dynamical low-rank approximation (DLRA), combined with asymptotic-preserving discretizations, offers a promising direction, but until now its use for nonlinear TRT has been fundamentally limited: stability regions of existing DLRA integrators are unknown in realistic nonlinear regimes, and coefficient updates remain computationally costly. We present an asymptotic-preserving, locally conservative, rank-adaptive, and parallel integrator for a macro–micro decomposition-based DLRA of the nonlinear TRT equations. Unlike previous approaches, our method is provably energy stable in the nonlinear setting, with step-size restrictions that capture both hyperbolic and parabolic CFL conditions. The integrator is constructed from the parallel BUG integrator, thus eliminating the need for augmented coefficient updates. In the setting of the parallel integrator and micro-macro decompositions, we propose a strategy to enforce reflection-transmission type boundary conditions in the low-rank factors. These advances resolve long-standing stability and efficiency obstacles, enabling DLRA to be applied robustly to nonlinear TRT with stability guarantees. Numerical experiments confirm the accuracy and efficiency of the proposed approach.

KEYWORDS

Thermal radiative transfer; nonlinear energy stability; asymptotic–preserving; dynamical low-rank approximation; parallel BUG integrator

1. Introduction

The field of thermal radiative transfer models the interaction of particles traveling through and interacting with a background material. Physical phenomena governed by the thermal radiative transfer equations include star

CONTACT Chinmay Patwardhan chinmay.patwardhan@kit.edu Department of Mathematics, Karlsruhe Institute of Technology, Karlsruhe, 76139 Germany.

formation, supernova explosions, radiation from a hohlraum striking a fusion target, and laser wakefield acceleration driven by pressure waves. To numerically simulate such problems, particles are commonly described by a phase space density $f(t, \boldsymbol{x}, \boldsymbol{\Omega})$ where t is time, $\boldsymbol{x} \in \mathbb{R}^3$ is the spatial position, and $\boldsymbol{\Omega} \in \mathbb{S}^2$ is the direction of flight. Then, the number of particles at time t with spatial position in $\mathrm{d}\boldsymbol{x}$ around $\boldsymbol{x}$ and direction of travel in $\mathrm{d}\boldsymbol{\Omega}$ around $\boldsymbol{\Omega}$ is given as $f(t, \boldsymbol{x}, \boldsymbol{\Omega})\mathrm{dx}\mathrm{d}\boldsymbol{\Omega}$.

Two central challenges exist in determining the phase space density: First, the phase space is six-dimensional, which poses a challenge to store and evolve the phase space density on a finely resolved computational grid. Second, the underlying dynamics are commonly governed on strongly varying time scales and numerical methods must be designed to accurately capture all essential solution characteristics while not having to resolve prohibitively small scales. In particular, if many particles are absorbed on a small time scale, the dynamics of the thermal radiative transfer equations asymptotically converge to a diffusive nonlinear partial differential equation called the Rosseland equation (Rosseland 1931). Numerical methods that capture a discrete analog of this behavior while not requiring the resolution of prohibitively small time scales are often called asymptotic–preserving (AP). To be specific, a numerical scheme is considered to be an AP scheme if it has the following three properties (Jin 1999): (1) asymptotic consistency, (2) asymptotic stability, and (3) asymptotic efficiency. The numerical scheme is asymptotically consistent if, in the diffusion limit, the solution of the kinetic equation converges to the solution of the diffusion limit. A numerical scheme is considered to be asymptotically stable if it does not require prohibitively small step sizes in the diffusion limit, and asymptotically efficient if the stability does not come at a high cost. A non-comprehensive list of AP schemes includes the AP unified gas kinetic scheme (UGKS) (Sun, Jiang, and Xu 2015; Sun, Jiang, Xu, et al. 2015; Sun et al. 2017; Li et al. 2024), the high-order/low-order (HOLO) scheme (Peng and McClarren 2021), and high-order IMEX schemes (Jang et al. 2014; Fu et al. 2022).

To address the high-dimensionality of thermal radiative transfer problems, recently developed numerical methods employ dynamical low-rank approximations (DLRA) introduced in Koch and Lubich (2007). The main idea of DLRA is to represent the solution as a low-rank factorization and then derive evolution equations for the low-rank factors such that the full-rank dynamics is captured as closely as possible. While DLRA can significantly reduce memory and computational requirements, it has several additional challenges. Most importantly, the evolution equations for low-rank factors are ill-conditioned, and a large amount of research has been devoted to constructing numerical time integrators that are robust to stiffness. The most frequently used robust integrators are the projector–splitting integrator (Lubich and

Oseledets 2014), and basis-update & Galerkin (BUG) integrators (Ceruti, Kusch, et al. 2022, 2024; Ceruti and Lubich 2022), which allow for an extension to higher order (Ceruti, Einkemmer, et al. 2024; Kusch 2025). Besides the construction of robust integrators, numerical methods for DLRA are commonly required to preserve certain characteristics of the original problem, e.g., the preservation of local conservation laws (Einkemmer, Kusch, et al. 2023; Einkemmer, Ostermann, et al. 2023; Baumann et al. 2024; Coughlin et al. 2024; Koellermeier et al. 2024; Frank et al. 2025), asymptotic limits (Ding et al. 2021; Einkemmer et al. 2021, 2024, 2025; Frank et al. 2025), or stability regions (Kusch et al. 2023; Baumann et al. 2024; Einkemmer et al. 2024; Frank et al. 2025). Such structure–preserving properties are often problem-dependent and require a careful modification of the standard integrators for individual applications. Here, the augmented BUG integrator (Ceruti and Lubich 2022) has proven to be beneficial since it allows for increased flexibility to incorporate solution structures while, unlike the projector–splitting integrators, not requiring steps backward in time. The augmented BUG integrator simplifies the construction of structure–preserving low-rank integrators; however, it requires additional costs compared to the parallel BUG integrator (Ceruti, Kusch, et al. 2024), which evolves all low-rank factors in parallel while not requiring a coefficient update at an increased rank.

Several structure–preserving DLRA methods have been developed for the thermal radiative transfer equations. A DLRA scheme to solve the one-dimensional thermal radiative transfer equation has been proposed in Ceruti, Frank, et al. (2022); however, without stability guarantees, it requires a parameter study to determine a sufficiently small time step size. In Baumann et al. (2024), a provable energy-stable and locally conservative DLRA scheme has been derived in the one-dimensional setting for the Su-Olson closure (Su and Olson 1997). Though not physically motivated, the Su-Olson closure significantly simplifies the evolution equation as it eliminates nonlinear effects in the coupling of the material and particles. Moreover, in Frank et al. (2025), the authors propose a DLRA method that is asymptotic–preserving, locally conservative, and energy–stable in a one-dimensional and linearized setting. In Fu et al. (2022), the authors propose an AP IMEX scheme for the nonlinear thermal radiative transfer equation, where energy stability is shown under hyperbolic and parabolic Courant–Friedrichs–Lewy (CFL) conditions. However, the scheme requires construction and propagation of the full phase space density $f(t, \boldsymbol{x}, \Omega)$ and has not been extended to the macro-micro or the low-rank setting.

It is important to note that the stability of previously derived low-rank methods is only understood in *simplified* settings, using *linearizations* or *simplified closure relations*. Moreover, while the methods proposed in Baumann et al. (2024) and Frank et al. (2025) allow for rank-adaptivity,

their construction as augmented BUG integrators leads to increased computational costs since the time evolution of low-rank coefficients requires a sequential time update at an increased rank. An additional challenge for DLRA schemes not addressed in Baumann et al. (2024); Frank et al. (2025) is the efficient implementation of boundary conditions for complex two- and three-dimensional geometries. Due to the nonlinear ansatz, which separates the basis in each phase space variable, describing boundary conditions for low-rank schemes is not straightforward. A few techniques for incorporating boundary conditions in the DLRA scheme have been proposed in Uschmajew and Zeiser (2024), Kusch et al. (2022), and Sapsis and Lermusiaux (2009). However, since the dynamics of the parallel BUG integrator are completely determined by the initial conditions, the described methods are not applicable to the parallel BUG integrator. This work aims to develop a structure-preserving DLRA method for thermal radiative transfer that overcomes these limitations. The main contributions of this paper are:

- Provable energy stability for the nonlinear problem. A key distinction from all previously derived DLRA integrators is the rigorous proof of energy stability for the DLRA scheme applied to the fully nonlinear thermal radiative transfer equations. While prior stability analyses have been confined to simplified closures or linearizations, we prove that our integrator is stable for the physical closure given by the Stefan-Boltzmann law. Our analysis yields a practical time step restriction that naturally combines hyperbolic and parabolic CFL conditions.
- A highly efficient, parallel, and structure-preserving integrator. We introduce a novel, rank-adaptive integrator based on a macro-micro decomposition within the parallel BUG framework. The resulting scheme is simultaneously asymptotic-preserving and locally conservative. Critically, its parallel nature avoids the computationally expensive substep at twice the rank that is required by alternative structure-preserving approaches (e.g., augmented BUG integrators).
- An efficient implementation of physical boundary conditions. We propose a novel technique to incorporate reflection-transmission type boundary conditions directly into the evolution of the low-rank factors. This method is specifically tailored for the parallel BUG integrator, where standard approaches are not applicable.

The rest of the paper is organized into four sections. Section 2 introduces the thermal radiative transfer equations, the macro–micro decomposition, and the fundamentals of dynamical low-rank approximation and the parallel BUG integrator. Section 3 presents an asymptotic–preserving

discretization for the macro–micro equations using discrete ordinates, a first-order upwind discretization on staggered grids, and an implicit-explicit (IMEX) time-stepping scheme. We show that the proposed full-rank scheme for the nonlinear closure given by the Stefan-Boltzmann law is energy stable under a mixed hyperbolic and parabolic CFL condition. Section 4 proposes a computationally inexpensive and memory-efficient low-rank scheme based on the parallel BUG integrator for the macro–micro equations. It also describes an efficient algorithm for incorporating reflection-transmission type boundary conditions in the parallel BUG integrator. This scheme is shown to be asymptotic–preserving and energy stable for the nonlinear closure, given by the Stefan-Boltzmann law, under the same CFL condition as the full-rank scheme. Finally, Section 5 presents numerical experiments for Gaussian, Marshak wave, and hohlraum test cases.

2. Background

2.1. Thermal radiative transfer equations

The gray thermal radiative transfer equations model the interaction of radiation particles with the background material through the interplay of radiation and material heat. In dimensionless form, they read

$$\frac{\varepsilon^2}{c}\partial_t f + \varepsilon\ \boldsymbol{\Omega}\cdot\nabla_{\boldsymbol{x}} f = \sigma^a(B(T)-f) + \sigma^s(\phi - f), \tag{1a}$$

$$\varepsilon^2 c_\nu \partial_t T = \int_{\mathbb{S}^2} \sigma^a(f - B(T))\mathrm{d}\boldsymbol{\Omega}. \tag{1b}$$

Here, $f(t,\boldsymbol{x},\boldsymbol{\Omega})$ describes the particle density at time $t \in \mathbb{R}_{\geq 0}$, position $\boldsymbol{x} = (x,y,z) \in \mathcal{D} \subset \mathbb{R}^3$ and direction of flight $\boldsymbol{\Omega} = (\Omega_x, \Omega_y, \Omega_v) \in \mathbb{S}^2$. The material temperature, denoted by $T(t,\boldsymbol{x})$, varies in time and space, and the specific heat of the material is denoted by c_ν. ε, known as the Knudsen number, specifies the ratio of the mean free path of particles between collisions to the relevant spatial scale. Since most particles fly through the material without any interaction, we specify the probability of the different types of interaction. The two main particle-material interactions are absorption and scattering, and their probabilities are given by $\sigma^a(\boldsymbol{x})$ and $\sigma^s(\boldsymbol{x})$, respectively. We define the total cross-section as $\sigma^t(\boldsymbol{x}) = \sigma^a(\boldsymbol{x}) + \sigma^s(\boldsymbol{x})$ and assume that $\sigma^a(\boldsymbol{x}) \geq \sigma_0^a > 0$ and $\sigma^t(\boldsymbol{x}) \geq \sigma_0^t > 0$. We introduce the short-hand notation $\langle\cdot\rangle = \int_{\mathbb{S}^2}\cdot\,\mathrm{d}\boldsymbol{\Omega}$ to denote the integration over the unit sphere $\mathbb{S}^2$. Then, the scalar flux, ϕ, defined as $\phi(t,\boldsymbol{x}) := \frac{1}{4\pi}\langle f(t,\boldsymbol{x},\boldsymbol{\Omega})\rangle$ satisfies the following local conservation law obtained by integrating (1a) over $\boldsymbol{\Omega}$ and adding (1b):

$$\partial_t\left(\frac{4\pi}{c}\phi + c_\nu T\right) + \frac{1}{\varepsilon}\nabla_{\boldsymbol{x}} \cdot \langle \Omega f\rangle = 0. \tag{2}$$

The absorption of particles by the material increases its temperature and, due to blackbody radiation, the material emits particles proportional to the fourth power of its current temperature. To be precise, the rate at which particles are emitted by the material, represented by $B(T)$, is given by the Stefan-Boltzmann law, which reads

$$B(T) = \frac{ac}{4\pi}T^4$$

where a is the radiation constant and c is the speed of light.

To complete the description of the thermal radiative transfer equations, we must specify f and T at the initial time $t_0 \in \mathbb{R}_{\geq 0}$ and the boundaries of the domain. The initial conditions are given by

$$f(t_0, \boldsymbol{x}, \Omega) = f_I(\boldsymbol{x}, \Omega), \quad T(t_0, \boldsymbol{x}) = T_I(\boldsymbol{x}), \quad \boldsymbol{x} \in \mathcal{D}, \Omega \in \mathbb{S}^2.$$

Let $\partial\mathcal{D}$ denote the boundary of $\mathcal{D}$ and $\hat{\boldsymbol{x}} \in \partial\mathcal{D}$ be a point on the boundary. If $\boldsymbol{n}(\hat{\boldsymbol{x}})$ denotes the outward unit normal to the boundary at $\hat{\boldsymbol{x}}$, the reflection-transmission type boundary conditions for the thermal radiative transfer equations are given by

$$f(t, \hat{\boldsymbol{x}}, \Omega) = \begin{cases} \rho(\boldsymbol{n}\cdot\Omega) f(t, \hat{\boldsymbol{x}}, \Omega') + (1-\rho(\boldsymbol{n}\cdot\Omega)) f_B(\hat{\boldsymbol{x}}, \Omega), & \text{if } \boldsymbol{n}\cdot\Omega < 0 \\ f(t, \hat{\boldsymbol{x}}, \Omega), & \text{if } \boldsymbol{n}\cdot\Omega \geq 0 \end{cases}, \tag{3a}$$

$$T(t, \hat{\boldsymbol{x}}) = T_B(\hat{\boldsymbol{x}}), \tag{3b}$$

where f_B denotes the particle density transmitted into the domain from outside, $0 \leq \rho \leq 1$ specifies reflectivity and $\Omega' = \Omega - 2\boldsymbol{n}(\boldsymbol{n}\cdot\Omega)$. Note that $\rho = 1$ corresponds to a purely reflective boundary while $\rho = 0$ corresponds to a transmission or inflow boundary condition.

Absorption of a large number of particles at small time scales is equivalent to $\varepsilon \to 0$. In this limiting case, $\varepsilon \to 0$, the particle density $f = B(T)$ and the evolution of the material temperature T is given by the nonlinear diffusion-type equation known as the Rosseland equation (Rosseland 1931) which reads

$$c_\nu \partial_t T + \frac{4\pi}{c}\partial_t B(T) = \frac{4\pi}{3}\nabla_{\boldsymbol{x}} \cdot \left(\frac{1}{\sigma^t}\nabla_{\boldsymbol{x}} B(T)\right). \tag{4}$$

Remark 1. The initial and boundary conditions for the Rosseland equation (4) are found by solving an initial and boundary layer problem. A detailed analysis can be found in Klar and Schmeiser (2001); Klar and Siedow (1998). However, treating boundary layer problems is out of the scope of

this work, and thus we adopt the so-called equilibrium boundary conditions proposed in Klar and Schmeiser (2001). That is, we assume $(1-\rho)(f_B - B(T_B)) = 0$ almost everywhere on $\partial\mathcal{D} \times \mathbb{S}^2_- = \{(\hat{\boldsymbol{x}}, \boldsymbol{\Omega}) \text{ s.t. } \hat{\boldsymbol{x}} \in \partial\mathcal{D}, \boldsymbol{n}(\hat{\boldsymbol{x}}) \cdot \boldsymbol{\Omega} < 0\}$. Then, if $\mathcal{D} \subset \mathbb{R}^3$ has a smooth boundary $\partial\mathcal{D}$ and we assume that the initial and the boundary data is bounded and sufficiently smooth on the domain, the solution pair (f, T) converges as $\varepsilon \to 0$ to the solution of the Rosseland equation (Klar and Schmeiser 2001). The initial and boundary conditions for the Rosseland equation are then given by $T_I(\boldsymbol{x})$ and $T_B(\hat{\boldsymbol{x}})$, respectively. The reader is referred to Klar and Schmeiser (2001) for further details.

2.1.1. Macro–micro decomposition

The thermal radiative transfer equations involve effects varying at different time scales. Thus, to avoid mixing scales, we use a macro-micro decomposition (Lemou and Mieussens 2008) which decomposes the particle density into unscaled equilibrium variables and scaled non-equilibrium variables. Specifically, we use the following macro–micro ansatz described in Klar and Schmeiser (2001):

$$f(t, \boldsymbol{x}, \boldsymbol{\Omega}) = B(T(t, \boldsymbol{x})) + \varepsilon g(t, \boldsymbol{x}, \boldsymbol{\Omega}) + \varepsilon^2 h(t, \boldsymbol{x}), \tag{5}$$

where $\langle g \rangle = 0$. Thus, the particle density is decomposed into its angular mean $\langle f \rangle = B(T) + \varepsilon^2 h$, and a correction term εg. Substituting this macro–micro ansatz in the thermal radiative transfer equations (1) and using the condition $\langle g \rangle = 0$ yields the macro–micro equations

$$\frac{\varepsilon^2}{c}\partial_t g + \varepsilon\left(\mathcal{I} - \frac{1}{4\pi}\langle\cdot\rangle\right)(\boldsymbol{\Omega}\cdot\nabla_{\boldsymbol{x}} g) + \boldsymbol{\Omega}\cdot\nabla_{\boldsymbol{x}}(B(T) + \varepsilon^2 h) = -\sigma^t g, \tag{6a}$$

$$\frac{\varepsilon^2}{c}\partial_t h + \frac{1}{c}\partial_t B(T) + \frac{1}{4\pi}\langle \boldsymbol{\Omega}\cdot\nabla_{\boldsymbol{x}} g\rangle = -\sigma^a h, \tag{6b}$$

$$c_\nu \partial_t T = 4\pi\sigma^a h. \tag{6c}$$

The macro–micro equations are equivalent to the thermal radiative transfer equation and have the same Rosseland diffusion limit. This can be seen by comparing $\mathcal{O}(1)$ terms in (6) which yield the Rosseland equation (4) in the limit $\varepsilon \to 0$. Additionally, since $\langle \boldsymbol{\Omega}(B(T) + \varepsilon^2 h)\rangle = 0$ the local conservation law (2) takes the following equivalent form:

$$\partial_t\left(\frac{4\pi}{c}\phi + c_\nu T\right) + \nabla_{\boldsymbol{x}}\cdot\langle\boldsymbol{\Omega} g\rangle = 0. \tag{7}$$

2.1.1.1. Initial and boundary conditions. The initial and boundary conditions for the macro–micro equations have been derived and analyzed in

Klar and Schmeiser (2001). We present the relevant details here. The initial conditions for g and h can be derived from the following relations:

$$g(t_0, \boldsymbol{x}, \boldsymbol{\Omega}) = \frac{1}{\varepsilon}\left(f_I(\boldsymbol{x}, \boldsymbol{\Omega}) - \frac{1}{4\pi}\langle f_I(\boldsymbol{x}, \boldsymbol{\Omega})\rangle\right), h(t_0, \boldsymbol{x})$$
$$= \frac{1}{\varepsilon^2}\left(\frac{1}{4\pi}\langle f_I(\boldsymbol{x}, \boldsymbol{\Omega})\rangle - B(T_I)(\boldsymbol{x})\right).$$

The boundary condition for g is obtained by substituting the macro–micro ansatz (5) into the boundary conditions for f given in (3a). Thus, for $\hat{\boldsymbol{x}} \in \partial\mathcal{D}$, the boundary condition for g is given by:

$$g(t, \hat{\boldsymbol{x}}, \boldsymbol{\Omega}) = \begin{cases} \rho g(t, \hat{\boldsymbol{x}}, \boldsymbol{\Omega}') + (1-\rho)\left(\dfrac{f_B(t, \hat{\boldsymbol{x}}, \boldsymbol{\Omega}) - B(T_B)(t, \hat{\boldsymbol{x}})}{\varepsilon} - \epsilon h(t, \hat{\mathbf{x}})\right), & \text{if } \boldsymbol{n}\cdot\boldsymbol{\Omega} < 0, \\ g(t, \hat{\boldsymbol{x}}, \boldsymbol{\Omega}), & \text{if } \boldsymbol{n}\cdot\boldsymbol{\Omega} \geq 0. \end{cases}$$

The boundary condition for h is set such that the macro–micro decomposition is consistent at the boundaries, i.e., we compute h such that the $\langle g\rangle = 0$ is satisfied at the boundaries. Thus, h must satisfy the following condition at the boundary:

$$\int_{\boldsymbol{n}\cdot\Omega>0} (1 + \rho(-\boldsymbol{n}\cdot\Omega))g \ \mathrm{d}\Omega + \int_{\boldsymbol{n}\cdot\Omega<0} (1-\rho)\left(\frac{f_B - B(T_B)}{\varepsilon} - \epsilon h\right) \ \mathrm{d}\Omega = 0,$$
$$\hat{\boldsymbol{x}} \in \partial\mathcal{D},$$

when the boundary is not purely reflective, i.e., $0 \leq \rho < 1$. For a purely reflective boundary, i.e., $\rho = 1$, the boundary conditions for h are not required (Klar and Schmeiser 2001). Since we assume equilibrium boundaries, the above conditions simplify to

$$g(t, \hat{\boldsymbol{x}}, \boldsymbol{\Omega}) = \begin{cases} \rho g(t, \hat{\boldsymbol{x}}, \boldsymbol{\Omega}') - (1-\rho)\varepsilon h(t, \hat{\boldsymbol{x}}), & \text{if } \boldsymbol{n}\cdot\boldsymbol{\Omega} < 0, \\ g(t, \hat{\boldsymbol{x}}, \boldsymbol{\Omega}), & \text{if } \boldsymbol{n}\cdot\boldsymbol{\Omega} \geq 0, \end{cases}$$
$$\varepsilon\int_{\boldsymbol{n}\cdot\boldsymbol{\Omega}<0} (1-\rho)h\mathrm{d}\boldsymbol{\Omega} = \int_{\mathbf{n}\cdot\boldsymbol{\Omega}>0} (1 + \rho(-\boldsymbol{n}\cdot\boldsymbol{\Omega}))g\mathrm{d}\boldsymbol{\Omega}.$$

2.2. Dynamical low-rank approximation

In this section, we present a summary of DLRA (Koch and Lubich 2007) for solving time-dependent problems on the manifold of low-rank matrices. The central idea is to evolve the solution on the low-rank manifold by projecting the dynamics onto the tangent space. Let $\mathbf{g}(t) \in \mathbb{R}^{N_{\boldsymbol{x}}\times N_q}$ denote the matrix form of g discretized in $\boldsymbol{x}$ and $\boldsymbol{\Omega}$ with $N_{\boldsymbol{x}}$ spatial cells and N_q discrete directions. That is, $(\mathbf{g})_{ik} = g(t, \boldsymbol{x}_i, \boldsymbol{\Omega}_k)$. Then, (6a) can be written as the matrix-valued differential equation

$$\dot{\mathbf{g}}(t) = \mathbf{F}(t, \mathbf{g}(t)).$$

Let $\mathcal{M}_r$ denote the manifold of $N_x \times N_q$ rank-r matrices. Then, a low-rank approximation $\mathbf{Y}(t) \in \mathcal{M}_r$ of $\mathbf{g}(t)$ admits the factorization

$$\mathbf{Y}(t) = \mathbf{X}(t)\mathbf{S}(t)\mathbf{V}(t)^\top,$$

where $\mathbf{X}(t) \in \mathbb{R}^{N_x \times r}$, $\mathbf{V}(t) \in \mathbb{R}^{N_q \times r}$ are orthonormal basis matrices and $\mathbf{S}(t) \in \mathbb{R}^{r \times r}$ is the invertible coefficient matrix. Let $\mathcal{T}_{\mathbf{Y}}\mathcal{M}_r$ denote the tangent space to $\mathcal{M}_r$ at $\mathbf{Y}$. Then, to ensure that $\mathbf{Y}(t) \in \mathcal{M}_r$ approximates $\mathbf{g}(t)$ we find $\dot{\mathbf{Y}}(t) \in \mathcal{T}_{\mathbf{Y}(t)}\mathcal{M}_r$ such that for all times t the minimization problem

$$\min_{\dot{\mathbf{Y}}(t) \in \mathcal{T}_{\mathbf{Y}(t)}\mathcal{M}_r} \left|\left|\dot{\mathbf{Y}}(t) - \mathbf{F}(t, \mathbf{Y}(t))\right|\right|_F$$

is satisfied with respect to the Frobenius norm $||\cdot||_F$. Reformulating the minimization problem as a Galerkin condition on the tangent space, we see that the minimization problem is satisfied by

$$\dot{\mathbf{Y}}(t) = \mathbf{P}(\mathbf{Y}(t))\mathbf{F}(t, \mathbf{Y}(t)), \tag{8}$$

where $\mathbf{P}(\mathbf{Y}(t))$ denotes the orthogonal projection onto the tangent space and has the form $\mathbf{P}(\mathbf{Y})\mathbf{Z} = \mathbf{X}\mathbf{X}^\top\mathbf{Z} - \mathbf{X}\mathbf{X}^\top\mathbf{Z}\mathbf{V}\mathbf{V}^\top + \mathbf{Z}\mathbf{V}\mathbf{V}^\top$ (Koch and Lubich 2007, Lemma 4.1), for any $\mathbf{Z} \in \mathbb{R}^{N_x \times N_q}$. This allows us to derive differential equations for $\mathbf{X}(t)$, $\mathbf{S}(t)$, and $\mathbf{V}(t)$. However, these equations are stiff in the case of rank over-approximation due to the presence of near-zero singular values (Koch and Lubich 2007).

In recent years, several structure–preserving integrators (Lubich and Oseledets 2014; Ceruti and Lubich 2022; Ceruti, Einkemmer, et al. 2024; Ceruti, Kusch, et al. 2024; Kusch 2025) have been developed that are robust to this stiffness when solving the projected equation (8). In this work, we use the parallel BUG integrator (Ceruti, Kusch, et al. 2024), which evolves all the factors $\mathbf{X}$, $\mathbf{S}$, and $\mathbf{V}$ in parallel, resulting in a reduced number of potentially expensive projection operations while also allowing for rank-adaptivity. One step of the parallel BUG integrator for an initial rank-r approximation $\mathbf{Y}^0 = \mathbf{X}^0\mathbf{S}^0\mathbf{V}^{0,\top}$ at time t_0 updates the factors to $\mathbf{X}^1$, $\mathbf{S}^1$, $\mathbf{V}^1$ of rank r_1 at $t_1 = t_0 + \Delta t$ in three steps:

1. **Parallel update**: Update $\mathbf{X}$, $\mathbf{S}$, and $\mathbf{V}$ in parallel and construct augmented basis matrices $\hat{\mathbf{X}} \in \mathbb{R}^{N_x \times 2r}$ and $\hat{\mathbf{V}} \in \mathbb{R}^{N_q \times 2r}$:

K-step: For $\mathbf{K}(t_0) = \mathbf{X}^0\mathbf{S}^0$ solve from t_0 to t_1

$$\dot{\mathbf{K}}(t) = \mathbf{F}(t, \mathbf{K}(t)\mathbf{V}^{0,\top})\mathbf{V}^0.$$

Determine $\hat{\mathbf{X}} = (\mathbf{X}^0, \tilde{\mathbf{X}}^1) \in \mathbb{R}^{N_x \times 2r}$ as an orthonormal basis of $(\mathbf{X}^0, \mathbf{K}(t_1))$ (e.g., by QR decomposition). The $N_x \times r$ matrix $\tilde{\mathbf{X}}^1$ is filled with zero

columns if $\text{rank}(\mathbf{X}^0, \mathbf{K}(t_1)) < r$. Compute and store the matrix $\tilde{\mathbf{S}}_1^K = \tilde{\mathbf{X}}^{1,\top}\mathbf{K}(t_1)$.

L-step: For $\mathbf{L}(t_0) = \mathbf{V}^0\mathbf{S}^{0,\top}$ solve from t_0 to t_1

$$\dot{\mathbf{L}}(t) = \mathbf{F}(t, \mathbf{X}^0\mathbf{L}(t)^\top)^\top\mathbf{X}^0.$$

Determine $\hat{\mathbf{V}} = (\mathbf{V}^0, \tilde{\mathbf{V}}^1) \in \mathbb{R}^{N_q \times 2r}$ as an orthonormal basis of $(\mathbf{V}^0, \mathbf{L}(t_1))$ (e.g., by QR decomposition). The $N_q \times r$ matrix $\tilde{\mathbf{V}}^1$ is filled with zero columns if $\text{rank}(\mathbf{V}^0, \mathbf{L}(t_1)) < r$. Compute and store the matrix $\tilde{\mathbf{S}}_1^L = \mathbf{L}(t_1)^\top\tilde{\mathbf{V}}^1$.

S-step: For $\overline{\mathbf{S}}(t_0) = \mathbf{S}^0$ solve from t_0 to t_1

$$\dot{\overline{\mathbf{S}}}(t) = \mathbf{X}^{0,\top}\mathbf{F}(t, \mathbf{X}^0\overline{\mathbf{S}}(t)\mathbf{V}^{0,\top})\mathbf{V}^0.$$

2. **Augmentation**: Construct the augmented coefficient matrix $\hat{\mathbf{S}} \in \mathbb{R}^{2r\times 2r}$

$$\hat{\mathbf{S}} = \begin{bmatrix} \overline{\mathbf{S}}(t_1) & \tilde{\mathbf{S}}_1^L \\ \tilde{\mathbf{S}}_1^K & \mathbf{0} \end{bmatrix}.$$

3. **Truncate**: Compute the singular value decomposition of the coefficient matrix $\hat{\mathbf{S}} = \hat{\mathbf{P}}\hat{\Sigma}\hat{\mathbf{Q}}^\top$ where $\hat{\Sigma}$ has the singular values, $\hat{\sigma}_j$, of $\hat{\mathbf{S}}$ on its diagonal. The new rank r_1 is chosen as the minimal $r_1 < 2r$ such that, for a given tolerance ϑ, the following inequality is satisfied

$$\left(\sum_{j=r_1+1}^{2r} \hat{\sigma}_j^2\right)^{1/2} \leq \vartheta.$$

The updated coefficient matrix $\mathbf{S}_1$ is set as the diagonal matrix containing the first r_1 singular values of $\hat{\Sigma}$. To set the updated basis, we define $\mathbf{P}_{r_1}$ and $\mathbf{Q}_{r_1}$ to be the matrices containing the first r_1 columns of $\hat{\mathbf{P}}$ and $\hat{\mathbf{Q}}$, respectively. Then, the updated factors are set as $\mathbf{X}^1 = \hat{\mathbf{X}}\mathbf{P}_{r_1}$ and $\mathbf{V}^1 = \hat{\mathbf{V}}\mathbf{Q}_{r_1}$.

The approximation at time t_1 is then $\mathbf{Y}^1 = \mathbf{X}^1\mathbf{S}^1\mathbf{V}^{1,\top}$.

3. An AP scheme for the macro–micro equations

To simulate the thermal radiative transfer equations, we discretize the macro–micro equations (6) in their phase space variables $(t, \boldsymbol{x}, \Omega)$. There are three important considerations when constructing a numerical scheme for the macro-micro equations. First, the numerical scheme should consistently discretize the Rosseland equation in the diffusive limit $\varepsilon \to 0$, i.e., the scheme should be AP. However, in the diffusive limit, the right-hand side

of the macro–micro equations becomes stiff, and naive schemes require prohibitively small $\mathcal{O}(\varepsilon)$ step sizes for stability. Thus, the proposed numerical scheme should not require prohibitively small step sizes to capture the correct dynamics of the system in the diffusive limit. Finally, the numerical scheme should reduce the computational costs and memory requirements arising from the high-dimensional phase space of g.

In this section, we propose a numerical scheme based on the discrete ordinates method (Lewis and Miller 1984) for $\mathbf{\Omega}$, a first-order upwind discretization on staggered grids (LeVeque 2002; Küpper et al. 2016) for $\boldsymbol{x}$, and a first-order IMEX scheme (Frank et al. 2025) for t. In Sections 3.3 and 3.4, the proposed scheme, dubbed the full-rank macro–micro scheme, is shown to be AP and energy stable for the nonlinear Stefan-Boltzmann closure with mixed hyperbolic and parabolic CFL conditions.

3.1. Angular discretization

The discrete ordinates, or S_N, method (Lewis and Miller 1984) uses a quadrature rule on the unit sphere $\mathbb{S}^2$ and solves the macro–micro equations in these discrete directions. The S_N method has been a popular choice for angular discretization of kinetic equations due to its ease of implementation and handling of boundary conditions (Einkemmer et al. 2021, 2021) compared to other methods like the method of moments (Case and Zweifel 1967) or the minimal entropy method (Levermore et al. 1998).

In this work, we use the tensorized Gauss-Legendre quadrature rule, also called the product quadrature, of order q on the unit sphere. Let $\{\mathbf{\Omega}^\ell\}_{\ell=1,\dots,N_q}$ be N_q quadrature points with the associated (quadrature) weights $\{w^\ell\}_{\ell=1,\dots,N_q}$ and let $g_\ell(\cdot,\cdot) := g(\cdot,\cdot,\mathbf{\Omega}^\ell)$. Then, the macro–micro equations in the ℓth discrete direction are given by

$$\begin{aligned}
&\frac{\varepsilon^2}{c}\partial_t g_\ell + \varepsilon\left(\mathbf{\Omega}^\ell\cdot\nabla_{\mathbf{x}} g_\ell - \frac{1}{4\pi}\sum_{\ell'=1}^{N_q} w^{\ell'}\mathbf{\Omega}^{\ell'}\cdot\nabla_{\mathbf{x}} g_{\ell'}\right) + \mathbf{\Omega}^\ell\cdot\nabla_{\mathbf{x}}(B(T)+\varepsilon^2 h) = -\sigma^t g_\ell,\\
&\frac{\varepsilon^2}{c}\partial_t h + \frac{1}{c}\partial_t B(T) + \frac{1}{4\pi}\sum_{\ell'=1}^{N_q} w^{\ell'}\mathbf{\Omega}^\ell\cdot\nabla_{\mathbf{x}} g_{\ell'} = -\sigma^a h,\\
&c_v\partial_t T = 4\pi\sigma^a h.
\end{aligned} \tag{9}$$

Let $\mathbf{\Omega}^\ell := (\Omega_x^\ell, \Omega_y^\ell, \Omega_z^\ell)^\top$ and $\mathcal{J}_{\boldsymbol{x}} := \{x, y, z\}$. If $\boldsymbol{g} := (g_1, \dots, g_{N_q})^\top \in \mathbb{R}^{N_q}$, then we can write the above system of N_q equations as

$$\frac{\varepsilon^2}{c}\partial_t \boldsymbol{g} + \varepsilon\left(\mathbf{I} - \frac{1}{4\pi}\mathbb{1}\boldsymbol{w}^\top\right)\sum_{v\in\mathcal{J}_{\boldsymbol{x}}}\mathbf{Q}_v\partial_v\boldsymbol{g} + \sum_{v\in\mathcal{J}_{\boldsymbol{x}}}\mathbf{Q}_v\mathbb{1}\partial_v(B(T)+\varepsilon^2 h) = -\sigma^t\boldsymbol{g}, \tag{10a}$$

$$\frac{\varepsilon^2}{c}\partial_t h + \frac{1}{c}\partial_t B(T) + \frac{1}{4\pi}\boldsymbol{w}^\top \sum_{v\in\mathcal{J}_{\boldsymbol{x}}} \mathbf{Q}_v \partial_v \boldsymbol{g} = -\sigma^a h, \tag{10b}$$

$$c_v \partial_t T = 4\pi\sigma^a h, \tag{10c}$$

where $\boldsymbol{w} = (w_1, \ldots, w_{N_q})^\top$ and $\mathbb{1} = (1, \ldots, 1)^\top$ are vectors in $\mathbb{R}^{N_q}$. In the above equations, $\mathbf{I} \in \mathbb{R}^{N_q \times N_q}$ denotes the identity matrix and, for $v \in \mathcal{J}_{\boldsymbol{x}}$,

$$\mathbf{Q}_v := \begin{bmatrix} \Omega_v^1 & & \\ & \ddots & \\ & & \Omega_v^{N_q} \end{bmatrix} \in \mathbb{R}^{N_q \times N_q}.$$

3.2. Spatio-temporal discretization

To discretize (10) in $\boldsymbol{x}$, we use a first-order upwind discretization on staggered grids (Küpper et al. 2016; Einkemmer et al. 2021) and a first-order IMEX scheme in t. This staggered-grid approach for constructing AP schemes was first described in Küpper et al. (2016) for the multi-scale transport equation and in Einkemmer et al. (2021) for the macro–micro decomposition of the radiation transport equation. For brevity, we restrict the presentation of the discretization to two spatial dimensions on a rectangular domain, i.e., $\boldsymbol{x} = (x, y) \in [x_L, x_R] \times [y_B, y_T] \subset \mathbb{R}^2$. Note that in this projected geometry, $\boldsymbol{\Omega} \in P(\mathbb{S}^2)$ where $P(\mathbb{S}^2)$ is the projection of the unit sphere in $\mathbb{R}^3$ onto the two dimensional plane. This is defined as

$$P(\mathbb{S}^2) := \left\{ (\sqrt{1-\mu^2}\sin(\theta), \sqrt{1-\mu^2}\cos(\theta)) | 0 \le \mu \le 1, \theta \in [0, 2\pi] \right\}.$$

Note that the normalization constant 4π in (1) is replaced by 2π in this projected geometry and $\mathcal{J}_{\boldsymbol{x}} = \{x, y\}$.

We construct two one-dimensional equidistant staggered grids, in x and y domains, with cell size $\Delta x = (x_R - x_L)/N_x$ and $\Delta y = (y_T - y_B)/N_y$, for some $N_x, N_y \in \mathbb{N}$. The interfaces between intervals are given by $\{x_{i+1/2}\}_{i=0}^{N_x}$ and $\{y_{j+1/2}\}_{j=0}^{N_y}$ while their mid-points are denoted by $\{x_i\}_{i=1}^{N_x}$ and $\{y_j\}_{j=1}^{N_y}$. Note that the discretization is set up such that x_1, x_{N_x}, y_1, and y_{N_y} lie on the boundaries of the domain. Following Küpper et al. (2016) and Einkemmer et al. (2021), we discretize (6) such that

- T and h are evaluated at (x_i, y_j) and $(x_{i+1/2}, y_{j+1/2})$ (red colored circles in Figure 1),
- $\boldsymbol{g}$ is evaluated at $(x_{i+1/2}, y_j)$ and $(x_i, y_{j+1/2})$ (blue colored diamonds in Figure 1).

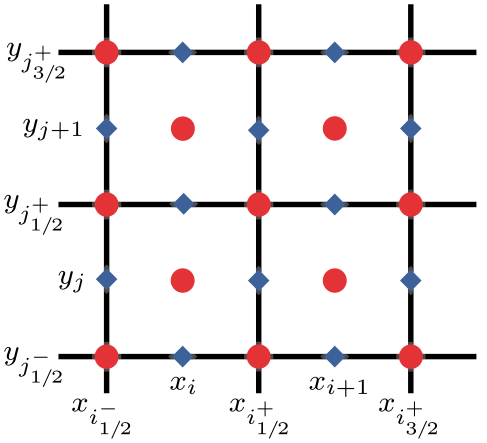

Figure 1. Two-dimensional staggered grid as described in Küpper et al. (2016). h and T are evaluated at the red circles whereas g is evaluated at the blue diamonds.

For an illustration of the grid, see Figure 1.

We introduce the following notation to simplify the presentation of the numerical scheme. Let $k^{\pm}_{1/2} := k \pm 1/2$, such that the cell interfaces are denoted by $x_{i^{\pm}_{1/2}}$ and $y_{j^{\pm}_{1/2}}$. To further simplify notation, we define $B^n_{ij} := \frac{ac}{2\pi}(T^n_{ij})^4$ at (x_i, y_j) and analogously $B^n_{i^+_{1/2}j^+_{1/2}} := \frac{ac}{2\pi}(T^n_{i^+_{1/2}j^+_{1/2}})^4$ at $(x_{i^+_{1/2}}, y_{j^+_{1/2}})$.

Let $|\mathbf{Q}_v| \in \mathbb{R}^{N_q \times N_q}$, $v \in \mathcal{J}_{\boldsymbol{x}}$, be the diagonal matrix with entries $(|\mathbf{Q}_v|)_{\ell\ell} = |\Omega^{\ell}_v|$, $\ell = 1, \ldots, N_q$. Then, we define the matrices $\mathbf{Q}^{\pm}_v := (\mathbf{Q}_v \pm |\mathbf{Q}_v|)/2$, $v \in \mathcal{J}_{\boldsymbol{x}}$. For $(\alpha, \beta) = (i^+_{1/2}, j)$ or $(\alpha, \beta) = (i, j^+_{1/2})$ let $\boldsymbol{g}_{\alpha,\beta}(t) := \boldsymbol{g}(t, x_\alpha, y_\beta)$ and $h_{\alpha\beta}(t) := h(t, x_\alpha, y_\beta)$, then the first-order upwind differential operators at the interfaces (omitting t dependence) are defined as

$$\mathcal{D}^+_x \boldsymbol{g}_{\alpha\beta} := \frac{1}{\Delta x}(\boldsymbol{g}_{\alpha+1,\beta} - \boldsymbol{g}_{\alpha\beta}), \quad \mathcal{D}^-_x \boldsymbol{g}_{\alpha\beta} := \frac{1}{\Delta x}(\boldsymbol{g}_{\alpha\beta} - \boldsymbol{g}_{\alpha-1,\beta}),$$
$$\mathcal{D}^+_y \boldsymbol{g}_{\alpha\beta} := \frac{1}{\Delta y}(\boldsymbol{g}_{\alpha,\beta+1} - \boldsymbol{g}_{\alpha\beta}), \quad \mathcal{D}^-_y \boldsymbol{g}_{\alpha\beta} := \frac{1}{\Delta y}(\boldsymbol{g}_{\alpha\beta} - \boldsymbol{g}_{\alpha,\beta-1}),$$
$$\delta^0_x h_{\alpha\beta} := \frac{1}{\Delta x}(h_{\alpha^+_{1/2}\beta} - h_{\alpha^-_{1/2}\beta}), \quad \delta^0_y h_{\alpha\beta} := \frac{1}{\Delta y}(h_{\alpha\beta^+_{1/2}} - h_{\alpha\beta^-_{1/2}}),$$

where recall that $\alpha^+_{1/2} = \alpha + 1/2$ and $\beta^+_{1/2} = \beta + 1/2$. Additionally, for $(\alpha, \beta) = (i, j)$ or $(\alpha, \beta) = (i^+_{1/2}, j^+_{1/2})$, we define the following centered difference operator at the cell centers and corners

$$\mathcal{D}^0_x \boldsymbol{g}_{\alpha\beta} := \frac{1}{\Delta x}(\boldsymbol{g}_{\alpha^+_{1/2}\beta} - \boldsymbol{g}_{\alpha^-_{1/2}\beta}), \quad \mathcal{D}^0_y \boldsymbol{g}_{\alpha\beta} := \frac{1}{\Delta y}(\boldsymbol{g}_{\alpha\beta^+_{1/2}} - \boldsymbol{g}_{\alpha\beta^-_{1/2}}).$$

Note that though $\mathcal{D}^0$ and δ^0 are both central difference operators, $\mathcal{D}^0$ approximates the derivative of g at the cell centers and corners while δ^0 approximates the derivatives of h and T at the interfaces. Finally, using an IMEX scheme similar to Frank et al. (2025) for discretizing in time, the full-rank macro–micro scheme reads

$$\frac{\varepsilon^2}{c\Delta t}\left(\boldsymbol{g}^{n+1}_{i^+_{1/2},j}-\boldsymbol{g}^{n}_{i^+_{1/2},j}\right)+\varepsilon\left(\mathbf{I}-\frac{1}{2\pi}\mathbb{1}\boldsymbol{w}^\top\right)\mathcal{L}_x\boldsymbol{g}^{n}_{i^+_{1/2}j}+\varepsilon\left(\mathbf{I}-\frac{1}{2\pi}\mathbb{1}\boldsymbol{w}^\top\right)\mathcal{L}_y\boldsymbol{g}^{n}_{i^+_{1/2}j}$$
$$+\mathbf{Q}_x\mathbb{1}\delta^0_x\left(B^n_{i^+_{1/2}j}+\varepsilon^2h^n_{i^+_{1/2}j}\right)+\mathbf{Q}_y\mathbb{1}\delta^0_y\left(B^n_{i^+_{1/2}j}+\varepsilon^2h^n_{i^+_{1/2}j}\right)=-\sigma^t_{i^+_{1/2}j}\boldsymbol{g}^{n+1}_{i^+_{1/2}j}, \tag{11a}$$

$$\frac{\varepsilon^2}{c\Delta t}\left(h^{n+1}_{ij}-h^n_{ij}\right)+\frac{1}{c\Delta t}\left(B^{n+1}_{ij}-B^n_{ij}\right)+\frac{1}{2\pi}\boldsymbol{w}^\top\mathbf{Q}_x\mathcal{D}^0_x\boldsymbol{g}^{n+1}_{ij}+\frac{1}{2\pi}\boldsymbol{w}^\top\mathbf{Q}_y\mathcal{D}^0_y\boldsymbol{g}^{n+1}_{ij}$$
$$=-\sigma^a_{ij}h^{n+1}_{ij}, \tag{11b}$$

$$\frac{c_\nu}{\Delta t}\left(T^{n+1}_{ij}-T^n_{ij}\right)=2\pi\sigma^a_{ij}h^{n+1}_{ij}, \tag{11c}$$

where, for $\nu\in\mathcal{J}_{\boldsymbol{x}}$,

$$\mathcal{L}_\nu\boldsymbol{g}^n_{i^+_{1/2}j}=\left(\mathbf{Q}^-_\nu\mathcal{D}^+_\nu+\mathbf{Q}^+_\nu\mathcal{D}^-_\nu\right)\boldsymbol{g}^n_{i^+_{1/2}j}.$$

The scheme is analogously defined at $(x_i, y_{j^+_{1/2}})$ for g and at $(x_{i^+_{1/2}}, y_{j^+_{1/2}})$ for h and T.

Remark 2. To update the solution from t_n to $t_{n+1}=t_n+\Delta t$ with the above scheme, we first update g using (11a) and then simultaneously update h and T using (11b),(11c). In the latter step, we first express h^{n+1} in terms of h^n, B^{n+1}, B^n, and g^{n+1} by re-writing (11b). Then, we substitute h^{n+1} in (11c) and solve a fourth order polynomial equation to obtain T^{n+1}. In the numerical implementation, we use the `Roots.jl` package from Julia to solve the fourth-order polynomial equation.

The full-rank macro–micro scheme satisfies a discrete version of the local conservation law (7), which is obtained by substituting the macro–micro ansatz in (2). Note that $\phi^n_{ij}=B^n_{ij}+\varepsilon^2h^n_{ij}$ (analogously, $\phi^n_{i^+_{1/2}j^+_{1/2}}$) denotes the scalar flux at time t_n. Thus, re-writing (11b) in terms of ϕ^n_{ij}, balancing constants and adding the resulting equation to (11c) yields that the full-rank macro–micro scheme (11) satisfies the following discrete local conservation law:

$$\frac{1}{\Delta t}\left(\frac{2\pi}{c}\phi^{n+1}_{ij}+c_\nu T^{n+1}_{ij}-\frac{2\pi}{c}\phi^n_{ij}-c_\nu T^n_{ij}\right)+\boldsymbol{w}^\top\mathbf{Q}_x\mathcal{D}^0_x\boldsymbol{g}^{n+1}_{ij}+\boldsymbol{w}^\top\mathbf{Q}_y\mathcal{D}^0_y\boldsymbol{g}^{n+1}_{ij}=0. \tag{12}$$

3.3. AP property

Theorem 3.1. *The full-rank macro–micro scheme (11) is asymptotic–preserving for the thermal radiative transfer equations. That is, it preserves the discrete Rosseland diffusion equation given by*

$$\frac{c_\nu}{\Delta t}\left(T_{ij}^{n+1}-T_{ij}^{n}\right)+\frac{2\pi}{c\Delta t}\left(B_{ij}^{n+1}-B_{ij}^{n}\right)=\frac{2\pi}{3}\left[\mathcal{D}_x^0\left(\frac{1}{\sigma^t}\delta_x^0 B^n\right)_{ij}+\mathcal{D}_y^0\left(\frac{1}{\sigma^t}\delta_y^0 B^n\right)_{ij}\right]. \tag{13}$$

This is a 5-point centered difference discretization for the Rosseland diffusion equation (4) *on a staggered grid with an explicit time discretization. A similar relation holds at* $(x_{i^+_{1/2}}, y_{j^+_{1/2}})$.

Proof. From (11a) and the analogous definition at $(x_i, y_{j^+_{1/2}})$, we see that as $\varepsilon \to 0$ we get

$$\boldsymbol{g}_{i^+_{1/2}j}^{n+1}=-\frac{1}{\sigma^t_{i^+_{1/2}j}}\left(\mathbf{Q}_x\mathbb{1}\delta_x^0+\mathbf{Q}_y\mathbb{1}\delta_y^0\right)B^n_{i^+_{1/2}j},$$

$$\boldsymbol{g}_{ij^+_{1/2}}^{n+1}=-\frac{1}{\sigma^t_{ij^+_{1/2}}}\left(\mathbf{Q}_x\mathbb{1}\delta_x^0+\mathbf{Q}_y\mathbb{1}\delta_y^0\right)B^n_{ij^+_{1/2}}.$$

Similarly, taking the limit $\varepsilon \to 0$ in (11b) yields

$$\sigma_{ij}^a h_{ij}^{n+1}=-\frac{1}{2\pi}\boldsymbol{w}^\top\mathbf{Q}_x\mathcal{D}_x^0\boldsymbol{g}_{ij}^{n+1}-\frac{1}{2\pi}\boldsymbol{w}^\top\mathbf{Q}_y\mathcal{D}_y^0\boldsymbol{g}_{ij}^{n+1}-\frac{1}{c\Delta t}\left(B_{ij}^{n+1}-B_{ij}^{n}\right). \tag{14}$$

Since $\mathcal{D}_x^0\boldsymbol{g}_{ij}^{n+1}=(\boldsymbol{g}_{i^+_{1/2}j}^{n+1}-\boldsymbol{g}_{i^-_{1/2}j}^{n+1})/\Delta x$, substituting $\boldsymbol{g}_{i^+_{1/2}j}^{n+1}$ and $\boldsymbol{g}_{ij^+_{1/2}}^{n+1}$ in $\mathcal{D}_x^0\boldsymbol{g}_{ij}^{n+1}$ gives

$$\begin{aligned}
\mathcal{D}_x^0\boldsymbol{g}_{ij}^{n+1}&=\frac{-1}{\Delta x}\left(\frac{1}{\sigma^t_{i^+_{1/2}j}}\left(\mathbf{Q}_x\mathbb{1}\delta_x^0+\mathbf{Q}_y\mathbb{1}\delta_y^0\right)B^n_{i^+_{1/2}j}-\frac{1}{\sigma^t_{i^-_{1/2}j}}\left(\mathbf{Q}_x\mathbb{1}\delta_x^0+\mathbf{Q}_y\mathbb{1}\delta_y^0\right)B^n_{i^-_{1/2}j}\right)\\
&=\frac{-1}{\Delta x}\left(\frac{1}{\sigma^t_{i^+_{1/2}j}}\mathbf{Q}_x\mathbb{1}\delta_x^0B^n_{i^+_{1/2}j}-\frac{1}{\sigma^t_{i^-_{1/2}j}}\mathbf{Q}_x\mathbb{1}\delta_x^0B^n_{i^-_{1/2}j}\right)\\
&\quad-\frac{1}{\Delta x}\left(\frac{1}{\sigma^t_{i^+_{1/2}j}}\mathbf{Q}_y\mathbb{1}\delta_y^0B^n_{i^+_{1/2}j}-\frac{1}{\sigma^t_{i^-_{1/2}j}}\mathbf{Q}_y\mathbb{1}\delta_y^0B^n_{i^-_{1/2}j}\right)\\
&=-\mathcal{D}_x^0\left(\frac{1}{\sigma^t_{ij}}\mathbf{Q}_x\mathbb{1}\delta_x^0B^n_{ij}\right)-\mathcal{D}_x^0\left(\frac{1}{\sigma^t_{ij}}\mathbf{Q}_y\mathbb{1}\delta_y^0B^n_{ij}\right).
\end{aligned}$$

A similar expression can be derived for $\mathcal{D}_y^0\boldsymbol{g}_{ij}^{n+1}=(\boldsymbol{g}_{ij^+_{1/2}}^{n+1}-\boldsymbol{g}_{ij^-_{1/2}}^{n+1})/\Delta y$. Substituting $\mathcal{D}_x^0\boldsymbol{g}_{ij}^{n+1}$ and $\mathcal{D}_y^0\boldsymbol{g}_{ij}^{n+1}$ in (14) yields

$$\sigma_{ij}^a h_{ij}^{n+1} = \frac{1}{2\pi}\boldsymbol{w}^\top \mathbf{Q}_x \left[\mathbf{Q}_x \mathbb{1}\mathcal{D}_x^0\left(\frac{1}{\sigma_{ij}^t}\delta_x^0 B_{ij}^n\right) + \mathbf{Q}_y \mathbb{1}\mathcal{D}_x^0\left(\frac{1}{\sigma_{ij}^t}\delta_y^0 B_{ij}^n\right)\right]$$
$$+\frac{1}{2\pi}\boldsymbol{w}^\top \mathbf{Q}_y \left[\mathbf{Q}_x \mathbb{1}\mathcal{D}_y^0\left(\frac{1}{\sigma_{ij}^t}\delta_x^0 B_{ij}^n\right) + \mathbf{Q}_y \mathbb{1}\mathcal{D}_y^0\left(\frac{1}{\sigma_{ij}^t}\delta_y^0 B_{ij}^n\right)\right] - \frac{1}{c\Delta t}\left(B_{ij}^{n+1} - B_{ij}^n\right).$$

Since by the choice of our quadrature $\boldsymbol{w}^\top \mathbf{Q}_x \mathbf{Q}_x \mathbb{1} = \int_{P(\mathbb{S}^2)} (\Omega_x)^2 \mathrm{d}\Omega = 2\pi/3$, $\boldsymbol{w}^\top \mathbf{Q}_y \mathbf{Q}_y \mathbb{1} = \int_{P(\mathbb{S}^2)} (\Omega_y)^2 \mathrm{d}\Omega = 2\pi/3$, and $\boldsymbol{w}^\top \mathbf{Q}_x \mathbf{Q}_y \mathbb{1} = \int_{\mathbb{P}(\mathbb{S}^2)} \Omega_x \Omega_y \mathrm{d}\Omega = 0$, we get

$$\sigma_{ij}^a h_{ij}^{n+1} = \frac{1}{3}\left[\mathcal{D}_x^0\left(\frac{1}{\sigma_{ij}^t}\delta_x^0 B_{ij}^n\right) + \mathcal{D}_y^0\left(\frac{1}{\sigma_{ij}^t}\delta_y^0 B_{ij}^n\right)\right] - \frac{1}{c\Delta t}\left(B_{ij}^{n+1} - B_{ij}^n\right).$$

Finally, substituting the value of h_{ij}^{n+1} in (11c) yields (13) at (x_i, y_j). A similar equality can be shown to hold at $(x_{i_{1/2}^+}, y_{j_{1/2}^+})$ in the limit $\varepsilon \to 0$. ■

3.4. Energy stability

In this section, we show that the full-rank macro–micro scheme (11) dissipates energy under a mixed CFL condition, for a suitable definition of energy. Let $N_{\boldsymbol{x}}^I$ denote the number of cell interface points and $N_{\boldsymbol{x}}^C$ denote the combined number of cell centers and corners. Let $\mathcal{K}^I$ denote the set of all spatial indices (α, β) such that (x_α, y_β) lies on the interface of two cells, i.e., it is of the form $(x_{i_{1/2}^+}, y_j)$ or $(x_i, y_{j_{1/2}^+})$. Then, to map $g_{\kappa,\ell}$, $\kappa \in \mathcal{K}^I$, $\ell = 1, \ldots, N_q$, to the matrix $\mathbf{g} \in \mathbb{R}^{N_{\boldsymbol{x}}^I \times N_q}$ we define the bijective index map $\varrho^I : \mathcal{K}^I \to \{1, \ldots, N_{\boldsymbol{x}}^I\}$ such that $(\mathbf{g})_{\varrho^I(\kappa),\ell} = g_{\kappa,\ell}$. Similarly, let $\mathcal{K}^C$ denote the set of all spatial indices (α, β) such that (x_α, y_β) is either the corner of a cell or its center and $\varrho^C : \mathcal{K}^C \to \{1, \ldots, N_{\boldsymbol{x}}^C\}$ denote the corresponding bijective index map. Then, we define $\boldsymbol{h} \in \mathbb{R}^{N_{\boldsymbol{x}}^C}$ and $\boldsymbol{T} \in \mathbb{R}^{N_{\boldsymbol{x}}^C}$ with elements $(\boldsymbol{h})_{\varrho^C(\kappa)} = h_\kappa$ and $(\boldsymbol{T})_{\varrho^C(\kappa)} = T_\kappa$, respectively. For $\Delta\zeta = \Delta x \Delta y$, the discrete-$L^2$ norms of $\boldsymbol{h}$, $\boldsymbol{T}$, and $\mathbf{g}$ are given as

$$||\boldsymbol{h}||^2 := \sum_{\kappa\in\mathcal{K}^C} h_\kappa^2 \Delta\zeta, \quad ||\boldsymbol{T}||^2 := \sum_{\kappa\in\mathcal{K}^C} T_\kappa^2 \Delta\zeta, \quad ||\boldsymbol{g}||_\Omega^2 := \sum_{\kappa\in\mathcal{K}^I} \boldsymbol{g}_\kappa^\top \mathbf{M}^2 \boldsymbol{g}_\kappa$$
$$\Delta\zeta = \sum_{\kappa\in\mathcal{K}^I}\sum_{\ell} w_\ell g_{\kappa,\ell}^2 \Delta\zeta,$$

where $\boldsymbol{g}_\kappa = (g_{\kappa,1}, \ldots, g_{\kappa,N_q})^\top$ and $(\mathbf{M})_{ij} = \sqrt{w_i}\delta_{ij}$, for $\delta_{ij} = 1$, if $i = j$ and 0 otherwise. The energy at time t_n is then defined as

$$e^n := \left|\left|\frac{1}{c}\boldsymbol{B}^n + \frac{\varepsilon^2}{c}\boldsymbol{h}^n\right|\right|^2 + \frac{1}{2\pi}\left|\left|\frac{\varepsilon}{c}\mathbf{g}^n\right|\right|_\Omega^2 + \frac{2}{5}\left|\left|\frac{\sqrt{ac_\nu}}{2\pi}(\boldsymbol{T}^n)^{5/2}\right|\right|^2. \tag{15}$$

Note that in the remainder of the paper, we drop the subscript Ω from $||\cdot||_\Omega$ and denote it by $||\cdot||$ when it is clear from the context that $||\cdot||_\Omega$ is chosen.

Theorem 3.2. *For a given spatial grid size $\Delta x, \Delta y$, let the step size Δt satisfy the following CFL condition for all $\Omega_x^\ell, \Omega_y^\ell \neq 0$,*

$$\Delta t \leq \frac{1}{3c}\min\left\{\varepsilon\Delta x + \frac{\sigma_0^t \Delta x^2}{4\left|\Omega_x^\ell\right|}, \varepsilon\Delta y + \frac{\sigma_0^t \Delta y^2}{4\left|\Omega_y^\ell\right|}\right\}. \tag{16}$$

Then, the full-rank macro–micro scheme given by (11) is energy stable, i.e., $e^{n+1} \leq e^n$, where the energy is defined in (15).

To keep the main part of the paper short, the proof of the theorem has been shifted to Appendix B.

4. An AP parallel low-rank scheme for macro–micro equations

From Theorem 3.1 we see that in the diffusive limit, $\varepsilon \to 0$, the full-rank macro–micro scheme is a consistent discretization of the Rosseland equation. Additionally, Theorem 3.2 shows that in the diffusive limit, the full-rank macro–micro scheme doesn't need to resolve small time scales to capture the correct dynamics of the system. Thus, the scheme (11) addresses the first two challenges outlined at the beginning of Section 3, namely the AP property and energy stability without restrictive CFL conditions.

However, the full-rank macro–micro scheme requires storing and updating g at each pair $(\boldsymbol{x}_\kappa, \Omega_\ell)$, for $\kappa \in \mathcal{K}^I$ and $\ell = 1, \ldots, N_q$, and hence has a high computational cost and memory footprint. Thus, further modifications must be made to address the high-dimensional phase space of g and reduce the computational costs of the scheme. In Frank et al. (2025), the authors propose to use DLRA (Koch and Lubich 2007) to reduce the computational costs of the thermal radiative transfer equations using the augmented BUG integrator (Ceruti, Kusch, et al. 2022). However, the proposed macro–micro augmented BUG scheme requires a serial S-step at twice the current rank. This increases the overall computational cost and memory requirement for the scheme. Moreover, only far-field boundaries have been considered in Frank et al. (2025), and thus efficient methods of implementing boundary conditions for the macro–micro low-rank schemes remain an open topic. In this section, we outline the use of the parallel BUG integrator (Ceruti,

Kusch, et al. 2024) to update all the factors in parallel and outline a procedure to efficiently incorporate boundary conditions.

For $v \in \mathcal{J}_x$, let $\mathbf{D}_v^{\pm} \in \mathbb{R}^{N_x^I \times N_x^I}$, $\mathbf{d}_v^0 \in \mathbb{R}^{N_x^I \times N_x^C}$, and $\mathbf{D}_v^0 \in \mathbb{R}^{N_x^C \times N_x^I}$ denote the matrix form of the operators $\mathcal{D}_v^{\pm}$, δ_v^0, and $\mathcal{D}_v^0$, respectively. Thus, for $v \in \mathcal{J}_x$ and $k = 1, \ldots, N_x^I$, we get $(\mathbf{D}_v^{\pm}\mathbf{g})_{k,\ell} = \mathcal{D}_v^{\pm} g_{(\varrho^I)^{-1}(k),\ell}$, and $(\mathbf{d}_v^0 \boldsymbol{h})_k = \delta_v^0 h_{(\varrho^I)^{-1}(k)}$, where $\ell = 1, \ldots, N_q$. Similarly, for $v \in \mathcal{J}_x$ and $k' = 1, \ldots, N_x^C$, we have $(\mathbf{D}_v^0 \mathbf{g})_{k',\ell} = \mathcal{D}_v^0 g_{(\varrho^C)^{-1}(k'),\ell}$, where $\ell = 1, \ldots, N_q$.

To begin, we consider the time-continuous evolution of $\mathbf{g}(t) \in \mathbb{R}^{N_x^I \times N_q}$ which reads

$$\frac{\varepsilon^2}{c}\dot{\mathbf{g}} = -\varepsilon \mathbf{L}_x \mathbf{g}\left(\mathbf{I} - \frac{1}{2\pi}\mathbb{1}\boldsymbol{w}^\top\right)^\top - \mathbf{d}_x^0(B(\boldsymbol{T}) + \varepsilon^2 \boldsymbol{h})\mathbb{1}^\top \mathbf{Q}_x - \Sigma^t \mathbf{g}, \tag{17}$$

where $B(\boldsymbol{T}\,)$ is computed component-wise. In the above equation, we have used the following short-hand notation $\mathbf{L}_x\mathbf{g} = (\mathbf{D}_x^+ \mathbf{g}\mathbf{Q}_x^- + \mathbf{D}_x^- \mathbf{g}\mathbf{Q}_x^+) + (\mathbf{D}_y^+ \mathbf{g}\mathbf{Q}_y^- + \mathbf{D}_y^- \mathbf{g}\mathbf{Q}_y^+)$, and $\mathbf{d}_x^0(B(\boldsymbol{T}\,) + \varepsilon^2\boldsymbol{h})\mathbb{1}^\top\mathbf{Q}_x = \mathbf{d}_x^0(B(\boldsymbol{T}\,) + \varepsilon^2\boldsymbol{h})\mathbb{1}^\top\mathbf{Q}_x + \mathbf{d}_y^0(B(\boldsymbol{T}\,) + \varepsilon^2\boldsymbol{h})\mathbb{1}^\top\mathbf{Q}_y$. If $\Sigma^a, \Sigma^s \in \mathbb{R}^{N_x^I \times N_x^I}$ such that $(\Sigma^a)_{(\rho(\kappa),\rho(\kappa))} = \sigma_\kappa^a$ and $(\Sigma^s)_{(\rho(\kappa),\rho(\kappa))} = \sigma_\kappa^s$, for $\kappa \in \mathcal{K}^I$, then the total cross section Σ^t is given by $\Sigma^t = \Sigma^a + \Sigma^s$.

We make the following low-rank ansatz for $\mathbf{g}$

$$\mathbf{g}(t) \approx \mathbf{X}(t)\mathbf{S}(t)\mathbf{V}(t)^\top,$$

where $\mathbf{X}(t) \in \mathbb{R}^{N_x^I \times r}$, $\mathbf{V}(t) \in \mathbb{R}^{N_q \times r}$ are orthonormal and $\mathbf{S}(t) \in \mathbb{R}^{r \times r}$ is invertible. The parallel BUG update scheme for (17) can be derived by following the steps outlined in Section 2.2 with $\mathbf{F}(t, \mathbf{X}\mathbf{S}\mathbf{V}^\top) = -\varepsilon \mathbf{L}_x \mathbf{X}\mathbf{S}\mathbf{V}^\top\left(\mathbf{I} - \frac{1}{2\pi}\mathbb{1}\boldsymbol{w}^\top\right)^\top - \mathbf{d}_x^0(B(\boldsymbol{T}) + \varepsilon^2\boldsymbol{h})\mathbb{1}^\top\mathbf{Q}_x - \Sigma^t\mathbf{X}\mathbf{S}\mathbf{V}^\top$. From Theorem 3.1 we know that a crucial step in showing the AP property for the full-rank macro–micro scheme is that, in the limit $\varepsilon \to 0$, we get

$$\mathbf{g}^{n+1} = -(\Sigma^t)^{-1}\mathbf{d}_x^0 B(\boldsymbol{T}^n)\mathbb{1}^\top\mathbf{Q}_x.$$

Thus, for the low-rank parallel BUG scheme to be AP, $(\Sigma^t)^{-1}\mathbf{d}_x^0 B(\boldsymbol{T}\,)$ must be in the range space of $\mathbf{X}^{n+1}$ at time t_{n+1} while $\mathbb{1}^\top\mathbf{Q}_x$ must be in the range space of $\mathbf{V}^{n+1}$. It can be shown that $(\Sigma^t)^{-1}\mathbf{d}_x^0 B(\boldsymbol{T}\,) \in \text{range}(\hat{\mathbf{X}})$ and $\mathbb{1}^\top\mathbf{Q}_x \in \text{range}(\hat{\mathbf{V}})$ (see Theorem 4.1). However, due to the truncation step of the parallel BUG integrator, the range space of the augmented basis $\hat{\mathbf{X}}$ and $\hat{\mathbf{V}}$ need not be preserved in $\mathbf{X}^{n+1}$, $\mathbf{V}^{n+1}$. In general, this also holds for the class of rank-adaptive BUG integrators (Ceruti, Kusch, et al. 2022, 2024), which augment and truncate the basis up to a given tolerance. Based on the conservative truncation proposed in Einkemmer, Ostermann, et al.

(2023), a mitigation tactic was proposed in Frank et al. (2025). The basis vectors $(\Sigma^t)^{-1}\mathbf{d}_x^0 B(\boldsymbol{T}\ )$ and $\mathbb{1}^\top \mathbf{Q}_x$ are augmented to the updated factors $\hat{\mathbf{X}}$ and $\hat{\mathbf{V}}$ to ensure that the sequential S-step captures the $\varepsilon \to 0$ information. This is sufficient since the S-step determines the dynamics of the problem. Finally, a conservative truncation strategy is used to ensure that the truncation step preserves the range space of the augmented basis. This guarantees that the resulting scheme is AP (Frank et al. 2025, Theorem 4.5). However, such a technique cannot be used for the parallel BUG integrator since the dynamics capturing the $\varepsilon \to 0$ information is not determined by the augmented basis $\hat{\mathbf{X}}$ and $\hat{\mathbf{V}}$ of the parallel BUG integrator. Thus, we propose the following modifications to the parallel BUG integrator to derive a low-rank AP scheme for the thermal radiative transfer equations.

For the initial rank-r_n data $\boldsymbol{T}^n$, $\boldsymbol{h}^n$, $\mathbf{X}^n$, $\mathbf{S}^n$ and $\mathbf{V}^n$ at time t_n the low-rank factors are updated in four steps:

1. **Pre-augmentation**: The spatially Discretized gradient $\frac{1}{\sigma^t}\nabla_{\boldsymbol{x}} B(T)$ at time t_n is augmented to the spatial basis $\mathbf{X}^n$ and Ω to the angular basis $\mathbf{V}^n$. That is, we set $\mathbf{X}^n_{\text{aug}}$ as an orthonormal basis of $\left[(\Sigma^t)^{-1}\mathbf{d}_x^0 B(\boldsymbol{T}^n), (\Sigma^t)^{-1}\mathbf{d}_y^0 B(\boldsymbol{T}^n), \mathbf{X}^n\right]$ and $\mathbf{V}^n_{\text{aug}}$ as an orthonormal basis of $\left[\mathbf{Q}_x\mathbb{1}, \mathbf{Q}_y\mathbb{1}, \mathbf{V}^n\right]$. Note that to satisfy $\langle g\rangle = 0$, $\mathbf{V}^n_{\text{aug}}$ is determined such that $(\mathbf{V}^n_{\text{aug}})^\top \boldsymbol{w} = 0$ component-wise. Then, we project the coefficient matrix onto the augmented basis, i.e. we set $\mathbf{S}^n_{\text{aug}} = \mathbf{X}^{n,\top}_{\text{aug}}\mathbf{X}^n\mathbf{S}^n\mathbf{V}^{n,\top}\mathbf{V}^n_{\text{aug}}$. The new initial rank is denoted by $\tilde{r}_n = r_n + 2$. *Note that the subscript* "aug" *is dropped in the rest of the paper and with abuse of notation we denote low-rank factors by* $\mathbf{X}^n$, $\mathbf{V}^n$, *and* $\mathbf{S}^n$.
2. **Parallel update**: **K-step**: For $\mathbf{K}^n = \mathbf{X}^n\mathbf{S}^n \in \mathbb{R}^{N_x^I \times \tilde{r}_n}$ update from t_n to $t_{n+1} = t_n + \Delta t$

$$\begin{aligned}\frac{\varepsilon^2}{c\Delta t}(\mathbf{K}^{n+1} - \mathbf{K}^n) = -\varepsilon\mathbf{L}_{\boldsymbol{x}}\mathbf{K}^n\mathbf{V}^{n,\top}\left(\mathbf{I} - \frac{1}{2\pi}\mathbb{1}\boldsymbol{w}^\top\right)^\top\mathbf{V}^n - \mathbf{d}_{\boldsymbol{x}}^0(B(\boldsymbol{T}^n)\\ +\varepsilon^2\boldsymbol{h}^n)\mathbb{1}^\top\mathbf{Q}_{\boldsymbol{x}}\mathbf{V}^n - \Sigma^t\mathbf{K}^{n+1}.\end{aligned} \tag{18}$$

Determine $\hat{\mathbf{X}} = (\mathbf{X}^n, \tilde{\mathbf{X}}^{n+1}) \in \mathbb{R}^{N_x^I \times 2\tilde{r}_n}$ and $\tilde{\mathbf{S}}^K = \tilde{\mathbf{X}}^{n+1,\top}\mathbf{K}^{n+1}$ as described in Section 2.2.

L-step: For $\mathbf{L}^n = \mathbf{V}^n\mathbf{S}^{n,\top} \in \mathbb{R}^{N_q \times \tilde{r}_n}$ update from t_n to $t_{n+1} = t_n + \Delta t$

$$\begin{aligned}\frac{\varepsilon^2}{c\Delta t}(\mathbf{L}^{n+1} - \mathbf{L}^n) = -\varepsilon\left(\mathbf{I} - \frac{1}{2\pi}\mathbb{1}\boldsymbol{w}^\top\right)\mathbf{L}^n\mathbf{X}^{n,\top}\mathbf{L}_{\mathbf{x}}^\top\mathbf{X}^n\\ -\mathbf{Q}_{\mathbf{x}}\mathbb{1}(B(\mathbf{T}^n) + \varepsilon^2\boldsymbol{h}^n)^\top(\mathbf{d}_{\mathbf{x}}^0)^\top\mathbf{X}^n - \mathbf{L}^{n+1}\mathbf{X}^{n,\top}\boldsymbol{\Sigma}^t\mathbf{X}^n.\end{aligned} \tag{19}$$

Determine $\hat{\mathbf{V}} = (\mathbf{V}^n, \tilde{\mathbf{V}}^{n+1}) \in \mathbb{R}^{N_q \times 2\tilde{r}_n}$ such that $\tilde{\mathbf{V}}^{n+1,\top}\boldsymbol{w} = 0$ and store the matrix $\tilde{\mathbf{S}}^L = \mathbf{L}^{n+1,\top}\tilde{\mathbf{V}}^{n+1}$ as described in Section 2.2

S-step: We update from t_n to $t_{n+1} = t_n + \Delta t$

$$\begin{aligned}\frac{\varepsilon^2}{c\Delta t}\left(\overline{\mathbf{S}}^{n+1} - \mathbf{S}^n\right) = &-\varepsilon \mathbf{X}^{n,\top}\mathbf{L}_x\mathbf{X}^n\mathbf{S}^n\mathbf{V}^{n,\top}\left(\mathbf{I} - \frac{1}{2\pi}\mathbb{1}\mathbf{w}^\top\right)^\top\mathbf{V}^n \\ &-\mathbf{X}^{n,\top}\mathbf{d}_x^0(B(\boldsymbol{T}^n) + \varepsilon^2\boldsymbol{h}^n)\mathbb{1}^\top\mathbf{Q}_x\mathbf{V}^n - \mathbf{X}^{n,\top}\boldsymbol{\Sigma}^t\mathbf{X}^n\overline{\mathbf{S}}^{n+1}.\end{aligned} \tag{20}$$

3. **Augmentation**: Perform the augmentation of the coefficient matrix, i.e. set $\hat{\mathbf{S}}$ to be

$$\hat{\mathbf{S}} = \begin{bmatrix} \overline{\mathbf{S}}^{n+1} & \tilde{\mathbf{S}}^L \\ \tilde{\mathbf{S}}^K & \mathbf{0} \end{bmatrix}.$$

4. **Conservative truncation**: A conservative truncation strategy, similar to the one used in Frank et al. (2025); Einkemmer, Ostermann, et al. (2023) is used to truncate the augmented basis while preserving the pre-augmented basis vectors at the next time step. A brief overview of the conservative truncation step has been added to Appendix A.

After the truncation step, we set the solution at t_{n+1} as $\mathbf{g}^{n+1} = \mathbf{X}^{n+1}\mathbf{S}^{n+1}\mathbf{V}^{n+1,\top}$ with rank $1 \leq r_{n+1} < 2\tilde{r}_n$. The update for h and T remain the same as (11) with the modification that $g^{n+1}_{\kappa,\ell} = (\mathbf{X}^{n+1}\mathbf{S}^{n+1}\mathbf{V}^{n+1,\top})_{\varrho(\kappa),\ell}$, for $\kappa \in \mathcal{K}^I$, $\ell = 1, \ldots, N_q$.

Remark 3. The macro–micro parallel BUG scheme is locally conservative, satisfying the discrete conservation law (12) with $g^{n+1}_{\kappa,\ell} = (\mathbf{X}^{n+1}\mathbf{S}^{n+1}\mathbf{V}^{n+1,\top})_{\varrho^C(\kappa),\ell}$, where $\kappa \in \mathcal{K}^C$.

4.1. Boundary conditions

An open question in dynamical low-rank approximation is the efficient implementation of boundary conditions. To impose boundary conditions, let us collect all spatial indices that lie on the boundary in the set $\mathcal{K}^I_{\mathrm{B}} := \{(\alpha,\beta) \in \mathcal{K}^I | (x_\alpha, y_\beta) \in \partial\mathcal{D}\}$ with $N_B := |\mathcal{K}^I_{\mathrm{B}}|$ boundary cells. Defining the bijective index map $\varrho^I_B : \mathcal{K}^I_{\mathrm{B}} \to \{1, \ldots, N_B\}$, we can define the solution on the boundary as $\tilde{\mathbf{g}} \in \mathbb{R}^{N_B \times N_q}$ with elements $\tilde{g}_{k\ell} = g_{\varrho^I_{\mathrm{B}}(\kappa),\ell}$ where $k \in \{1, \ldots, N_B\}$, $\kappa \in \mathcal{K}^I_{\mathrm{B}}$. Vise-versa, we have $g_{\kappa\ell} = \tilde{g}_{(\varrho^I_{\mathrm{B}})^{-1}(k),\ell}$. Now, to impose reflective-transmitive boundary conditions, we define

$$\hat{g}_{k\ell} = \begin{cases} \rho\tilde{g}^{n+1}_{k\ell'} - (1-\rho)\varepsilon h^n_{(\varrho^I_{\mathrm{B}})^{-1}(k)}, & \text{if } \boldsymbol{n}_k \cdot \boldsymbol{\Omega}_\ell < 0 \\ \tilde{g}^{n+1}_{k\ell}, & \text{if } \boldsymbol{n}_k \cdot \boldsymbol{\Omega}_\ell \geq 0 \end{cases}. \tag{21}$$

where $\boldsymbol{n}_k$ is the outward-pointing normal at position $\boldsymbol{x}_{(\varrho^I_{\mathrm{B}})^{-1}(k)}$ and $\boldsymbol{\Omega}_{\ell'}$ is the reflection of $\boldsymbol{\Omega}_\ell$ along $\boldsymbol{n}_k$. The value of $h^n_{(\varrho^I_{\mathrm{B}})^{-1}(k)}$ is interpolated at the boundary point. We note that $\tilde{\mathbf{g}}$ in (21) can be computed efficiently by restricting $\mathbf{X}^{n+1}$ to boundary points from ghost cells. Lastly, it remains to *efficiently* impose $\hat{\mathbf{g}} \in \mathbb{R}^{N_B \times N_q}$ on the low-rank factorized solution, which we do after the time update of the parallel integrator. That is, we manipulate $\mathbf{g}^{n+1} = \mathbf{X}^{n+1}\mathbf{S}^{n+1}\mathbf{V}^{n+1,\top}$ such that $g^{n+1}_{\kappa\ell} \equiv \hat{g}_{\varrho^I_{\mathrm{B}}(\kappa),\ell}$ for all $\kappa \in \mathcal{K}^I_{\mathrm{B}}$ without having to compute and store $\mathbf{g}^{n+1}$. To apply boundary conditions efficiently, we define $\hat{\mathbf{K}} = \hat{\mathbf{g}}\mathbf{V}^{n+}1 \in \mathbb{R}^{N_B \times r}$ and $\overline{\mathbf{K}} \in \mathbb{R}^{N_x \times r}$ such that $\overline{K}_{\kappa\ell} = \hat{K}_{\varrho^I_{\mathrm{B}}(\kappa),\ell}$ for $\kappa \in \mathcal{K}^I_{\mathrm{B}}$ and $\overline{K}_{j\ell} = \sum_i X_{ji}S_{i\ell}$ for $j \notin \mathcal{K}^I_{\mathrm{B}}$. Lastly, the basis $\mathbf{X}^{n+1}$ and coefficient $\mathbf{S}^{n+1}$ are recomputed as a QR decomposition of $\overline{\mathbf{K}}$, giving the factorized solution at time $n+1$ with reflective-transmitive boundary values imposed efficiently.

Note that in an abuse of notation, we did not define an intermediate low-rank solution for the step in between the parallel integrator and imposing boundary conditions. Instead, to simplify notation, we recycle the notation of $\mathbf{g}^{n+1} = \mathbf{X}^{n+1}\mathbf{S}^{n+1}\mathbf{V}^{n+1,\top}$. We also note that the above strategy does not impose boundary conditions exactly, similar to the projected boundary conditions, for example, used in (Kusch et al. 2022, Section 4) or Sapsis and Lermusiaux (2009). Alternatively, boundary conditions can be imposed exactly through an augmentation of the directional basis as is done for the projector–splitting (Lubich and Oseledets 2014) integrator in Hu and Wang (2022). However, we found in our numerical experiment that an approximate imposition through a projection is sufficient to obtain accurate results. Thus, to avoid a further increase in the computational cost of the method, we impose boundary conditions only through a projection.

4.2. AP property

Theorem 4.1. *The macro–micro parallel BUG scheme for the thermal radiative transfer equation is asymptotic–preserving. That is, in the limit* $\varepsilon \to 0$ *the scheme preserves the discrete Rosseland diffusion equation*

$$\begin{aligned} &\frac{c_\nu}{\Delta t}\left(\boldsymbol{T}^{n+1} - \boldsymbol{T}^n\right) + \frac{2\pi}{c\Delta t}\left(\boldsymbol{B}^{n+1} - \boldsymbol{B}^n\right) \\ &= \frac{2\pi}{3}\left[\mathbf{D}^0_x\left((\Sigma^t)^{-1}\mathbf{d}^0_x\boldsymbol{B}^n\right) + \mathbf{D}^0_y\left((\Sigma^t)^{-1}\mathbf{d}^0_y\boldsymbol{B}^n\right)\right]. \end{aligned}$$

This is a 5-point centered difference discretization for updating the diffusion equation (*4*) *on a staggered grid with an explicit time discretization.*

Proof. As $\varepsilon \to 0$, since $\tilde{\mathbf{S}}^K = \tilde{\mathbf{X}}^{n+1,\top}\mathbf{K}^{n+1}$, we get from the K-step (18)

$$\tilde{\mathbf{S}}^K = -\tilde{\mathbf{X}}^{n+1,\top}(\Sigma^t)^{-1}\Big(\mathbf{d}_x^0 B(\boldsymbol{T})\mathbb{1}^\top \mathbf{Q}_x + \mathbf{d}_y^0 B(\boldsymbol{T})\mathbb{1}^\top \mathbf{Q}_y\Big)\mathbf{V}^n.$$

Similarly, as $\varepsilon \to 0$ in the L-step (19) we get

$$(\mathbf{X}^{n,\top}\Sigma^t\mathbf{X}^n)\tilde{\mathbf{S}}^L = -\mathbf{X}^{n,\top}\Big(\mathbf{d}_x^0 B(\boldsymbol{T})\mathbb{1}^\top \mathbf{Q}_x + \mathbf{d}_y^0 B(\boldsymbol{T})\mathbb{1}^\top \mathbf{Q}_y\Big)\tilde{\mathbf{V}}^{n+1}.$$

By construction, $(\Sigma^t)^{-1}\mathbf{d}_x^0 B(\boldsymbol{T}^n), (\Sigma^t)^{-1}\mathbf{d}_y^0 B(\boldsymbol{T}^n) \in \text{range}(\mathbf{X}^n)$ which implies for $\nu \in \mathcal{J}_{\boldsymbol{x}}$

$$\mathbf{X}^{n,\top}\mathbf{d}_\nu^0 B(\boldsymbol{T}^n) = \mathbf{X}^{n,\top}\Sigma^t\mathbf{X}^n\mathbf{X}^{n,\top}(\Sigma^t)^{-1}\mathbf{d}_\nu^0 B(\boldsymbol{T}^n),$$

and thus if we assume that $(\mathbf{X}^{n,\top}\Sigma^t\mathbf{X}^n)$ has full rank

$$\tilde{\mathbf{S}}^L = -\mathbf{X}^{n,\top}(\Sigma^t)^{-1}\Big(\mathbf{d}_x^0 B(\boldsymbol{T})\mathbb{1}^\top \mathbf{Q}_x + \mathbf{d}_y^0 B(\boldsymbol{T})\mathbb{1}^\top \mathbf{Q}_y\Big)\tilde{\mathbf{V}}^{n+1}.$$

From the S-step (20) we get, as $\varepsilon \to 0$,

$$\overline{\mathbf{S}}^{n+1} = -\mathbf{X}^{n,\top}(\Sigma^t)^{-1}\Big(\mathbf{d}_x^0 B(\boldsymbol{T})\mathbb{1}^\top \mathbf{Q}_x + \mathbf{d}_y^0 B(\boldsymbol{T})\mathbb{1}^\top \mathbf{Q}_y\Big)\mathbf{V}^n.$$

Then,

$$\begin{aligned}\hat{\mathbf{X}}\hat{\mathbf{S}}\hat{\mathbf{V}}^\top &= \begin{bmatrix}\mathbf{X}^n & \tilde{\mathbf{X}}^n\end{bmatrix}\begin{bmatrix}\overline{\mathbf{S}}^{n+1} & \tilde{\mathbf{S}}^L \\ \tilde{\mathbf{S}}^K & \mathbf{0}\end{bmatrix}\begin{bmatrix}\mathbf{V}^{n,\top} \\ \tilde{\mathbf{V}}^{n,\top}\end{bmatrix} \\ &= -\mathbf{X}^n\mathbf{X}^{n,\top}(\boldsymbol{\Sigma}^t)^{-1}\Big(\mathbf{d}_x^0 B(\boldsymbol{T})\mathbb{1}^\top \mathbf{Q}_x + \mathbf{d}_y^0 B(\boldsymbol{T})\mathbb{1}^\top \mathbf{Q}_y\Big)\hat{\mathbf{V}}^n\hat{\mathbf{V}}^{n,\top} \\ &\quad -\tilde{\mathbf{X}}^{n+1}\tilde{\mathbf{X}}^{n+1,\top}(\boldsymbol{\Sigma}^t)^{-1}\Big(\mathbf{d}_x^0 B(\boldsymbol{T})\mathbb{1}^\top \mathbf{Q}_x + \mathbf{d}_y^0 B(\boldsymbol{T})\mathbb{1}^\top \mathbf{Q}_y\Big)\mathbf{V}^n\mathbf{V}^{n,\top}.\end{aligned}$$

Since $\mathbf{Q}_x\mathbb{1}, \mathbf{Q}_y\mathbb{1} \in \text{range}(\mathbf{V}^n)$ and $\mathbf{Q}_x\mathbb{1}, \mathbf{Q}_y\mathbb{1} \in \text{range}(\hat{\mathbf{V}})$, we get

$$\begin{aligned}\hat{\mathbf{X}}\hat{\mathbf{S}}\hat{\mathbf{V}}^\top &= -\mathbf{X}^n\mathbf{X}^{n,\top}(\boldsymbol{\Sigma}^t)^{-1}\Big(\mathbf{d}_x^0 B(\boldsymbol{T})\mathbb{1}^\top \mathbf{Q}_x + \mathbf{d}_y^0 B(\boldsymbol{T})\mathbb{1}^\top \mathbf{Q}_y\Big) \\ &\quad -\tilde{\mathbf{X}}^{n+1}\tilde{\mathbf{X}}^{n+1,\top}(\boldsymbol{\Sigma}^t)^{-1}\Big(\mathbf{d}_x^0 B(\boldsymbol{T})\mathbb{1}^\top \mathbf{Q}_x + \mathbf{d}_y^0 B(\boldsymbol{T})\mathbb{1}^\top \mathbf{Q}_y\Big) \\ &= -(\boldsymbol{\Sigma}^t)^{-1}\Big(\mathbf{d}_x^0 B(\boldsymbol{T})\mathbb{1}^\top \mathbf{Q}_x + \mathbf{d}_y^0 B(\boldsymbol{T})\mathbb{1}^\top \mathbf{Q}_y\Big),\end{aligned}$$

where we get the last equality since $(\Sigma^t)^{-1}\mathbf{d}_x^0 B(\boldsymbol{T}), (\Sigma^t)^{-1}\mathbf{d}_y^0 B(\boldsymbol{T}) \in \text{range}(\hat{\mathbf{X}})$.

It was shown in (Frank et al. 2025, Theorem 4.5) that the conservative truncation preserves the range space of the augmented spatial and angular basis. Thus, as $\varepsilon \to 0$ we get

$$\mathbf{g}^{n+1} = \mathbf{X}^{n+1}\mathbf{S}^{n+1}\mathbf{V}^{n+1,\top} = -(\boldsymbol{\Sigma}^t)^{-1}\Big(\mathbf{d}_x^0 B(\boldsymbol{T})\mathbb{1}^\top \mathbf{Q}_x + \mathbf{d}_y^0 B(\boldsymbol{T})\mathbb{1}^\top \mathbf{Q}_y\Big).$$

The rest of the proof follows on the lines of Theorem 3.1 with $g_{\kappa,\ell}^{n+1} = (\mathbf{g}^{n+1})_{\varrho(\kappa),\ell}$, for $\kappa \in \mathcal{K}^I$ and $\ell = 1, \ldots, N_q$. ■

4.3. Energy stability

Theorem 4.2. *For a given spatial grid size $\Delta x, \Delta y$, let the step size Δt satisfy the CFL condition (16) for all $\Omega_x^\ell, \Omega_y^\ell \neq 0$. Then, the proposed macro–micro parallel BUG scheme is energy stable, i.e.,*

$$e^{n+1} \leq e^n,$$

where the energy is defined as

$$e^n = \left|\left| \frac{1}{c} B^n + \frac{\varepsilon^2}{c} h^n \right|\right|^2 + \frac{1}{2\pi} \left|\left| \frac{\varepsilon}{c} \mathbf{X}^n \mathbf{S}^n \mathbf{V}^{n,\top} \right|\right|^2 + \frac{2}{5} \left|\left| \frac{\sqrt{a c_\nu}}{2\pi} (T^n)^{5/2} \right|\right|^2.$$

Remark 4. The proof of this theorem is based on the proof of Theorem 3.2 and the energy stability for the AP augmented BUG integrator for thermal radiative transfer equations in slab geometry in (Frank et al. 2025, Theorem 4.6). Note that energy stability in (Frank et al. 2025, Theorem 4.6) is for an associated linearized problem and thus the energy stability (Theorem 3.2) of the fully nonlinear problem (1) proved in this paper is a key ingredient.

The extension to the higher dimensional setting (1) and the change of angular discretization don't affect the stability of the augmented BUG integrator. Let $\hat{\mathbf{X}}_a$ and $\hat{\mathbf{V}}_a$ denote the orthonormal basis obtained after the K-step and the L-step of the AP-modified augmented BUG integrator (Frank et al. 2025) with the first r columns being replaced by $\mathbf{X}^n$ and $\mathbf{V}^n$, respectively. If $\tilde{\mathbf{S}}^n := \hat{\mathbf{X}}_a^\top \mathbf{X}^n \mathbf{S}^n \mathbf{V}^{n,\top} \hat{\mathbf{V}}_a = \hat{\mathbf{X}}_a^\top \mathbf{g}^n \hat{\mathbf{V}}_a$, then the S-step of the AP-modified augmented BUG scheme is given by

$$\begin{aligned} \frac{\varepsilon^2}{c\Delta t} \left(\hat{\mathbf{S}}_a^{n+1} - \tilde{\mathbf{S}}^n \right) = &-\varepsilon \hat{\mathbf{X}}_a^\top \mathbf{L}_{\mathbf{x}} \hat{\mathbf{X}}_a \tilde{\mathbf{S}}^n \hat{\mathbf{V}}_a^\top \left(\mathbf{I} - \frac{1}{2\pi} \mathbb{1} \boldsymbol{w}^\top \right)^\top \hat{\mathbf{V}}_a \\ &- \hat{\mathbf{X}}_a^\top \mathbf{d}_{\mathbf{x}}^0 (B(\boldsymbol{T}^n) + \varepsilon^2 \boldsymbol{h}^n) \mathbb{1}^\top \mathbf{Q}_{\mathbf{x}} \hat{\mathbf{V}}_a - \hat{\mathbf{X}}_a^\top \boldsymbol{\Sigma}^t \hat{\mathbf{X}}_a \hat{\mathbf{S}}_a^{n+1}. \end{aligned}$$

Then the solution to (17) at time t_{n+1} (before truncation) is given by $\hat{\mathbf{g}}_a^{n+1} = \hat{\mathbf{X}}_a \hat{\mathbf{S}}_a^{n+1} \hat{\mathbf{V}}_a^\top$. multiplying the S-step from left and right by $\hat{\mathbf{X}}_a^\top$ and $\hat{\mathbf{V}}_a$, respectively, we get

$$\begin{aligned} \frac{\varepsilon^2}{c\Delta t} \left(\hat{\mathbf{g}}_a^{n+1} - \mathbf{g}^n \right) = &-\varepsilon \mathbf{P}^{\hat{\mathbf{X}}_a} \mathbf{L}_{\boldsymbol{x}} \mathbf{g}^n \left(\mathbf{I} - \frac{1}{2\pi} \mathbb{1} \boldsymbol{w}^\top \right)^\top \mathbf{P}^{\hat{\mathbf{V}}_a} \\ &- \mathbf{P}^{\hat{\mathbf{X}}_a} \mathbf{d}_{\mathbf{x}}^0 (B(\boldsymbol{T}^n) + \varepsilon^2 \boldsymbol{h}^n) \mathbb{1}^\top \mathbf{Q}_{\mathbf{x}} \mathbf{P}^{\hat{\mathbf{V}}_a} - \mathbf{P}^{\hat{\mathbf{X}}_a} \boldsymbol{\Sigma}^t \hat{\mathbf{g}}_a^{n+1}, \end{aligned}$$

where $\mathbf{P}^{\hat{\mathbf{X}}_a} := \hat{\mathbf{X}}_a \hat{\mathbf{X}}_a^\top$, $\mathbf{P}^{\hat{\mathbf{V}}_a} := \hat{\mathbf{V}}_a \hat{\mathbf{V}}_a^\top$, and $\hat{\mathbf{X}}_a \tilde{\mathbf{S}}^n \hat{\mathbf{V}}_a^\top = \mathbf{g}^n$ since $\hat{\mathbf{X}}_a$ spans $\mathbf{X}^n$ and $\hat{\mathbf{V}}_a$ spans $\mathbf{V}^n$. Now, from (Frank et al.2025, Theorem 4.6), we get an expression similar to (B14) with $\mathbf{g}^{n+1}$ replaced by $\hat{\mathbf{g}}_a^{n+1}$. Further, following the steps from Theorem 3.2 we can show that the scheme with the augmented solution $\hat{\mathbf{g}}_a^{n+1}$ is energy stable for the nonlinear closure given by the Stefan-Boltzmann law in the sense of Theorem 3.2. Let $\mathbf{g}_a^{n+1} = \mathbf{X}_a^{n+1}\mathbf{S}_a^{n+1}\mathbf{V}_a^{n+1,\top}$ denote the solution at time t_{n+1} after truncation. Since the truncation step does not increase the norm of the solution, we conclude that the macro–micro augmented BUG scheme is energy stable.

The discussion in (Ceruti, Kusch, et al.2024, Section 3.2) shows that if $\mathbf{g}_p^{n+1} = \mathbf{X}_p^{n+1}\mathbf{S}_p^{n+1}\mathbf{V}_p^{n+1,\top}$ is the solution of the parallel BUG at time t_{n+1} then $\left|\left|\mathbf{g}_p^{n+1}\right|\right| \leq \left|\left|\mathbf{g}_a^{n+1}\right|\right|$. Thus, the macro–micro parallel BUG scheme is energy stable for the nonlinear closure given by the Stefan-Boltzmann law.

5. Numerical experiments

This section presents numerical examples to verify the theoretical properties of the integrators and demonstrate their efficiency.[1] In all examples, the initial condition is specified for the material temperature while the particle density is assumed to be at an equilibrium. That is, the initial particle density is set as $f_I(\boldsymbol{x}, \boldsymbol{\Omega}) = \frac{ac}{2\pi} T_I(\boldsymbol{x})^4$. The truncation tolerance, ϑ, of the macro–micro parallel BUG scheme is set as $\vartheta = 10^{-2}||\boldsymbol{\Sigma}||_2$ in all experiments, where $\boldsymbol{\Sigma}$ contains the singular values of the coefficient matrix. We are mainly interested in the case where the absorption effects are dominant and thus we set $\sigma^s = 0$ in all the test cases. We define the radiation temperature as $T_{\text{rad}} := (2\pi(B(T) + \varepsilon^2 h)/ac)^{1/4}$ and the following conserved quantity

$$q^n := \sum_{\alpha,\, \beta \in \mathcal{K}_C} \left(\frac{2\pi}{c} \left(B(T_{\alpha\beta}) + \varepsilon^2 h_{\alpha\beta} \right) + c_\nu T_{\alpha\beta} \right) \Delta x \Delta y. \tag{22}$$

Throughout this section, we refer to the full-rank macro–micro scheme (11) as the full solver/ integrator, and the corresponding material temperature, scalar flux, and radiation temperatures are denoted by T^{Full}, ϕ^{Full}, and $T_{\text{rad}}^{\text{Full}}$, respectively. The macro–micro parallel BUG scheme described in Section 4 is referred to as the parallel BUG solver/ integrator and T^ϑ, ϕ^ϑ, and T_{rad}^ϑ denote the corresponding material temperature, scalar flux, and radiation temperature, respectively, for a given tolerance ϑ. To study the behavior of our scheme

[1] All codes used to generate the results are openly available in the GitHub repository: https://github.com/chinsp/publication-parallel-AP-DLRA-for-non-linear-TRT.

in the asymptotic limit $\varepsilon \to 0$, we compare our schemes to the numerical solution of the Rosseland equation (4) with (13), which is denoted by T^R.

5.1. AP property

The first test case is set up to study the AP property, energy decay and conservation property of the proposed integrators and uses the parameters described in Ceruti, Frank, et al. (2022). The details are summarized in Table 1. The test case is defined for the spatial domain $\boldsymbol{x} \in [0, 0.002]^2$ with material density $\rho = 0.01$ g cm $^{-3}$ and the temperature is initially distributed as a Gaussian centered at $\boldsymbol{x}_0 = (0.001, 0.001)$, i.e.,

$$\tilde{T}_I(\boldsymbol{x}) = \frac{1}{2\pi\sigma^2} \cdot \exp\left(-\frac{||\boldsymbol{x} - \boldsymbol{x}_0||_2^2}{2\sigma^2}\right),$$

where $\sigma = 10^{-4}$. Furthermore, $T_I(\boldsymbol{x})$ is re-scaled such that the maximum temperature is 80 eV and the cutoff minimum is 0.02 eV, i.e.,

$$T_I(\boldsymbol{x}) = \begin{cases} \dfrac{80}{\max(\tilde{T}_I(\boldsymbol{x}))} \cdot \tilde{T}_I(\boldsymbol{x}), \text{if } \tilde{T}_I(\boldsymbol{x}) \geq 0.02, \\ 0.02, \qquad\qquad \text{otherwise.} \end{cases}$$

The initially distributed particles move in all directions, and as time progresses, they heat the background material. A temperature heat front, traveling outwards from the center of the domain, develops in the material, resulting in further emission of particles. The material temperature at the boundary is kept at a constant temperature of 0.02 eV.

To demonstrate the AP property of the full-rank and parallel BUG integrator we compute the solution at $t_{\text{end}} = 5$ ps for Knudsen numbers $\varepsilon \in \{1, 5 \cdot 10^{-1}, 10^{-1}, 5 \cdot 10^{-2}, 10^{-2}, 10^{-3}, 10^{-4}, 10^{-5}, 10^{-6}, 10^{-7}\}$. Note that simulations with $\varepsilon = 1$ correspond to the kinetic regime while $\varepsilon = 10^{-4}$ correspond to the diffusive regime. The solution of the integrators is compared to the solution of the Rosseland equation at t_{end}. The relative error between the material temperature of both the integrators and the Rosseland equation at t_{end} is plotted in Figure 2(a). We see that as $\varepsilon \to 0$, the solution of the full solver and the parallel BUG solver converge to the Rosseland equation. From Figure 2(b), we see that the solution of the parallel BUG integrator is compressed by over 97% compared to the full solver, where the compression ratio refers to the ratio of the largest rank (except initial rank) of the parallel BUG solver and the maximal possible rank of the full solver. Additionally, from Figure 2(c) we see that energy decays for both the full solver and the parallel BUG solver in the absence of a source term.

The run-time of the full solver and the parallel BUG solver, which generate Figure 2(a), has been stated in Table 2. From the table, we see that the

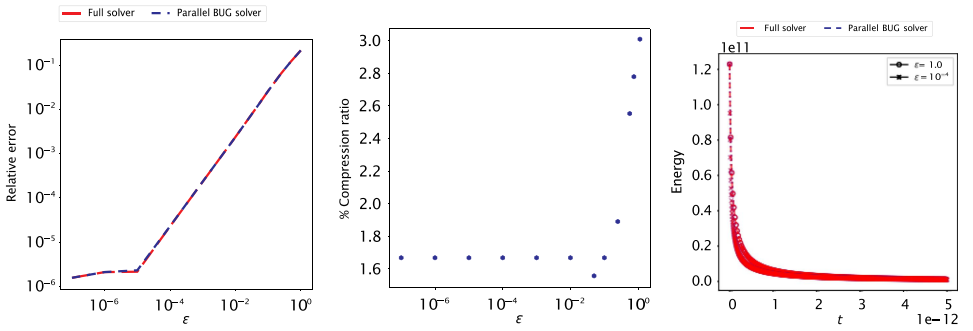

(a) AP property (b) Compression ratio (c) Energy decay over time

Figure 2. Left: Relative error of T^{Full} and T^{ϑ} compared to T^{R}, numerical solution of the Rosseland equation, for $\varepsilon \in \{1, 5 \cdot 10^{-1}, 10^{-1}, 5 \cdot 10^{-2}, 10^{-2}, 10^{-3}, 10^{-4}, 10^{-5}, 10^{-6}, 10^{-7}\}$. Middle: Compression ratio of the low-rank solution with respect to the full-rank solution computed as $r_{\max}/\min(N_x^l, N_q) \times 100$, where $r_{\max}$ is the largest rank of the parallel BUG solver (except initial rank). Right: Energy decay of the full solver and parallel BUG solver for $\varepsilon \in \{1.0, 10^{-4}\}$.

Table 1. Material constants and settings for the Gaussian and Marshak wave test case as given in Ceruti, Frank, et al. (2022).

Number of spatial cells, N_x, N_y	52,52
Quadrature order, q	30
Absorption coefficient, σ^a	$10,799.13607\ \text{cm}^{-1}$
Speed of light, c	$2.99792458 \cdot 10^{10}\ \text{cm s}^{-1}$
Radiation constant, a	$7.565766 \cdot 10^{-15}\ \text{erg cm}^{-3}\ \text{K}^{-4}$
Specific heat, c_ν	$0.831 \cdot 10^{5}\ \text{J g}^{-1}\ \text{K}^{-1}$

Table 2. Run-times of the full solver and the parallel BUG solver for $\varepsilon \in \{1.0, 0.05, 10^{-4}\}$ on the AP property test case 3.3, illustrating the relative computational performance and scalability of the two solvers as the problem transitions across regimes.

	$\varepsilon = 1.0$	$\varepsilon = 0.05$	$\varepsilon = 10^{-4}$
Full solver	3001.34	19070.77	27236.05
Parallel BUG solver	6737.39	42192.17	65438.80
Speed-up	2.24	2.21	2.4

parallel BUG solver roughly halves the simulation time while using only $1.5 - 3\%$ of the total degrees of freedom (rank) (see Figure 2b).

5.1.1. Conservation

To show that the proposed schemes are conservative, we consider a modification of the test case described in this section. The initial temperature distribution is set as

$$T_I(\boldsymbol{x}) = \begin{cases} \dfrac{80}{\max(\tilde{T}_I(\boldsymbol{x}))} \cdot \tilde{T}_I(\boldsymbol{x}), & \text{if } \tilde{T}_I(\boldsymbol{x}) \geq 0.02, \\ 0.0, & \text{otherwise,} \end{cases}$$

and the boundary temperature is given by $T_B = 0$ eV, given any $\hat{\boldsymbol{x}} \in \partial\mathcal{D}$. In addition, to ensure that all particles are contained in the system, we set $\tilde{\sigma}^a = 100 \cdot \sigma^a$, where σ^a is given in Table 1. The other parameters are the same as

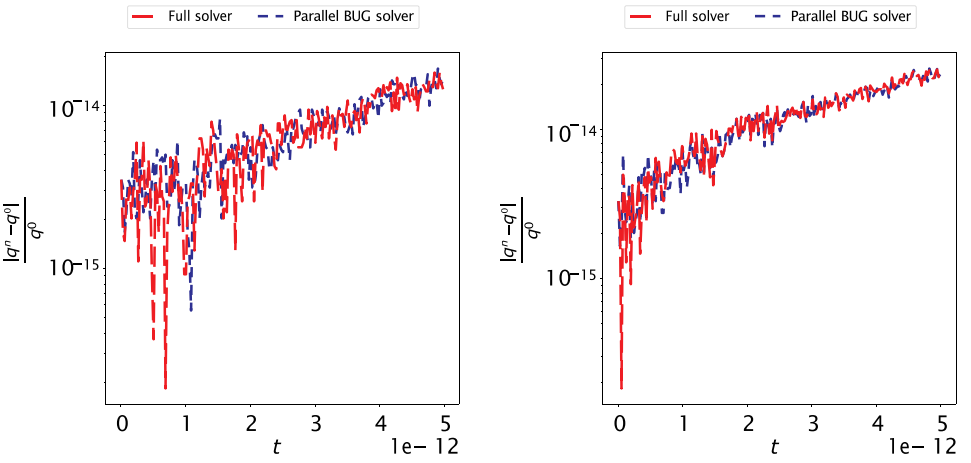

(a) $\varepsilon = 1.0$ (b) $\varepsilon = 10^{-5}$

Figure 3. Relative error of the conserved quantity q^n over the entire simulation for the modified problem.

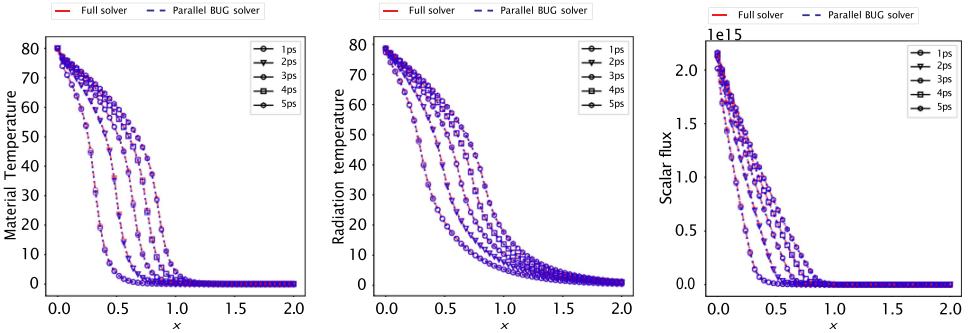

Figure 4. Cross-section of the material temperature, radiation temperature, and scalar flux for the Marshak wave test case at times 1, 2, 3, 4, and 5 ps through $y = 0.001$ for $\varepsilon = 1.0$.

those for the AP property. The relative error of the conserved quantity q^n for $\varepsilon = 1.0$ and $\varepsilon = 10^{-5}$ are plotted in Figure 3 and show that q^n is conserved.

5.2. Marshak wave

The Marshak wave test case is a two-dimensional extension of the test case presented in Ceruti, Frank, et al. (2022) for the one-dimensional thermal radiative transfer equations. The spatial domain and other parameters are the same as AP property test case and are given in Table 1. The initial temperature of the material is 0.02 eV, and a constant temperature source of 80 eV is applied to the left wall, which is switched on at the initial time, while the remaining boundaries are maintained at 0.02 eV.

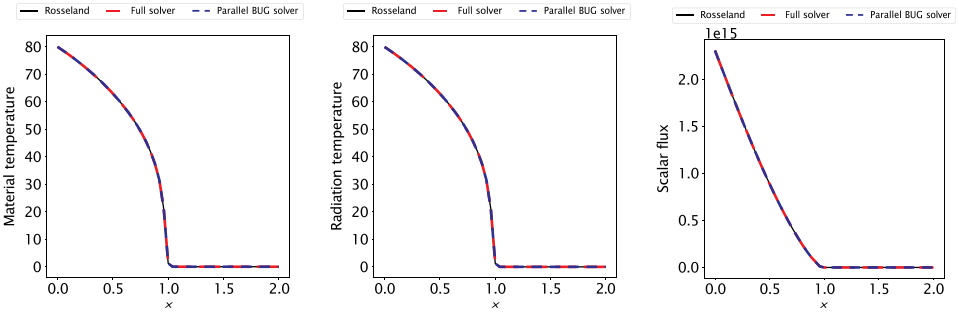

Figure 5. Cross-section of the material temperature, radiation temperature, and scalar flux for the Marshak wave test case at time 5 ps through $y = 0.001$ for the diffusive limit with $\varepsilon = 10^{-4}$.

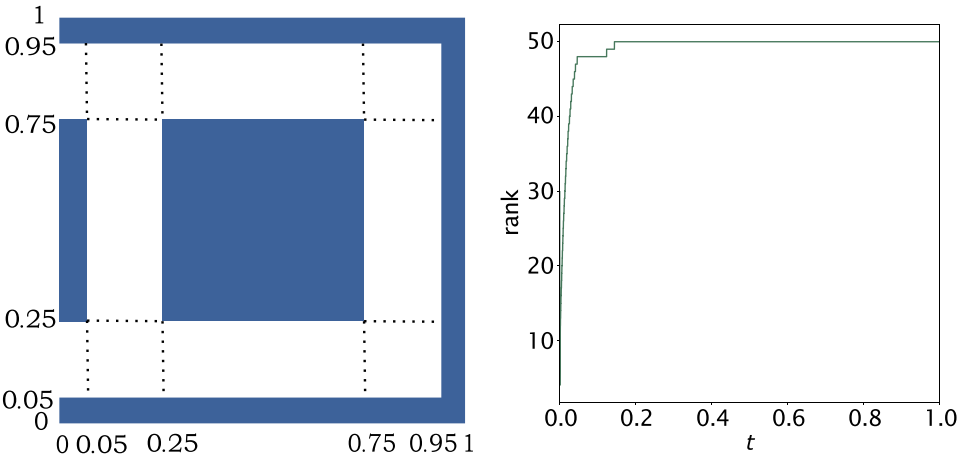

Figure 6. Left: Geometry of the hohlraum as described in McClarren and Hauck (2010). Right: Rank over time for the hohlraum test case with $\vartheta = 10^{-2}$ until 1 ns.

As time progresses, particles stream into the domain from the left wall, and a temperature heat front traveling to the right wall develops. For $\varepsilon = 1.0$, the cross-section of the material temperature and scalar flux through $y = 0.001$ at times $1, 2, 3, 4,$ and 5 ps are plotted in Figure 4. Additionally, for $\varepsilon = 10^{-4}$ we plot the material temperature and scalar flux through $y = 0.001$ at 5 ps for the full solver, parallel BUG solver, and the Rosseland equation in Figure 5. We see that the full solver and parallel BUG solver both accurately capture the Rosseland diffusion limit. Note that the Marshak wave test case has similar run-times as the AP property test case, for varying ε, since they have the same material parameters.

5.3. A Hohlraum problem

Next, we consider a version of the hohlraum test case described in (Bruner 2002; McClarren and Hauck 2010; Li et al. 2024). The test case models a

Table 3. Material constants and settings for the hohlraum test case (McClarren and Hauck 2010).

N_x, N_y	102,102
Quadrature order, q	30
Speed of light, c	29.98 m ns^{-1}
Radiation constant, a	0.01372 GJ cm^{-3} keV^{-4}

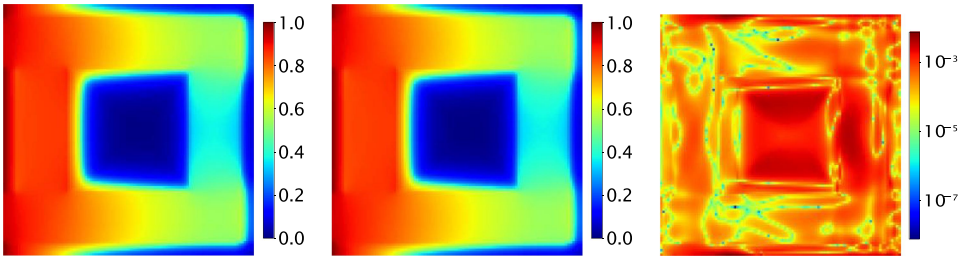

(a) $T^{\text{Full}}_{\text{rad}}$ (b) T^{9}_{rad} (c) $|T^{\text{Full}}_{\text{rad}} - T^{9}_{\text{rad}}|$

Figure 7. Radiation temperature at $t = 1$ ns for the hohlraum test case.

hohlraum for testing inertial confinement fusion in Cartesian coordinates. The problem's geometry and parameters are given in Figure 6 and Table 3, respectively. The blue regions in Figure 6 are pure absorbers with $\sigma^a = 100$ cm^{-1} and $\rho c_\nu = 5.0 \cdot 10^5$ GJ cm^{-3} keV^{-1} and the white region is a pure vacuum with $\sigma^a = 0$ cm^{-1} and $\rho c_\nu = 1.0 \cdot 10^{99}$GJ cm^{-3} keV^{-1}. Note that the absorption coefficient σ^a is kept constant following (Bruner 2002) while in (McClarren and Hauck 2010; Li et al. 2024) the absorption coefficient depends on temperature.

The initial temperature of the entire hohlraum is 10^{-3} keV. The left boundary is heated at a constant temperature of 1 keV, and the right boundary is maintained at 10^{-3} keV. There is an inflow of particles from the left and right boundaries into the hohlraum at equilibrium with the temperature, while the top and bottom boundaries are reflective. As particles stream into the hohlraum, a sharp radiation front develops near the edges of the absorbing block, and a shadow develops behind it. These boundary conditions for the hohlraum have been described in Li et al. (2024), and no analytical solution exists for this problem.

We simulate the hohlraum test case for $\varepsilon = 1.0$ until $t_{\text{end}} = 1$ ns. The material temperature and radiation temperature at t_{end} are plotted in Figures 7 and 8, respectively. We see that the parallel BUG solver approximates the full-rank solution accurately while only requiring 8551s compared to 15,311 s for the full solver. Since the solution has sharp fronts, we expect the solution to have a higher rank compared to the previous test cases. However, we see from Figure 6 that the rank of the parallel BUG solution does not grow beyond 50 despite the maximal rank being much higher.

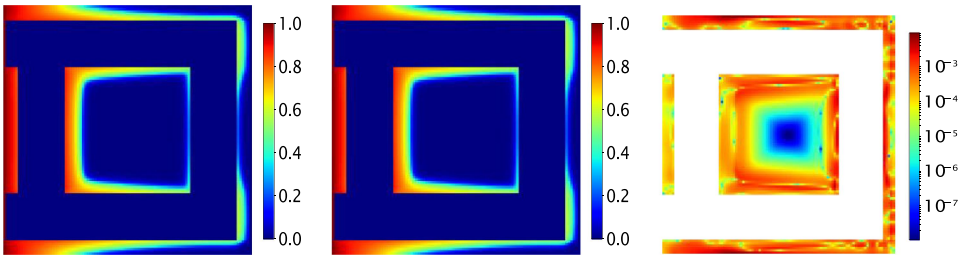

(a) T^{Full} (b) T^{ϑ} (c) $|T^{\text{Full}} - T^{\vartheta}|$

Figure 8. Material temperature at $t = 1$ ns for the hohlraum test case.

6. Conclusions and outlook

In this work, we have proposed a low-rank scheme for the nonlinear thermal radiative transfer equations based on macro–micro decomposition. Th proposed macro–micro parallel BUG scheme is asymptotic–preserving, locally conservative, rank-adaptive, and energy stable for the nonlinear Stefan-Boltzmann closure under a mixed hyperbolic and parabolic CFL condition. In addition, we also propose an efficient algorithm to implement reflection-transmission type boundary conditions for the macro–micro parallel BUG scheme. Several experiments demonstrating the efficacy of the proposed schemes are presented. It is observed that the macro–micro scheme captures the solution to a high degree of accuracy while being computationally and memory efficient.

Authors contributions

CRediT: **Chinmay Patwardhan**: Conceptualization, Formal analysis, Investigation, Methodology, Software, Validation, Visualization, Writing – original draft; **Jonas Kusch**: Conceptualization, Formal analysis, Methodology, Supervision, Writing – review & editing.

Disclosure statement

No potential conflict of interest was reported by the author(s).

Funding

The work of Chinmay Patwardhan was funded by the Deutsche Forschungsgemeinschaft (DFG, German Research Foundation) – Project-ID [258734477 – SFB 1173].

References

Baumann L, Einkemmer L, Klingenberg C, Kusch J. 2024. Energy stable and conservative dynamical low-rank approximation for the Su-Olson problem. SIAM J Sci Comput. 46(2):B137–B158. https://doi.org/10.1137/23M1586215

Bruner TA. 2002. Forms of approximate radiation transport. Sandia National Laboratories. https://doi.org/10.2172/800993

Case KM, Zweifel PF. 1967. Linear transport theory. Addison-Wesley.

Ceruti G, Einkemmer L, Kusch J, Lubich C. 2024. A robust second-order low-rank BUG integrator based on the midpoint rule. Bit Numer Math. 64(3):30–19. https://doi.org/10.1007/s10543-024-01032-x

Ceruti G, Frank M, Kusch J. 2022. Dynamical low-rank approximation for Marshak waves. CRC 1173 Preprint 2022/76. Karlsruhe Institute of Technology.

Ceruti G, Kusch J, Lubich C. 2022. A rank-adaptive robust integrator for dynamical low-rank approximation. Bit Numer Math. 62(4):1149–1174. https://doi.org/10.1007/s10543-021-00907-7

Ceruti G, Kusch J, Lubich C. 2024. A parallel rank-adaptive integrator for dynamical low-rank approximation. SIAM J Sci Comput. 46(3):B205–B228. https://doi.org/10.1137/23M1565103

Ceruti G, Lubich C. 2022. An unconventional robust integrator for dynamical low-rank approximation. Bit Numer Math. 62(1):23–44. https://doi.org/10.1007/s10543-021-00873-0

Coughlin J, Hu J, Shumlak U. 2024. Robust and conservative dynamical low-rank methods for the Vlasov equation via a novel macro-micro decomposition. J Comput Phys. 509: 113055. https://doi.org/10.1016/j.jcp.2024.113055

Ding Z, Einkemmer L, Li Q. 2021. Dynamical low-rank integrator for the linear Boltzmann equation: error analysis in the diffusion limit. SIAM J Numer Anal. 59(4):2254–2285. https://doi.org/10.1137/20M1380788

Einkemmer L, Hu J, Kusch J. 2024. Asymptotic-preserving and energy stable dynamical low-rank approximation. SIAM J Numer Anal. 62(1):73–92. https://doi.org/10.1137/23M1547603

Einkemmer L, Hu J, Wang Y. 2021. An asymptotic-preserving dynamical low-rank method for the multi-scale multi-dimensional linear transport equation. J Comput Phys. 439: 110353–110321. https://doi.org/10.1016/j.jcp.2021.110353

Einkemmer L, Hu J, Ying L. 2021. An efficient dynamical low-rank algorithm for the Boltzmann-BGK equation close to the compressible viscous flow regime. SIAM J Sci Comput. 43(5):B1057–B1080. https://doi.org/10.1137/21M1392772

Einkemmer L, Hu J, Zhang S. 2025. Asymptotic-preserving dynamical low-rank method for the stiff nonlinear Boltzmann equation. Comput Phys. 538:114112. https://doi.org/10.1016/j.jcp.2025.114112

Einkemmer L, Kusch J, Schotthöfer S. 2023. Conservation properties of the augmented basis update & Galerkin integrator for kinetic problems. https://papers.ssrn.com/sol3/papers.cfm?abstract_id=4668132

Einkemmer L, Ostermann A, Scalone C. 2023. A robust and conservative dynamical low-rank algorithm. Comput Phys. 484:112060. https://doi.org/10.1016/j.jcp.2023.112060

Frank M, Kusch J, Patwardhan C. 2025. Asymptotic-preserving and energy stable dynamical low-rank approximation for thermal radiative transfer equations. Multiscale Model Simul. 23(1):278–312. https://doi.org/10.1137/24M1646303

Fu J, Li W, Song P, Wang Y. 2022. An asymptotic-preserving IMEX method for nonlinear radiative transfer equation. J Sci Comput. 92(1):27–35. https://doi.org/10.1007/s10915-022-01870-3

Hu J, Wang Y. 2022. An adaptive dynamical low rank method for the nonlinear Boltzmann equation. J Sci Comput. 92(2):75–24. https://doi.org/10.1007/s10915-022-01934-4

Jang J, Li F, Qiu J-M, Xiong T. 2014. Analysis of asymptotic preserving DG-IMEX schemes for linear kinetic transport equations in a diffusive scaling. SIAM J Numer Anal. 52(4): 2048–2072. https://doi.org/10.1137/130938955

Jin S. 1999. Efficient asymptotic-preserving (AP) schemes for some multiscale kinetic equations. SIAM J Sci Comput. 21(2):441–454. https://doi.org/10.1137/S1064827598334599

Klar A, Schmeiser C. 2001. Numerical passage from radiative heat transfer to nonlinear diffusion models. Math Models Methods Appl Sci. 11(05):749–767. https://doi.org/10.1142/S0218202501001082

Klar A, Siedow N. 1998. Boundary layers and domain decomposition for radiative heat transfer and diffusion equations: applications to glass manufacturing process. Eur J Appl Math. 9(4):351–372. https://doi.org/10.1017/S0956792598003490

Koch O, Lubich C. 2007. Dynamical low-rank approximation. SIAM J Matrix Anal Appl. 29(2):434–454. https://doi.org/10.1137/050639703

Koellermeier J, Krah P, Kusch J. 2024. Macro-micro decomposition for consistent and conservative model order reduction of hyperbolic shallow water moment equations: a study using POD-Galerkin and dynamical low-rank approximation. Adv Comput Math. 50(4): 76–41. https://doi.org/10.1007/s10444-024-10175-y

Küpper K, Frank M, Jin S. 2016. An asymptotic preserving two-dimensional staggered grid method for multiscale transport equations. SIAM J Numer Anal. 54(1):440–461. https://doi.org/10.1137/140999992

Kusch J. 2025. Second-order robust parallel integrators for dynamical low-rank approximation. Bit Numer Math. 65(3):31. https://doi.org/10.1007/s10543-025-01073-w

Kusch J, Ceruti G, Einkemmer L, Frank M. 2022. Dynamical low-rank approximation for Burgers' equation with uncertainty. Int J Uncertain Quantif. 12(5):1–21. https://doi.org/10.1615/Int.J.UncertaintyQuantification.2022039345

Kusch J, Einkemmer L, Ceruti G. 2023. On the stability of robust dynamical low-rank approximations for hyperbolic problems. SIAM J Sci Comput. 45(1):A1–A24. https://doi.org/10.1137/21M1446289

Lemou M, Mieussens L. 2008. A new asymptotic preserving scheme based on micro-macro formulation for linear kinetic equations in the diffusion limit. SIAM J Sci Comput. 31(1):334–368. https://doi.org/10.1137/07069479X

LeVeque RJ. 2002. Finite volume methods for hyperbolic problems. Cambridge texts in applied mathematics. Cambridge University Press.

Levermore CD, Morokoff WJ, Nadiga BT. 1998. Moment realizability and the validity of the Navier-Stokes equations for rarefied gas dynamics. Phys. Fluids. 10(12):3214–3226. https://doi.org/10.1063/1.869849

Lewis EE, Miller WF. 1984. Computational methods of neutron transport. John Wiley and Sons, Inc.

Li W, Liu C, Song P. 2024. Unified gas-kinetic particle method for frequency-dependent radiation transport. J Comput Phys. 498(112663):112663. https://doi.org/10.1016/j.jcp.2023.112663

Lubich C, Oseledets IV. 2014. A projector-splitting integrator for dynamical low-rank approximation. Bit Numer Math. 54(1):171–188. https://doi.org/10.1007/s10543-013-0454-0

McClarren RG, Hauck CD. 2010. Robust and accurate filtered spherical harmonics expansions for radiative transfer. J Comput Phys. 229(16):5597–5614. https://doi.org/10.1016/j.jcp.2010.03.043

Peng Z, McClarren RG. 2021. A high-order/low-order (HOLO) algorithm for preserving conservation in time-dependent low-rank transport calculations. J Comput Phys. 447: 110672. https://doi.org/10.1016/j.jcp.2021.110672

Rosseland S. 1931. Astrophysik auf atomtheoretischer Grundlage. Struktur der Materie in Einzeldarstellungen. Vol. 11. Springer.

Sapsis TP, Lermusiaux PFJ. 2009. Dynamically orthogonal field equations for continuous stochastic dynamical systems. Physica D. 238(23–24):2347–2360. https://doi.org/10.1016/j.physd.2009.09.017

Su B, Olson GL. 1997. An analytical benchmark for non-equilibrium radiative transfer in an isotropically scattering medium. Ann Nucl Energy. 24(13):1035–1055. https://doi.org/10.1016/S0306-4549(96)00100-4

Sun W, Jiang S, Xu K. 2015. An asymptotic preserving unified gas kinetic scheme for gray radiative transfer equations. J Comput Phys. 285:265–279. https://doi.org/10.1016/j.jcp.2015.01.008

Sun W, Jiang S, Xu K. 2017. A multidimensional unified gas-kinetic scheme for radiative transfer equations on unstructured mesh. J Comput Phys. 351:455–472. https://doi.org/10.1016/j.jcp.2017.09.036

Sun W, Jiang S, Xu K, Li S. 2015. An asymptotic preserving unified gas kinetic scheme for frequency-dependent radiative transfer equations. J Comput Phys. 302:222–238. https://doi.org/10.1016/j.jcp.2015.09.002

Uschmajew A, Zeiser A. 2024. Dynamical low-rank approximation of the Vlasov-Poisson equation with piecewise linear spatial boundary. BIT. 64(2):19–26. https://doi.org/10.1007/s10543-024-01019-8

Appendix A: Conservative truncation

In this section, we provide a brief overview of the conservative truncation (Einkemmer, Ostermann, et al. 2023) strategy used to preserve the range space of the basis. Recall that after the pre-augmentation, parallel update, and augmentation steps of the parallel BUG integrator outlined in Section 4, we obtain $\hat{\mathbf{X}} \in \mathbb{R}^{N_x^l \times 2\tilde{r}_n}$, $\hat{\mathbf{V}} \in \mathbb{R}^{N_q \times 2\tilde{r}_n}$, and $\hat{\mathbf{S}} \in \mathbb{R}^{2\tilde{r}_n \times 2\tilde{r}_n}$. To preserve the first m basis vectors of $\hat{\mathbf{X}}$ and $\hat{\mathbf{V}}$, we first construct $\hat{\mathbf{K}}^{n+1} = \hat{\mathbf{X}}\hat{\mathbf{S}}$, and then split $\hat{\mathbf{K}}^{n+1} = \begin{bmatrix} \hat{\mathbf{K}}_{\text{ap}} & \hat{\mathbf{K}}_{\text{rem}} \end{bmatrix}$, where $\hat{\mathbf{K}}_{\text{ap}} \in \mathbb{R}^{N_x^l \times m}$, $\hat{\mathbf{K}}_{\text{rem}} \in \mathbb{R}^{N_x^l \times r_{\text{trunc}}}$, and $r_{\text{trunc}} = 2\tilde{r}_n - m$. Analogously, we split $\hat{\mathbf{V}} = \begin{bmatrix} \hat{\mathbf{V}}_{\text{ap}} & \hat{\mathbf{V}}_{\text{rem}} \end{bmatrix}$, where $\hat{\mathbf{V}}_{\text{ap}} \in \mathbb{R}^{N_q \times m}$ and $\hat{\mathbf{V}}_{\text{rem}} \in \mathbb{R}^{N_q \times r_{\text{trunc}}}$. Next, we compute the QR decomposition $\hat{\mathbf{K}}_{\text{rem}} = \hat{\mathbf{X}}_{\text{rem}}\hat{\mathbf{S}}_{\text{rem}}$ and subsequently the SVD of $\hat{\mathbf{S}}_{\text{rem}} = \mathbf{U}\Sigma\mathbf{W}^\top$. We perform a truncation step by selecting $1 \leq r_* \leq r_{\text{trunc}}$ such that, if σ_i, $i = 1, \ldots, r_{\text{trunc}}$ are singular values of $\hat{\mathbf{S}}_{\text{rem}}$, then for a given $\vartheta > 0$ the following is satisfied

$$\left(\sum_{i=r_*+1}^{r_{\text{trunc}}} \sigma_i^2 \right)^{1/2} \leq \vartheta.$$

The rank at time t_{n+1} is then $r_{n+1} = r_* + m$ and we set

$$\mathbf{X}_{\text{rem}} = \hat{\mathbf{X}}_{\text{rem}}\hat{\mathbf{U}}, \quad \mathbf{S}_{\text{rem}} = \hat{\Sigma}, \quad \tilde{\mathbf{W}} = \hat{\mathbf{V}}_{\text{rem}}\hat{\mathbf{W}},$$

where $\hat{\mathbf{U}} \in \mathbb{R}^{r_{\text{trunc}} \times r_*}$ and $\hat{\mathbf{W}} \in \mathbb{R}^{r_{\text{trunc}} \times r_*}$ contain the first r_* columns of $\mathbf{U}$ and $\mathbf{W}$, and $\hat{\Sigma} \in \mathbb{R}^{r_* \times r_*}$ is the first $r_* \times r_*$ block of Σ. The angular basis at time t_{n+1} is then defined as

$$\mathbf{V}^{n+1} := \begin{bmatrix} \hat{\mathbf{V}}_{\text{ap}} & \tilde{\mathbf{W}} \end{bmatrix}.$$

To set the updated spatial basis, we first compute a QR decomposition of the untruncated basis vectors, i.e., $\mathbf{X}_{\text{ap}}\mathbf{S}_{\text{ap}} = \hat{\mathbf{K}}_{\text{ap}}$ and define $\hat{\mathbf{X}}_* := \begin{bmatrix} \mathbf{X}_{\text{ap}} & \mathbf{X}_{\text{rem}} \end{bmatrix}$. Then by computing the QR decomposition of $\hat{\mathbf{X}}_*$ as $\hat{\mathbf{X}}_* = \mathbf{X}^{n+1}\mathbf{R}$ and setting

$$\mathbf{S}^{n+1} = \mathbf{R}\begin{bmatrix} \mathbf{S}_{\text{ap}} & \mathbf{0} \\ \mathbf{0} & \mathbf{S}_{\text{rem}} \end{bmatrix}.$$

Thus, we obtain the updated solution $\mathbf{X}^{n+1}$, $\mathbf{V}^{n+1}$, and $\mathbf{S}^{n+1}$ at time t_{n+1} while preserving the first m basis vectors of the augmented solution.

Appendix B: Proof of Theorem 2

We first state and prove several auxiliary lemmas to prove Theorem 3.2. To ease the presentation of the lemmas, we split the index sets $\mathcal{K}^I, \mathcal{K}^C$ as $\mathcal{K}^I = \mathcal{K}^I_{10} \cup \mathcal{K}^I_{01}$ and $\mathcal{K}^C = \mathcal{K}^C_{00} \cup \mathcal{K}^C_{11}$ where

$$\begin{aligned}
\mathcal{K}^I_{10} &:= \left\{(i^+_{1/2}, j) | \quad i \in \{0, ..., N_x\}, \quad j \in \{1, ..., N_y\}\right\}, \\
\mathcal{K}^I_{01} &:= \left\{(i, j^+_{1/2}) | \quad i \in \{1, ..., N_x\}, \quad j \in \{0, ..., N_y\}\right\} \\
\mathcal{K}^C_{00} &:= \left\{(i, j) | \quad i \in \{1, ..., N_x\}, \quad j \in \{1, ..., N_y\}\right\}, \\
\mathcal{K}^C_{11} &:= \left\{(i^+_{1/2}, j^+_{1/2}) \mid \quad i \in \{0, ..., N_x\}, \quad j \in \{0, ..., N_y\}\right\}.
\end{aligned}$$

Property 1.
For any $\{c_i\}_{i=0,\ldots,N_x} \in \mathbb{R}$ and $\{d_i\}_{i=0,\ldots,N_x} \in \mathbb{R}$ we have

$$\sum_i c_i d_i = \frac{1}{2}\sum_i c_i^2 + \frac{1}{2}\sum_i d_i^2 - \frac{1}{2}\sum_i (c_i - d_i)^2.$$

Lemma B.1. *Given any* $\boldsymbol{\varphi}_{i^+_{1/2}j} = (\varphi_{i^+_{1/2}j,1}, ..., \varphi_{i^+_{1/2}j,N_q})^\top \in \mathbb{R}^{N_q}$, $(i,j) \in \mathcal{K}^I_{10}$, $u_{ij} \in \mathbb{R}$, $(i,j) \in \mathcal{K}^C_{00}$, *and* $(\mathbf{M})_{\ell k} = \sqrt{w_\ell}\delta_{\ell k}$ *we have*

$$\begin{aligned}
\sum_{ij} \left(\boldsymbol{\varphi}_{i^+_{1/2}j}\right)^\top \mathbf{M}^2 \mathbb{1} \delta^0_x u_{i^+_{1/2}j} &= -\sum_{ij} \left(\mathcal{D}^0_x \boldsymbol{\varphi}_{ij}\right)^\top \mathbf{M}^2 \mathbb{1} u_{ij}, \quad \sum_{ij} \left(\boldsymbol{\varphi}_{i^+_{1/2}j}\right)^\top \mathbf{M}^2 \mathbb{1} \delta^0_y u_{i^+_{1/2}j} \\
&= -\sum_{ij} \left(\mathcal{D}^0_y \boldsymbol{\varphi}_{ij}\right)^\top \mathbf{M}^2 \mathbb{1} u_{ij},
\end{aligned}$$

where $\delta^0_x u_{i^+_{1/2}j}$ *and* $\mathcal{D}^0_x \boldsymbol{\varphi}_{ij}$ *are as defined in Section 3.2. Similarly, for* $\boldsymbol{\varphi}_{ij^+_{1/2}} = (\varphi_{j^+_{1/2},1}, ..., \varphi_{ij^+_{1/2},N_q})^\top \in \mathbb{R}^{N_q}$, $(i,j) \in \mathcal{K}^I_{01}$ *and* $u_{i^+_{1/2}j^+_{1/2}} \in \mathbb{R}$, $(i,j) \in \mathcal{K}^C_{11}$, *we have*

$$\begin{aligned}
\sum_{ij} \left(\boldsymbol{\varphi}_{ij^+_{1/2}}\right)^\top \mathbf{M}^2 \mathbb{1} \delta^0_x u_{ij^+_{1/2}} &= -\sum_{ij} \left(\mathcal{D}^0_x \boldsymbol{\varphi}_{i^+_{1/2}j^+_{1/2}}\right)^\top \mathbf{M}^2 \mathbb{1} u_{i^+_{1/2}j^+_{1/2}}, \\
\sum_{ij} \left(\boldsymbol{\varphi}_{ij^+_{1/2}}\right)^\top \mathbf{M}^2 \mathbb{1} \delta^0_y u_{ij^+_{1/2}} &= -\sum_{ij} \left(\mathcal{D}^0_y \boldsymbol{\varphi}_{i^+_{1/2}j^+_{1/2}}\right)^\top \mathbf{M}^2 \mathbb{1} u_{i^+_{1/2}j^+_{1/2}}.
\end{aligned}$$

Proof. Consider

$$\begin{aligned}\sum_{ij}\left(\boldsymbol{\varphi}_{i^+_{1/2}j}\right)^\top \mathbf{M}^2\mathbb{1}\delta^0_x u_{i^+_{1/2}j} &= \sum_\ell\sum_j\sum_i w_\ell \varphi_{i^+_{1/2}j,\ell}\delta^0_x u_{i^+_{1/2}j}\\ &= \frac{1}{\Delta x}\sum_\ell\sum_j\sum_i w_\ell \varphi_{i^+_{1/2}j,\ell}\left(u_{i+1,j}-u_{ij}\right)\\ &= -\frac{1}{\Delta x}\sum_\ell\sum_j\sum_i w_\ell\left(\varphi_{i^+_{1/2}j,\ell}-\varphi_{i^-_{1/2}j,\ell}\right)u_{ij}\\ &= -\frac{1}{\Delta x}\sum_\ell\sum_j\sum_i w_\ell\left(\mathcal{D}^0_x\varphi_{ij,\ell}\right)u_{ij}\\ &= -\sum_{ij}\left(\mathcal{D}^0_x\boldsymbol{\varphi}_{ij}\right)^\top\mathbf{M}^2\mathbb{1}u_{ij}.\end{aligned}$$

The other relations can be shown along similar lines. ■

Lemma B.2. *Let* $\boldsymbol{\varphi}_{i^+_{1/2}j} := (\varphi_{i^+_{1/2}j,1},\ldots,\varphi_{i^+_{1/2}j,N_q})^\top \in \mathbb{R}^{N_q}$, $\boldsymbol{\psi}_{i^+_{1/2}j} := (\psi_{i^+_{1/2}j,1},\ldots,\psi_{i^+_{1/2}j,N_q})^\top \in \mathbb{R}^{N_q}$ *for* $(i,j)\in\mathcal{K}^I_{10}$, *and* $\boldsymbol{\psi}_{-\frac{1}{2},j}=\boldsymbol{\varphi}_{N_x+\frac{1}{2},j}=0$. *Then, the following is satisfied:*

$$\sum_{ij}\left(\mathcal{D}^\pm_v\boldsymbol{\varphi}_{i^+_{1/2}j}\right)^\top\mathbf{S}\boldsymbol{\psi}_{i^+_{1/2}j}\Delta\zeta = -\sum_{ij}\left(\boldsymbol{\varphi}_{i^+_{1/2}j}\right)^\top\mathbf{S}\mathcal{D}^\mp_v\boldsymbol{\psi}_{i^+_{1/2}j}\Delta\zeta,\qquad v\in\mathcal{J}_{\boldsymbol{x}},\tag{B1}$$

where $\mathbf{S}\in\mathbb{R}^{N_q\times N_q}$ *is any symmetric matrix. Similarly, at* $(x_i,y_{j^+_{1/2}})$ *we get*

$$\sum_{ij}\left(\mathcal{D}^\pm_v\boldsymbol{\varphi}_{ij^+_{1/2}}\right)^\top\mathbf{S}\boldsymbol{\psi}_{ij^+_{1/2}}\Delta\zeta = -\sum_{ij}\left(\boldsymbol{\varphi}_{ij^+_{1/2}}\right)^\top\mathbf{S}\mathcal{D}^\mp_v\boldsymbol{\psi}_{ij^+_{1/2}}\Delta\zeta,\qquad v\in\mathcal{J}_{\boldsymbol{x}}.\tag{B2}$$

Proof. We show the result for $\mathcal{D}^+_v$, $v\in\mathcal{J}_{\boldsymbol{x}}$, since the proof for $\mathcal{D}^-_v$ follows from similar arguments. Recalling the definition of $\mathcal{D}^+_v$, we can write the left-hand side of (B1) as

$$\begin{aligned}\sum_{ij}\left(\mathcal{D}^+_v\boldsymbol{\varphi}_{i^+_{1/2}j}\right)^\top\mathbf{S}\boldsymbol{\psi}_{i^+_{1/2}j}\Delta\zeta &= \frac{1}{\Delta x}\sum_{j=1}^{N_y}\sum_{i=0}^{N_x}(\boldsymbol{\varphi}^\top_{i^+_{3/2}j}-\boldsymbol{\varphi}^\top_{i^+_{1/2}j})\mathbf{S}\boldsymbol{\psi}_{i^+_{1/2}j}\Delta\zeta\\ &= \frac{1}{\Delta x}\sum_{j=1}^{N_y}\sum_{i=0}^{N_x}\boldsymbol{\varphi}^\top_{i^+_{1/2}j}\mathbf{S}(\boldsymbol{\psi}_{i^+_{1/2}j}-\boldsymbol{\psi}_{i^+_{3/2}j})\Delta\zeta\quad\text{(rearranging terms)}\\ &= -\sum_{ij}\left(\boldsymbol{\varphi}_{i^+_{1/2}j}\right)^\top\mathbf{S}\mathcal{D}^\mp_v\boldsymbol{\psi}_{i^+_{1/2}j}\Delta\zeta.\end{aligned}$$

Using similar arguments, we can show that (B2) holds as well. ■

Lemma B.3. *For* $v\in\mathcal{J}_{\boldsymbol{x}}$, *we define*

$$\begin{aligned}\mathcal{E}_v = \frac{1}{2\pi}\Bigg[&\sum_{ij}\left(\mathcal{D}^0_v\boldsymbol{g}^{n+1}_{ij}\right)^\top\mathbf{M}^2\mathbf{Q}_v\mathbb{1}\left(\frac{1}{c}B^n_{ij}+\frac{\varepsilon^2}{c}h^n_{ij}-\frac{1}{c}B^{n+1}_{ij}-\frac{\varepsilon^2}{c}h^{n+1}_{ij}\right)\\ &+\sum_{ij}\left(\mathcal{D}^0_v\boldsymbol{g}^{n+1}_{i^+_{1/2}j^+_{1/2}}\right)^\top\mathbf{M}^2\mathbf{Q}_v\mathbb{1}\left(\frac{1}{c}B^n_{i^+_{1/2}j^+_{1/2}}+\frac{\varepsilon^2}{c}h^n_{i^+_{1/2}j^+_{1/2}}-\frac{1}{c}B^{n+1}_{i^+_{1/2}j^+_{1/2}}-\frac{\varepsilon^2}{c}h^{n+1}_{i^+_{1/2}j^+_{1/2}}\right)\Bigg]\Delta\zeta.\end{aligned}$$

Then, the following inequality holds

$$\mathcal{E}_v \leq \frac{\Delta t}{(2\pi)^2}\left[\sum_{ij}\left[\left(\mathcal{D}_v^0 \boldsymbol{g}_{ij}^{n+1}\right)^\top \mathbf{M}^2\mathbf{Q}_v\mathbb{1}\right]^2 + \sum_{ij}\left[\left(\mathcal{D}_v^0 \mathbf{g}_{i^+_{1/2}j^+_{1/2}}^{n+1}\right)^\top \mathbf{M}^2\mathbf{Q}_v\mathbb{1}\right]^2\right]\Delta\zeta + \frac{1}{4\Delta t}\left|\left|\frac{1}{c}B^n + \frac{\varepsilon^2}{c}h^n - \frac{1}{c}B^{n+1} - \frac{\varepsilon^2}{c}h^{n+1}\right|\right|^2.$$

Proof. Let

$$a_{ij}^v := \frac{1}{2\pi}\left(\mathcal{D}_v^0 \boldsymbol{g}_{ij}^{n+1}\right)^\top \mathbf{M}^2\mathbf{Q}_v\mathbb{1}, \quad b_{ij} := \left(\frac{1}{c}B_{ij}^n + \frac{\varepsilon^2}{c}h_{ij}^n - \frac{1}{c}B_{ij}^{n+1} - \frac{\varepsilon^2}{c}h_{ij}^{n+1}\right),$$

then we can write $\mathcal{E}_v$ as

$$\mathcal{E}_v = \sum_{ij} a_{ij}^v b_{ij}\Delta\zeta + \sum_{ij} a^v_{i^+_{1/2}j^+_{1/2}} b_{i^+_{1/2}j^+_{1/2}}\Delta\zeta.$$

Using Young's inequality we get

$$\mathcal{E}_v = \frac{1}{4\alpha}\sum_{ij}\left[(a_{ij}^v)^2 + (a^v_{i^+_{1/2}j^+_{1/2}})^2\right]\Delta\zeta + \alpha\sum_{ij}\left[(b_{ij})^2 + (b_{i^+_{1/2}j^+_{1/2}})^2\right]\Delta\zeta.$$

Since

$$\begin{aligned}\sum_{ij}\left[(b_{ij})^2 + (b_{i^+_{1/2}j^+_{1/2}})^2\right]\Delta\zeta &= \left[\sum_{ij}\left(\frac{1}{c}B_{ij}^n + \frac{\varepsilon^2}{c}h_{ij}^n - \frac{1}{c}B_{ij}^{n+1} - \frac{\varepsilon^2}{c}h_{ij}^{n+1}\right)^2\right.\\ &\quad\left. + \sum_{ij}\left(\frac{1}{c}B^n_{i^+_{1/2}j^+_{1/2}} + \frac{\varepsilon^2}{c}h^n_{i^+_{1/2}j^+_{1/2}} - \frac{1}{c}B^{n+1}_{i^+_{1/2}j^+_{1/2}} - \frac{\varepsilon^2}{c}h^{n+1}_{i^+_{1/2}j^+_{1/2}}\right)^2\right]\Delta\zeta\\ &= \left|\left|\frac{1}{c}B^n + \frac{\varepsilon^2}{c}h^n - \frac{1}{c}B^{n+1} - \frac{\varepsilon^2}{c}h^{n+1}\right|\right|^2,\end{aligned}$$

setting $\alpha = \frac{1}{4\Delta t}$ yields the required result. ∎

Lemma B.4. *If* $\boldsymbol{\varphi}_{i^+_{1/2}j} := (\varphi_{i^+_{1/2}j,1},\ldots,\varphi_{i^+_{1/2}j,N_q})^\top$, $(i,j)\in\mathcal{K}^I_{10}$, *and* $\boldsymbol{\varphi}_{ij^+_{1/2}} := (\varphi_{ij^+_{1/2},1},\ldots,\varphi_{ij^+_{1/2},N_q})^\top$, $(i,j)\in\mathcal{K}^I_{01}$, *in* $\mathbb{R}^{N_q}$, *then the following relations hold for the advection operator:*

$$\begin{aligned}\mathcal{L}_v\boldsymbol{\varphi}_{i^+_{1/2}j} &= \mathbf{Q}_v\mathcal{D}_v^c\boldsymbol{\varphi}_{i^+_{1/2}j} - \frac{\Delta v}{2}|\mathbf{Q}_v|\mathcal{D}_v^-\mathcal{D}_v^+\boldsymbol{\varphi}_{i^+_{1/2}j},\\ \mathcal{L}_v\boldsymbol{\varphi}_{ij^+_{1/2}} &= \mathbf{Q}_v\mathcal{D}_v^c\boldsymbol{\varphi}_{ij^+_{1/2}} - \frac{\Delta v}{2}|\mathbf{Q}_v|\mathcal{D}_v^-\mathcal{D}_v^+\boldsymbol{\varphi}_{ij^+_{1/2}},\end{aligned} \quad \text{where } v\in\mathcal{J}_x$$

$$\mathcal{D}_x^c\boldsymbol{\varphi}_{i^+_{1/2}j} := \frac{\boldsymbol{\varphi}_{i^+_{3/2}j} - \boldsymbol{\varphi}_{i^-_{1/2}j}}{2\Delta x}, \quad \mathcal{D}_x^c\boldsymbol{\varphi}_{ij^+_{1/2}} := \frac{\boldsymbol{\varphi}_{i+1,j^+_{1/2}} - \boldsymbol{\varphi}_{i-1,j^+_{1/2}}}{2\Delta x},$$

and $\mathcal{D}_y^c$ *is defined in a similar manner.*

Proof. For $\mathcal{L}_v\boldsymbol{\varphi}_{i^+_{1/2}j}$ we have,

$$\begin{aligned}
&\mathcal{L}_v\boldsymbol{\varphi}_{i^+_{1/2}j} = (\mathbf{Q}_v^-\mathcal{D}_v^+ + \mathbf{Q}_v^+\mathcal{D}_v^-)\boldsymbol{\varphi}_{i^+_{1/2}j}\\
&= \frac{1}{2}(\mathbf{Q}_v - |\mathbf{Q}_v|)\mathcal{D}_v^+\boldsymbol{\varphi}_{i^+_{1/2}j} + \frac{1}{2}(\mathbf{Q}_v + |\mathbf{Q}_v|)\mathcal{D}_v^-\boldsymbol{\varphi}_{i^+_{1/2}j}, \quad (\mathbf{Q}_v^\pm = \frac{1}{2}(\mathbf{Q}_v \pm |\mathbf{Q}_v|))\\
&= \mathbf{Q}_v\left(\frac{\mathcal{D}_v^+ + \mathcal{D}_v^-}{2}\right)\boldsymbol{\varphi}_{i^+_{1/2}j} - |\mathbf{Q}_v|\left(\frac{\mathcal{D}_v^+ - \mathcal{D}_v^-}{2}\right)\boldsymbol{\varphi}_{i^+_{1/2}j} = \mathbf{Q}_v\mathcal{D}_v^c\boldsymbol{\varphi}_{i^+_{1/2}j} - \frac{\Delta v}{2}|\mathbf{Q}_v|\mathcal{D}_v^-\mathcal{D}_v^+\boldsymbol{\varphi}_{i^+_{1/2}j}.
\end{aligned}$$

Similarly, we can show the relation for $\mathcal{L}_v\boldsymbol{\varphi}_{ij^+_{1/2}}$. ■

Lemma B.5. *Let* $\boldsymbol{\varphi}_{i^+_{1/2}j} = (\varphi_{i^+_{1/2}j,1},\ldots,\varphi_{i^+_{1/2}j,N_q})^\top \in \mathbb{R}^{N_q}$ *and* $\boldsymbol{\psi}_{i^+_{1/2}j} = (\psi_{i^+_{1/2}j,1},\ldots,\psi_{i^+_{1/2}j,N_q})^\top \in \mathbb{R}^{N_q}$, *for* $(i,j) \in \mathcal{K}^I_{10}$, *then we have the following inequality*

$$\begin{aligned}
&\left|\sum_{ij}[\mathbf{M}(\mathbf{Q}_v^+\mathcal{D}_v^+ + \mathbf{Q}_v^-\mathcal{D}_v^-)\boldsymbol{\varphi}_{i^+_{1/2}j}]^\top(\mathbf{M}\boldsymbol{\psi}_{i^+_{1/2}j})\Delta\zeta\right|\\
&\le \alpha\sum_{ij}(\boldsymbol{\psi}_{i^+_{1/2}j})^\top\mathbf{M}^2\boldsymbol{\psi}_{i^+_{1/2}j}\Delta\zeta + \frac{1}{4\alpha}\sum_{ij}(|\mathbf{Q}_v|\mathcal{D}_v^+\boldsymbol{\varphi}_{i^+_{1/2}j})^\top\mathbf{M}^2(|\mathbf{Q}_v|\mathcal{D}_v^+\boldsymbol{\varphi}_{i^+_{1/2}j})\Delta\zeta
\end{aligned} \tag{B3}$$

A similar result holds for $\boldsymbol{\varphi}_{ij^+_{1/2}} \in \mathbb{R}^{N_q}$ *and* $\boldsymbol{\psi}_{ij^+_{1/2}} \in \mathbb{R}^{N_q}$, *for* $(i,j) \in \mathcal{K}^I_{01}$.

Proof. Using Young's inequality for the left-hand side we get

$$\begin{aligned}
&\left|\sum_{ij}[\mathbf{M}(\mathbf{Q}_v^+\mathcal{D}_v^+ + \mathbf{Q}_v^-\mathcal{D}_v^-)\boldsymbol{\varphi}_{i^+_{1/2}j}]^\top(\mathbf{M}\boldsymbol{\psi}_{i^+_{1/2}j})\Delta\zeta\right|\\
&\le \alpha\sum_{ij}(\boldsymbol{\psi}_{i^+_{1/2}j})^\top\mathbf{M}^2\boldsymbol{\psi}_{i^+_{1/2}j}\Delta\zeta + \frac{1}{4\alpha}\sum_{ij}[\mathbf{M}(\mathbf{Q}_v^+\mathcal{D}_v^+ + \mathbf{Q}_v^-\mathcal{D}_v^-)\boldsymbol{\varphi}_{i^+_{1/2}j}]^2\Delta\zeta.
\end{aligned}$$

Now consider the second term on the right-hand side of the above inequality,

$$\begin{aligned}
\sum_{ij}\left[\mathbf{M}(\mathbf{Q}_v^+\mathcal{D}_v^+ + \mathbf{Q}_v^-\mathcal{D}_v^-)\boldsymbol{\varphi}_{i^+_{1/2}j}\right]^2\Delta\zeta &= \sum_{ij}(\mathcal{D}_v^+\boldsymbol{\varphi}_{i^+_{1/2}j})^\top\mathbf{Q}_v^+\mathbf{M}^2\mathbf{Q}_v^+(\mathcal{D}_v^+\boldsymbol{\varphi}_{i^+_{1/2}j})\Delta\zeta\\
&+ \sum_{ij}(\mathcal{D}_v^-\boldsymbol{\varphi}_{i^+_{1/2}j})^\top\mathbf{Q}_v^-\mathbf{M}^2\mathbf{Q}_v^-(\mathcal{D}_v^-\boldsymbol{\varphi}_{i^+_{1/2}j})\Delta\zeta\\
&+ 2\sum_{ij}(\mathcal{D}_v^+\boldsymbol{\varphi}_{i^+_{1/2}j})^\top\mathbf{Q}_v^+\mathbf{M}^2\mathbf{Q}_v^-(\mathcal{D}_v^-\boldsymbol{\varphi}_{i^+_{1/2}j})\Delta\zeta.
\end{aligned} \tag{B4}$$

We have that $\mathbf{Q}_v^+ = (\mathbf{Q}_v + |\mathbf{Q}_v|)/2$, $\mathbf{Q}_v^- = (\mathbf{Q}_v - |\mathbf{Q}_v|)/2$ and since $\mathbf{Q}_v$ and $\mathbf{M}$ are diagonal matrices

$$\mathbf{Q}_v^+\mathbf{M}^2\mathbf{Q}_v^- = 0.$$

Moreover,

$$\sum_{ij}(\mathcal{D}_v^-\boldsymbol{\varphi}_{i^+_{1/2}j})^\top\mathbf{Q}_v^-\mathbf{M}^2\mathbf{Q}_v^-(\mathcal{D}_v^-\phi_{i^+_{1/2}j})\Delta\zeta = \sum_{ij}(\mathcal{D}_v^+\boldsymbol{\varphi}_{i^+_{1/2}j})^\top\mathbf{Q}_v^-\mathbf{M}^2\mathbf{Q}_v^-(\mathcal{D}_v^+\boldsymbol{\varphi}_{i^+_{1/2}j})\Delta\zeta.$$

Thus by substituting $\mathbf{Q}_v^+$ and $\mathbf{Q}_v^-$ in (B4) we get

$$\begin{aligned}
&\sum_{ij}\left[\mathbf{M}(\mathbf{Q}_v^+\mathcal{D}_v^+ + \mathbf{Q}_v^-\mathcal{D}_v^-)\boldsymbol{\varphi}_{i_{1/2}^+j}\right]^2\Delta\zeta = \frac{1}{2}\sum_{ij}(\mathcal{D}_v^+\boldsymbol{\varphi}_{i_{1/2}^+j})^\top\mathbf{Q}_v\mathbf{M}^2\mathbf{Q}_v(\mathcal{D}_v^+\boldsymbol{\varphi}_{i_{1/2}^+j})\Delta\zeta\\
&+\frac{1}{2}\sum_{ij}(\mathcal{D}_v^+\boldsymbol{\varphi}_{i_{1/2}^+j})^\top|\mathbf{Q}_v|\mathbf{M}^2|\mathbf{Q}_v|(\mathcal{D}_v^+\boldsymbol{\varphi}_{i_{1/2}^+j})\Delta\zeta\\
&\leq \sum_{ij}(\mathcal{D}_v^+\boldsymbol{\varphi}_{i_{1/2}^+j})^\top|\mathbf{Q}_v|\mathbf{M}^2|\mathbf{Q}_v|(\mathcal{D}_v^+\boldsymbol{\varphi}_{i_{1/2}^+j})\Delta\zeta.
\end{aligned}$$

The result for $\left|\sum_{ij}\left[\mathbf{M}(\mathbf{Q}_v^+\mathcal{D}_v^+ + \mathbf{Q}_v^-\mathcal{D}_v^-)\boldsymbol{\varphi}_{ij_{1/2}^+}\right]^\top(\mathbf{M}\boldsymbol{\psi}_{ij_{1/2}^+})\Delta\zeta\right|$ can be shown in a similar manner. ■

Lemma B.6. *For the advection operator $\mathcal{L}_v, v \in \mathcal{J}_x$, if $\boldsymbol{\psi}_{i_{1/2}^+j} = (\psi_{i_{1/2}^+j,1},\ldots,\psi_{i_{1/2}^+j,N_q})^\top \in \mathbb{R}^{N_q}$, for $(i,j)\in\mathcal{K}_{10}^I$, $\boldsymbol{\psi}_{ij_{1/2}^+} = (\psi_{ij_{1/2}^+,1},\ldots,\psi_{ij_{1/2}^+,N_q})^\top \in \mathbb{R}^{N_q}$, for $(i,j)\in\mathcal{K}_{01}^I$, the following holds*

$$\left[\sum_{ij}\left(\boldsymbol{\psi}_{i_{1/2}^+j}^{n+1}\right)^\top\mathbf{M}^2\mathcal{L}_v\boldsymbol{\psi}_{i_{1/2}^+j}^{n} + \sum_{ij}\left(\boldsymbol{\psi}_{ij_{1/2}^+}^{n+1}\right)^\top\mathbf{M}^2\mathcal{L}_v\boldsymbol{\psi}_{ij_{1/2}^+}^{n}\right]\Delta\zeta = \mathcal{A}_v + \mathcal{B}_v, \tag{B5}$$

where

$$\begin{aligned}
\mathcal{A}_v &= \frac{\Delta v}{2}\left[\sum_{ij}(\mathcal{D}_v^+\boldsymbol{\psi}_{i_{1/2}^+j}^{n+1})^\top\mathbf{M}^2|\mathbf{Q}_v|\mathcal{D}_v^+\boldsymbol{\psi}_{i_{1/2}^+j}^{n+1}\right.\\
&\qquad\left.+\sum_{ij}(\mathcal{D}_v^+\boldsymbol{\psi}_{ij_{1/2}^+}^{n+1})^\top\mathbf{M}^2|\mathbf{Q}_v|\mathcal{D}_v^+\boldsymbol{\psi}_{ij_{1/2}^+}^{n+1}\right]\Delta\zeta,\\
\mathcal{B}_v &= -\left[\sum_{ij}((\mathbf{Q}_v^+\mathcal{D}_v^+ + \mathbf{Q}_v^-\mathcal{D}_v^-)\boldsymbol{\psi}_{i_{1/2}^+j}^{n+1})^\top\mathbf{M}^2(\boldsymbol{\psi}_{i_{1/2}^+j}^{n} - \boldsymbol{\psi}_{i_{1/2}^+j}^{n+1})\right.\\
&\qquad\left.+\sum_{ij}((\mathbf{Q}_v^+\mathcal{D}_v^+ + \mathbf{Q}_v^-\mathcal{D}_v^-)\boldsymbol{\psi}_{ij_{1/2}^+}^{n+1})^\top\mathbf{M}^2(\boldsymbol{\psi}_{ij_{1/2}^+}^{n} - \boldsymbol{\psi}_{ij_{1/2}^+}^{n+1})\right]\Delta\zeta.
\end{aligned}$$

Additionally, we have

$$\mathcal{B}_v \geq -\frac{\varepsilon}{4c\Delta t}\left|\left|\Psi^n - \Psi^{n+1}\right|\right|^2 - \frac{c\Delta t}{\varepsilon}\left|\left||\mathbf{Q}_v|\mathcal{D}_v^+\Psi^{n+1}\right|\right|^2.$$

Proof. First, we rewrite the first term on the left-hand side of (B5) as

$$\begin{aligned}
&\sum_{ij}\left(\boldsymbol{\psi}_{i_{1/2}^+j}^{n+1}\right)^\top\mathbf{M}^2\mathcal{L}_v\boldsymbol{\psi}_{i_{1/2}^+j}^{n}\Delta\zeta = \sum_{ij}\left(\boldsymbol{\psi}_{i_{1/2}^+j}^{n+1}\right)^\top\mathbf{M}^2\mathcal{L}_v\boldsymbol{\psi}_{i_{1/2}^+j}^{n+1}\Delta\zeta\\
&+\sum_{ij}\left(\boldsymbol{\psi}_{i_{1/2}^+j}^{n+1}\right)^\top\mathbf{M}^2\mathcal{L}_v\left(\boldsymbol{\psi}_{i_{1/2}^+j}^{n} - \boldsymbol{\psi}_{i_{1/2}^+j}^{n+1}\right)\Delta\zeta.
\end{aligned} \tag{B6}$$

Using Lemma B.4, the first term on the right-hand side of (B6) is given by

$$\begin{aligned}
&\sum_{ij}\left(\boldsymbol{\psi}_{i_{1/2}^+j}^{n+1}\right)^\top\mathbf{M}^2\mathcal{L}_v\boldsymbol{\psi}_{i_{1/2}^+j}^{n+1}\Delta\zeta = \sum_{ij}\left(\boldsymbol{\psi}_{i_{1/2}^+j}^{n+1}\right)^\top\mathbf{M}^2\mathbf{Q}_v\mathcal{D}_v^c\boldsymbol{\psi}_{i_{1/2}^+j}^{n+1}\Delta\zeta\\
&-\frac{\Delta v}{2}\sum_{ij}\left(\boldsymbol{\psi}_{i_{1/2}^+j}^{n+1}\right)^\top\mathbf{M}^2|\mathbf{Q}_v|\mathcal{D}_v^-\mathcal{D}_v^+\boldsymbol{\psi}_{i_{1/2}^+j}^{n+1}\Delta\zeta\\
&=\frac{\Delta v}{2}\sum_{ij}\left(\mathcal{D}_v^+\boldsymbol{\psi}_{i_{1/2}^+j}^{n+1}\right)^\top\mathbf{M}^2|\mathbf{Q}_v|\mathcal{D}_v^+\boldsymbol{\psi}_{i_{1/2}^+j}^{n+1}\Delta\zeta,
\end{aligned}$$

where we use Lemma B.2 and

$$\sum_{ij}\left(\boldsymbol{\psi}^{n+1}_{i^+_{1/2}j}\right)^\top \mathbf{M}^2\mathbf{Q}_v\mathcal{D}_v^c\boldsymbol{\psi}^{n+1}_{i^+_{1/2}j}\Delta\zeta = \frac{1}{\Delta x}\sum_{ij}\left(\boldsymbol{\psi}^{n+1}_{i^+_{1/2}j}\right)^\top \mathbf{M}^2\mathbf{Q}_v\boldsymbol{\psi}^{n+1}_{i^+_{3/2}j}\Delta\zeta$$
$$-\frac{1}{\Delta x}\sum_{ij}\left(\boldsymbol{\psi}^{n+1}_{i^+_{1/2}j}\right)^\top \mathbf{M}^2\mathbf{Q}_v\boldsymbol{\psi}^{n+1}_{i^-_{1/2}j}\Delta\zeta$$
$$\overset{\text{shifting index}}{=} 0.$$

Using Lemma B.2 for the second term on the right-hand side of (B6) we get

$$\begin{aligned}&\textstyle\sum_{ij}\left(\boldsymbol{\psi}^{n+1}_{i^+_{1/2}j}\right)^\top \mathbf{M}^2\mathcal{L}_v\left(\boldsymbol{\psi}^{n}_{i^+_{1/2}j}-\boldsymbol{\psi}^{n+1}_{i^+_{1/2}j}\right)\Delta\zeta\\ &=\textstyle\sum_{ij}\left((\mathbf{Q}_v^+\mathcal{D}_v^+ + \mathbf{Q}_v^-\mathcal{D}_v^-)\boldsymbol{\psi}^{n+1}_{i^+_{1/2}j}\right)^\top \mathbf{M}^2\left(\boldsymbol{\psi}^{n}_{i^+_{1/2}j}-\boldsymbol{\psi}^{n+1}_{i^+_{1/2}j}\right)\Delta\zeta.\end{aligned} \tag{B7}$$

We get similar expressions at $(x_i, y_{j^+_{1/2}})$. Combining with the expressions at $(x_{i^+_{1/2}}, y_j)$ yields the first part of the lemma. To prove the remaining lemma, we use Lemma B.5 for the right-hand side of (B7) which gives

$$\begin{aligned}&-\sum_{ij}((\mathbf{Q}_v^+\mathcal{D}_v^+ + \mathbf{Q}_v^-\mathcal{D}_v^-)\boldsymbol{\psi}^{n+1}_{i^+_{1/2}j})^\top \mathbf{M}^2(\boldsymbol{\psi}^{n}_{i^+_{1/2}j}-\boldsymbol{\psi}^{n+1}_{i^+_{1/2}j})\Delta\zeta\\ &\geq -\alpha\sum_{ij}(\boldsymbol{\psi}^{n}_{i^+_{1/2}j}-\boldsymbol{\psi}^{n+1}_{i^+_{1/2}j})^\top \mathbf{M}^2(\boldsymbol{\psi}^{n}_{i^+_{1/2}j}-\boldsymbol{\psi}^{n+1}_{i^+_{1/2}j})\Delta\zeta\\ &-\frac{1}{4\alpha}\sum_{ij}(|\mathbf{Q}_v|\mathcal{D}_v^+\boldsymbol{\psi}^{n+1}_{i^+_{1/2}j})^\top \mathbf{M}^2(|\mathbf{Q}_v|\mathcal{D}_v^+\boldsymbol{\psi}^{n+1}_{i^+_{1/2}j})\Delta\zeta.\end{aligned} \tag{B8}$$

Similarly, at $(x_i, y_{j^+_{1/2}})$ we get

$$\begin{aligned}&-\sum_{ij}((\mathbf{Q}_v^+\mathcal{D}_v^+ + \mathbf{Q}_v^-\mathcal{D}_v^-)\boldsymbol{\psi}^{n+1}_{ij^+_{1/2}})^\top \mathbf{M}^2(\boldsymbol{\psi}^{n}_{ij^+_{1/2}}-\boldsymbol{\psi}^{n+1}_{ij^+_{1/2}})\Delta\zeta\\ &\geq -\alpha\sum_{ij}(\boldsymbol{\psi}^{n}_{ij^+_{1/2}}-\boldsymbol{\psi}^{n+1}_{ij^+_{1/2}})^\top \mathbf{M}^2(\boldsymbol{\psi}^{n}_{ij^+_{1/2}}-\boldsymbol{\psi}^{n+1}_{ij^+_{1/2}})\Delta\zeta\\ &-\frac{1}{4\alpha}\sum_{ij}(|\mathbf{Q}_v|\mathcal{D}_v^+\boldsymbol{\psi}^{n+1}_{ij^+_{1/2}})^\top \mathbf{M}^2(|\mathbf{Q}_v|\mathcal{D}_v^+\boldsymbol{\psi}^{n+1}_{ij^+_{1/2}})\Delta\zeta.\end{aligned} \tag{B9}$$

Adding (B8) and (B9) and setting $\alpha = \frac{\varepsilon}{4c\Delta t}$ completes the proof of the lemma. ■

Lemma B.7. *Given any $\boldsymbol{\varphi} \in \mathbb{R}^{N_q}$ the following inequality holds for $v \in \mathcal{J}_x$:*

$$\boldsymbol{\varphi}^\top\mathbf{Q}_v\boldsymbol{w}\boldsymbol{w}^\top\mathbf{Q}_v\boldsymbol{\varphi} \leq \pi\boldsymbol{\varphi}^\top|\mathbf{Q}_v|\mathbf{M}^2\boldsymbol{\varphi}.$$

Proof. Expanding the left-hand side, we get

$$\boldsymbol{\varphi}^\top\mathbf{Q}_v\boldsymbol{w}\boldsymbol{w}^\top\mathbf{Q}_v\boldsymbol{\varphi} = \left(\sum_\ell w_\ell\Omega_v^\ell\varphi_\ell\right)^2 \leq \left(\sum_\ell w_\ell|\Omega_v^\ell|\varphi_\ell\right)^2 \leq \sum_{\ell'} w_{\ell'}|\Omega_v^{\ell'}|\sum_\ell w_\ell|\Omega_v^\ell|\varphi_\ell^2.$$

Since $\sum_{\ell'} w_{\ell'}|\Omega_x^{\ell'}| = \int_{P(\mathbb{S}^2)}|\Omega_x|\mathrm{d}\Omega = \pi$ and $\sum_{\ell'} w_{\ell'}|\Omega_y^{\ell'}| = \int_{P(\mathbb{S}^2)}|\Omega_y|\mathrm{d}\Omega = \pi$, we get the desired result for $v \in \mathcal{J}_x$. ■

Lemma B.8. *The following holds for* $\boldsymbol{\varphi}_{i^+_{1/2}j} \in \mathbb{R}^{N_q}$, $(i,j) \in \mathcal{K}^I_{10}$,

$$\sum_{ij} (\mathcal{D}^+_v \boldsymbol{\varphi}_{i^+_{1/2}j})^\top \mathbf{M}^2 |\mathbf{Q}_v| (\mathcal{D}^+_v \boldsymbol{\varphi}_{i^+_{1/2}j}) \leq \frac{4}{\Delta v^2} \sum_{ij} \boldsymbol{\varphi}^\top_{i^+_{1/2}j} \mathbf{M}^2 |\mathbf{Q}_v| \boldsymbol{\varphi}_{i^+_{1/2}j}, \quad v \in \mathcal{J}_{\boldsymbol{x}}. \tag{B10}$$

A similar result holds for $\boldsymbol{\varphi}_{ij^+_{1/2}}$ *at* $(i, j^+_{1/2})$.

Proof. Expanding the left-hand side of (B10) yields

$$\sum_{ij} (\mathcal{D}^+_v \boldsymbol{\varphi}_{i^+_{1/2}j})^\top \mathbf{M}^2 |\mathbf{Q}_v| (\mathcal{D}^+_v \boldsymbol{\varphi}_{i^+_{1/2}j}) = \sum_\ell w_\ell |\Omega^\ell_v| \sum_j \sum_i (\mathcal{D}^+_v \boldsymbol{\varphi}_{i^+_{1/2}j})^2.$$

For a fixed j, using (Frank et al. 2025, Lemma A.2) we get

$$\begin{aligned} &\sum_{ij} (\mathcal{D}^+_v \boldsymbol{\varphi}_{i^+_{1/2}j})^\top \mathbf{M}^2 |\mathbf{Q}_v| (\mathcal{D}^+_v \boldsymbol{\varphi}_{i^+_{1/2}j}) \leq \frac{4}{\Delta v^2} \sum_\ell w_\ell |\Omega^\ell_v| \sum_j \sum_i (\boldsymbol{\varphi}_{i^+_{1/2}j})^2 \\ &= \frac{4}{\Delta v^2} \sum_{ij} \boldsymbol{\varphi}^\top_{i^+_{1/2}j} \mathbf{M}^2 |\mathbf{Q}_v| \boldsymbol{\varphi}_{i^+_{1/2}j}. \end{aligned}$$

Similarly, we can show the results for $\boldsymbol{\varphi}_{ij^+_{1/2}}$ at $(i, j^+_{1/2})$. ∎

Lemma B.9. *For* $a, b > 0$ *we have that the following inequality holds:*

$$a^4(a-b) - \frac{1}{5}(a^5 - b^5) \geq 0.$$

Proof. For $a = b$ we get that the left-hand side of the inequality is zero and thus we consider the case $a \neq b$. Thus we have two cases $a < b$ or $a > b$ and without loss of generality we consider the case $a < b$ and prove the inequality by contradiction. So assume that the given inequality is not true and thus we have

$$(a-b) \cdot (4a^4 - a^3 b - a^2 b^2 - a b^3 - b^4) < 0.$$

Since $a < b$ we have $4a^4 > a^3 b + a^2 b^2 + a b^3 + b^4$. However, we have

$$a^3 b + a^2 b^2 + a b^3 + b^4 > 4a^4,$$

which is a contradiction. ∎

Finally, we now give the proof of Theorem 2:

Proof. We denote the scalar flux by $\phi^n_{ij} = B^n_{ij} + \varepsilon^2 h^n_{ij}$. Then, rearranging (11b) yields

$$\frac{1}{\Delta t}\left[\frac{1}{c}\phi^{n+1}_{ij} - \frac{1}{c}\phi^n_{ij}\right] + \frac{1}{2\pi} \boldsymbol{w}^\top \mathbf{Q}_x \mathcal{D}^0_x \boldsymbol{g}^{n+1}_{ij} + \frac{1}{2\pi} \boldsymbol{w}^\top \mathbf{Q}_y \mathcal{D}^0_y \boldsymbol{g}^{n+1}_{ij} = -\sigma^a_{ij} h^{n+1}_{ij}. \tag{B11}$$

Multiplying (B11) by $\left(\frac{1}{c}\phi^{n+1}_{ij}\right)\Delta\zeta$ and summing over i, j

$$\begin{aligned} &\frac{1}{2\Delta t} \sum_{ij} \left[\left(\frac{1}{c}\phi^{n+1}_{ij}\right)^2 - \left(\frac{1}{c}\phi^n_{ij}\right)^2 + \left(\frac{1}{c}\phi^{n+1}_{ij} - \frac{1}{c}\phi^n_{ij}\right)^2\right]\Delta\zeta \\ &+ \frac{1}{2\pi}\sum_{ij} (\mathcal{H}^1_x)^{n+1,n+1}_{ij} \Delta\zeta + \frac{1}{2\pi}\sum_{ij} (\mathcal{H}^1_y)^{n+1,n+1}_{ij} \Delta\zeta = -\sum_{ij} (\mathcal{H}^2)^{n+1,n+1}_{ij} \Delta\zeta, \end{aligned} \tag{B12}$$

where

$$
\begin{aligned}
(\mathcal{H}_v^1)_{ij}^{n+1,n+1} &:= \boldsymbol{w}^\top \mathbf{Q}_v \mathcal{D}_v^0 \boldsymbol{g}_{ij}^{n+1}\left(\frac{1}{c}\phi_{ij}^{n+1}\right), \quad v \in \mathcal{J}_{\boldsymbol{x}},\\
(\mathcal{H}^2)_{ij}^{n+1,n+1} &:= \sigma_{ij}^a h_{ij}^{n+1}\left(\frac{1}{c}\phi_{ij}^{n+1}\right).
\end{aligned}
$$

The double temporal index on $(\mathcal{H}_v^1)_{ij}^{n+1,n+1}$ are for $\boldsymbol{g}^{n+1}$ and ϕ^{n+1}, respectively. A similar equality is obtained at $(x_{i_{1/2}^+}, y_{j_{1/2}^+})$; adding this to (B12) and summing over i,j yields

$$
\frac{1}{2\Delta t}\left[\left|\left|\frac{1}{c}\phi^{n+1}\right|\right|^2 - \left|\left|\frac{1}{c}\phi^{n}\right|\right|^2 + \left|\left|\frac{1}{c}\phi^{n+1} - \frac{1}{c}\phi^{n}\right|\right|^2\right] + \frac{1}{2\pi}(\mathcal{H}^1)^{n+1,n+1} = -(\mathcal{H}^2)^{n+1,n+1},
\tag{B13}
$$

where

$$
\begin{aligned}
(\mathcal{H}_v^1)^{n+1,n+1} &:= \left[\sum_{ij}(\mathcal{H}_v^1)_{ij}^{n+1,n+1} + \sum_{ij}(\mathcal{H}_v^1)_{i_{1/2}^+ j_{1/2}^+}^{n+1,n+1}\right]\Delta\zeta, \quad v \in \mathcal{J}_{\mathbf{x}},\\
(\mathcal{H}^1)^{n+1,n+1} &:= (\mathcal{H}_x^1)^{n+1,n+1} + \left(\mathcal{H}_y^1\right)^{n+1,n+1},\\
(\mathcal{H}^2)^{n+1,n+1} &:= \left[\sum_{ij}(\mathcal{H}^2)_{ij}^{n+1,n+1} + \sum_{ij}(\mathcal{H}^2)_{i_{1/2}^+ j_{1/2}^+}^{n+1,n+1}\right]\Delta\zeta.
\end{aligned}
$$

Similarly, multiplying (11a) by $(\boldsymbol{g}_{i_{1/2}^+ j}^{n+1})^\top \mathbf{M}^2 \Delta\zeta$ and the equivalent equation at $(x_i, y_{j_{1/2}^+})$ by $(\boldsymbol{g}_{ij_{1/2}^+}^{n+1})^\top \mathbf{M}^2 \Delta\zeta$, summing over i,j and adding them yields

$$
\begin{aligned}
&\frac{1}{2\Delta t}\left[\frac{1}{c}\left|\left|\boldsymbol{g}^{n+1}\right|\right|^2 - \frac{1}{c}||\boldsymbol{g}^n||^2 + \frac{1}{c}\left|\left|\boldsymbol{g}^{n+1} - \boldsymbol{g}^n\right|\right|^2\right]\\
&+\frac{1}{\varepsilon}\left[\sum_{ij}\left(\boldsymbol{g}_{i_{1/2}^+ j}^{n+1}\right)^\top \mathbf{M}^2\left(\mathbf{I} - \frac{1}{2\pi}\mathbb{1}\boldsymbol{w}^\top\right)\mathcal{L}_x \boldsymbol{g}_{i_{1/2}^+ j}^{n+1} + \sum_{ij}\left(\boldsymbol{g}_{ij_{1/2}^+}^{n+1}\right)^\top \mathbf{M}^2\left(\mathbf{I} - \frac{1}{2\pi}\mathbb{1}\boldsymbol{w}^\top\right)\mathcal{L}_x \boldsymbol{g}_{ij_{1/2}^+}^{n+1}\right]\Delta\zeta\\
&+\frac{1}{\varepsilon}\left[\sum_{ij}\left(\boldsymbol{g}_{i_{1/2}^+ j}^{n+1}\right)^\top \mathbf{M}^2\left(\mathbf{I} - \frac{1}{2\pi}\mathbb{1}\boldsymbol{w}^\top\right)\mathcal{L}_y \boldsymbol{g}_{i_{1/2}^+ j}^{n+1} + \sum_{ij}\left(\boldsymbol{g}_{ij_{1/2}^+}^{n+1}\right)^\top \mathbf{M}^2\left(\mathbf{I} - \frac{1}{2\pi}\mathbb{1}\boldsymbol{w}^\top\right)\mathcal{L}_y \boldsymbol{g}_{ij_{1/2}^+}^{n+1}\right]\Delta\zeta\\
&+\frac{c}{\varepsilon^2}(\mathcal{G}^1)^{n+1,n} = -\frac{1}{\varepsilon^2}\left[\sum_{ij}\sigma_{i_{1/2}^+ j}^t\left(\boldsymbol{g}_{i_{1/2}^+ j}^{n+1}\right)^\top \mathbf{M}^2 \boldsymbol{g}_{i_{1/2}^+ j}^{n+1} + \sum_{ij}\sigma_{ij_{1/2}^+}^t\left(\boldsymbol{g}_{ij_{1/2}^+}^{n+1}\right)^\top \mathbf{M}^2 \mathbf{g}_{ij_{1/2}^+}^{n+1}\right]\Delta\zeta,
\end{aligned}
\tag{B14}
$$

where

$$
\begin{aligned}
(\mathcal{G}_v^1)_{i_{1/2}^+ j}^{n+1,n} &:= \left(\boldsymbol{g}_{i_{1/2}^+ j}^{n+1}\right)^\top \mathbf{M}^2 \mathbf{Q}_v \mathbb{1}\delta_v^0\left(\frac{1}{c}\phi_{i_{1/2}^+ j}^{n}\right), \quad v \in \mathcal{J}_{\mathbf{x}},\\
(\mathcal{G}_v^1)^{n+1,n} &:= \left[\sum_{ij}(\mathcal{G}_v^1)_{i_{1/2}^+ j}^{n+1,n} + \sum_{ij}(\mathcal{G}_v^1)_{ij_{1/2}^+}^{n+1,n}\right]\Delta\zeta, \quad v \in \mathcal{J}_{\mathbf{x}},\\
(\mathcal{G}^1)^{n+1,n} &:= (\mathcal{G}_x^1)^{n+1,n} + \left(\mathcal{G}_y^1\right)^{n+1,n}.
\end{aligned}
$$

Since $\sigma^t(\boldsymbol{x}) \geq \sigma_0^t, \forall \boldsymbol{x}$, $\mathbf{M}^2\mathbb{1} = \boldsymbol{w}$, and $0 = \langle \boldsymbol{g} \rangle = \boldsymbol{g}_{i^+_{1/2}j}^\top \boldsymbol{w} = \boldsymbol{g}_{ij^+_{1/2}}^\top \boldsymbol{w}$, we get

$$
\begin{aligned}
&-\frac{1}{\varepsilon^2}\left[\sum_{ij}\sigma^t_{i^+_{1/2}j}\left(\boldsymbol{g}^{n+1}_{i^+_{1/2}j}\right)^\top \mathbf{M}^2 \boldsymbol{g}^{n+1}_{i^+_{1/2}j} + \sum_{ij}\sigma^t_{ij^+_{1/2}}\left(\boldsymbol{g}^{n+1}_{ij^+_{1/2}}\right)^\top \mathbf{M}^2 \boldsymbol{g}^{n+1}_{ij^+_{1/2}}\right]\Delta\zeta \leq -\frac{\sigma_0^t}{\varepsilon^2}||\boldsymbol{g}^{n+1}||^2\\
&\left(\boldsymbol{g}^{n+1}_{i^+_{1/2}j}\right)^\top \mathbf{M}^2\mathbb{1} = \left(\boldsymbol{g}^{n+1}_{i^+_{1/2}j}\right)^\top \mathbf{w} = 0,\\
&\left(\boldsymbol{g}^{n+1}_{ij^+_{1/2}}\right)^\top \mathbf{M}^2\mathbb{1} = \left(\boldsymbol{g}^{n+1}_{ij^+_{1/2}}\right)^\top \mathbf{w} = 0.
\end{aligned}
$$

Hence (B14) reduces to

$$
\begin{aligned}
\frac{1}{2\Delta t}\left[\frac{1}{c}||\mathbf{g}^{n+1}||^2 - \frac{1}{c}||\mathbf{g}^n||^2 \quad + \frac{1}{c}||\mathbf{g}^{n+1}-\mathbf{g}^n||^2\right] + \frac{1}{\varepsilon}(\mathcal{G}^2)^{n+1,n+1}\\
+\frac{c}{\varepsilon^2}(\mathcal{G}^1)^{n+1,n} \leq -\frac{\sigma_0^t}{\varepsilon^2}||\mathbf{g}^{n+1}||^2,
\end{aligned}
\tag{B15}
$$

where

$$
\begin{aligned}
\left(\mathcal{G}^2_v\right)^{n+1,n+1}_{i^+_{1/2}j} &:= \left(\boldsymbol{g}^{n+1}_{i^+_{1/2}j}\right)^\top \mathbf{M}^2 \mathcal{L}_v \boldsymbol{g}^{n+1}_{i^+_{1/2}j}, \quad v \in \mathcal{J}_{\mathbf{x}},\\
\left(\mathcal{G}^2_v\right)^{n+1,n+1} &:= \left[\textstyle\sum_{ij}\left(\mathcal{G}^2_v\right)^{n+1,n+1}_{i^+_{1/2}j} + \sum_{ij}\left(\mathcal{G}^2_v\right)^{n+1,n+1}_{ij^+_{1/2}}\right]\Delta\zeta, \quad v \in \mathcal{J}_{\mathbf{x}},\\
(\mathcal{G}^2)^{n+1,n+1} &:= \left(\mathcal{G}^2_x\right)^{n+1,n+1} + \left(\mathcal{G}^2_y\right)^{n+1,n+1}.
\end{aligned}
$$

Adding, (B13) + $\frac{\varepsilon^2}{2\pi c}$ (B15) yields

$$
\begin{aligned}
\frac{1}{2\Delta t}\Bigg[\left|\left|\frac{1}{c}\phi^{n+1}\right|\right|^2 + \frac{1}{2\pi}\left|\left|\frac{\varepsilon}{c}\mathbf{g}^{n+1}\right|\right|^2 - \left|\left|\frac{1}{c}\phi^{n}\right|\right|^2 - \frac{1}{2\pi}\left|\left|\frac{\varepsilon}{c}\mathbf{g}^{n}\right|\right|^2 + \left|\left|\frac{1}{c}\phi^{n+1} - \frac{1}{c}\phi^{n}\right|\right|^2\\
+\frac{1}{2\pi}\left|\left|\frac{\varepsilon}{c}\mathbf{g}^{n+1} - \frac{\varepsilon}{c}\mathbf{g}^{n}\right|\right|^2\Bigg] + \frac{\varepsilon}{2\pi c}(\mathcal{G}^2)^{n+1,n+1} + \frac{1}{2\pi}(\mathcal{H}^1)^{n+1,n+1}\\
\leq -\frac{\sigma_0^t}{2\pi c}||\mathbf{g}^{n+1}||^2 - (\mathcal{H}^2)^{n+1,n+1} - \frac{1}{2\pi}(\mathcal{G}^1)^{n+1,n}.
\end{aligned}
\tag{B16}
$$

Since $\mathbf{M}^2\mathbf{Q}_v\mathbb{1} = \boldsymbol{w}^\top \mathbf{Q}_v$, $v \in \mathcal{J}_{\boldsymbol{x}}$, using Lemma B.1 for $(\mathcal{G}^1)^{n+1,n}$ we have

$$
\sum_{ij}(\mathcal{G}^1_v)^{n+1,n}_{i^+_{1/2}j} = -\sum_{ij}(\mathcal{D}^0_v \mathbf{g}^{n+1}_{ij})^\top \mathbf{M}^2\mathbf{Q}_v\mathbb{1}(\frac{1}{c}\phi^n_{ij}) = -\sum_{ij}(\mathcal{H}^1_v)^{n+1,n}_{ij}.
$$

Then, we get

$$
\begin{aligned}
\frac{1}{2\Delta t}\Bigg[\left|\left|\frac{1}{c}\phi^{n+1}\right|\right|^2 + \frac{1}{2\pi}\left|\left|\frac{\varepsilon}{c}\mathbf{g}^{n+1}\right|\right|^2 - \left|\left|\frac{1}{c}\phi^{n}\right|\right|^2 - \frac{1}{2\pi}\left|\left|\frac{\varepsilon}{c}\mathbf{g}^{n}\right|\right|^2 + \left|\left|\frac{1}{c}\phi^{n+1} - \frac{1}{c}\phi^{n}\right|\right|^2\\
+\frac{1}{2\pi}\left|\left|\frac{\varepsilon}{c}\mathbf{g}^{n+1} - \frac{\varepsilon}{c}\mathbf{g}^{n}\right|\right|^2\Bigg] + \frac{\varepsilon}{2\pi c}(\mathcal{G}^2)^{n+1,n+1} + \frac{1}{2\pi}(\mathcal{H}^1)^{n+1,n+1}\\
\leq -\frac{\sigma_0^t}{2\pi c}\left|\left|\mathbf{g}^{n+1}\right|\right|^2 - (\mathcal{H}^2)^{n+1,n+1} + \frac{1}{2\pi}(\mathcal{H}^1)^{n+1,n}.
\end{aligned}
\tag{B17}
$$

Subtracting $(\mathcal{H}^1)^{n+1,n+1}$ from $(\mathcal{H}^1)^{n+1,n}$ and using Lemma B.3 we get

$$
\frac{1}{2\pi}\left[(\mathcal{H}^1)^{n+1,n} - (\mathcal{H}^1)^{n+1,n+1}\right] = \frac{\Delta t}{(2\pi)^2}(\mathcal{G}^3)^{n+1,n+1} + \frac{1}{2\Delta t}\left|\left|\frac{1}{c}\phi^n - \frac{1}{c}\phi^{n+1}\right|\right|^2,
$$

where

$$(\mathcal{G}^3)^{n+1,n+1} := \left[\sum_{ij}\left[\left(\mathcal{D}_x^0 \boldsymbol{g}_{ij}^{n+1}\right)^\top \mathbf{M}^2\mathbf{Q}_x\mathbb{1}\right]^2 + \sum_{ij}\left[\left(\mathcal{D}_x^0 \boldsymbol{g}_{i^+_{1/2}j^+_{1/2}}^{n+1}\right)^\top \mathbf{M}^2\mathbf{Q}_x\mathbb{1}\right]^2\right]\Delta\zeta + \left[\sum_{ij}\left[\left(\mathcal{D}_y^0 \boldsymbol{g}_{ij}^{n+1}\right)^\top \mathbf{M}^2\mathbf{Q}_y\mathbb{1}\right]^2 + \sum_{ij}\left[\left(\mathcal{D}_y^0 \boldsymbol{g}_{i^+_{1/2}j^+_{1/2}}^{n+1}\right)^\top \mathbf{M}^2\mathbf{Q}_y\mathbb{1}\right]^2\right]\Delta\zeta.$$

Using Lemma B.7 and the definition of the differential operators $\mathcal{D}_v^0$, we get for the last two terms on the right-hand side

$$\frac{\Delta t}{(2\pi)^2}(\mathcal{G}^3)^{n+1,n+1} \le \frac{\Delta t}{4\pi}\left(\tilde{\mathcal{G}}^3\right)^{n+1,n+1}. \tag{B18}$$

where

$$\begin{aligned}
\left(\tilde{\mathcal{G}}_v^3\right)^{n+1,n+1}_{i^+_{1/2}j} &:= \left(\mathcal{D}_v^+ \boldsymbol{g}_{i^+_{1/2}j}^{n+1}\right)^\top |\mathbf{Q}_v|\mathbf{M}^2\mathcal{D}_x^+ \boldsymbol{g}_{i^+_{1/2}j}^{n+1}, \quad v \in \mathcal{J}_{\mathbf{x}},\\
\left(\tilde{\mathcal{G}}_v^3\right)^{n+1,n+1} &:= \left[\sum_{ij}\left(\tilde{\mathcal{G}}_v^3\right)^{n+1,n+1}_{i^+_{1/2}j} + \sum_{ij}\left(\tilde{\mathcal{G}}_v^3\right)^{n+1,n+1}_{ij^+_{1/2}}\right]\Delta\zeta, \quad v \in \mathcal{J}_{\mathbf{x}},\\
\left(\tilde{\mathcal{G}}^3\right)^{n+1,n+1} &:= \left(\tilde{\mathcal{G}}_x^3\right)^{n+1,n+1} + \left(\tilde{\mathcal{G}}_y^3\right)^{n+1,n+1}.
\end{aligned}$$

Putting it all together we get

$$\begin{aligned}
&\frac{1}{2\Delta t}\left[\left|\left|\frac{1}{c}\phi^{n+1}\right|\right|^2 + \frac{1}{2\pi}\left|\left|\frac{\varepsilon}{c}\boldsymbol{g}^{n+1}\right|\right|^2 - \left|\left|\frac{1}{c}\phi^{n}\right|\right|^2 - \frac{1}{2\pi}\left|\left|\frac{\varepsilon}{c}\boldsymbol{g}^{n}\right|\right|^2 + \frac{1}{2\pi}\left|\left|\frac{\varepsilon}{c}\boldsymbol{g}^{n+1} - \frac{\varepsilon}{c}\boldsymbol{g}^{n}\right|\right|^2\right]\\
&+\frac{\varepsilon}{2\pi c}(\mathcal{G}^2)^{n+1,n+1} \le -\frac{\sigma_0^t}{2\pi c}\left|\left|\boldsymbol{g}^{n+1}\right|\right|^2 - (\mathcal{H}^2)^{n+1,n+1} + \frac{\Delta t}{4\pi}\left(\tilde{\mathcal{G}}^3\right)^{n+1,n+1}.
\end{aligned} \tag{B19}$$

Multiplying (11c) by $\left(\frac{1}{c}B_{ij}^{n+1}\right)\Delta\zeta$ and its equivalent at $(x_{i^+_{1/2}}, y_{j^+_{1/2}})$ by $\left(\frac{1}{c}B^{n+1}_{i^+_{1/2}j^+_{1/2}}\right)\Delta\zeta$, respectively, and summing over i,j yields

$$\frac{1}{\Delta t}\sum_{ij}\frac{ac_\nu}{(2\pi)^2}(T_{ij}^{n+1})^4\left(T_{ij}^{n+1} - T_{ij}^{n}\right)\Delta\zeta = \sum_{ij}\frac{1}{c}B_{ij}^{n+1}\sigma_{ij}^a h_{ij}^{n+1}\Delta\zeta,$$

$$\frac{1}{\Delta t}\sum_{ij}\frac{ac_\nu}{(2\pi)^2}(T^{n+1}_{i^+_{1/2}j^+_{1/2}})^4\left(T^{n+1}_{i^+_{1/2}j^+_{1/2}} - T^{n}_{i^+_{1/2}j^+_{1/2}}\right)\Delta\zeta = \sum_{ij}\frac{1}{c}B^{n+1}_{i^+_{1/2}j^+_{1/2}}\sigma^a_{i^+_{1/2}j^+_{1/2}} h^{n+1}_{i^+_{1/2}j^+_{1/2}}\Delta\zeta.$$

Using Lemma B.9 we get

$$\frac{1}{\Delta t}\sum_{ij}\frac{ac_\nu}{5(2\pi)^2}\left(\left(T_{ij}^{n+1}\right)^5 - \left(T_{ij}^{n}\right)^5\right)\Delta\zeta \le \sum_{ij}\frac{1}{c}B_{ij}^{n+1}\sigma_{ij}^a h_{ij}^{n+1}\Delta\zeta, \tag{B20}$$

$$\frac{1}{\Delta t}\sum_{ij}\frac{ac_\nu}{5(2\pi)^2}\left(\left(T^{n+1}_{i^+_{1/2}j^+_{1/2}}\right)^5 - \left(T^{n}_{i^+_{1/2}j^+_{1/2}}\right)^5\right)\Delta\zeta \le \sum_{ij}\frac{1}{c}B^{n+1}_{i^+_{1/2}j^+_{1/2}}\sigma^a_{i^+_{1/2}j^+_{1/2}} h^{n+1}_{i^+_{1/2}j^+_{1/2}}\Delta\zeta. \tag{B21}$$

Combining (B20) and (B21), yields

$$\begin{aligned}
&\frac{1}{2\Delta t}\left[\frac{2}{5}\left|\left|\frac{\sqrt{ac_\nu}}{2\pi}(T^{n+1})^{5/2}\right|\right|^2 - \frac{2}{5}\left|\left|\frac{\sqrt{ac_\nu}}{2\pi}(T^{n})^{5/2}\right|\right|^2\right]\\
&\qquad\le \frac{1}{c}\left[\sum_{ij}B_{ij}^{n+1}\sigma_{ij}^a h_{ij}^{n+1} + \sum_{ij}B^{n+1}_{i^+_{1/2}j^+_{1/2}}\sigma^a_{i^+_{1/2}j^+_{1/2}} h^{n+1}_{i^+_{1/2}j^+_{1/2}}\right]\Delta\zeta.
\end{aligned} \tag{B22}$$

Since $\sigma^a(\boldsymbol{x}) \geq \sigma_0^a$

$$-\left[\sum_{ij}\frac{\varepsilon^2}{c}h_{ij}^{n+1}\sigma_{ij}^a h_{ij}^{n+1}+\sum_{ij}\frac{\varepsilon^2}{c}h_{i_{1/2}^+j_{1/2}^+}^{n+1}\sigma_{i_{1/2}^+j_{1/2}^+}^a h_{i_{1/2}^+j_{1/2}^+}^{n+1}\right]\Delta\zeta \leq -\frac{\sigma_0^a}{c}\left|\left|\varepsilon h^{n+1}\right|\right|^2.$$

Thus, adding (B19) and (B22) yields

$$\begin{aligned}&\frac{1}{2\Delta t}\left[e^{n+1}-e^n+\frac{1}{2\pi}\left|\left|\frac{\varepsilon}{c}\mathbf{g}^{n+1}-\frac{\varepsilon}{c}\mathbf{g}^n\right|\right|^2\right]+\frac{\varepsilon}{2\pi c}(\mathcal{G}^2)^{n+1,n+1}\\&\leq -\frac{\sigma_0^t}{2\pi c}\left|\left|\mathbf{g}^{n+1}\right|\right|^2-\frac{\sigma_0^a}{c}\left|\left|\varepsilon h^{n+1}\right|\right|^2+\frac{\Delta t}{4\pi}\left(\tilde{\mathcal{G}}^3\right)^{n+1,n+1}.\end{aligned} \tag{B23}$$

Note that we bound $-\frac{\sigma_0^a}{c}\left|\left|\varepsilon h^{n+1}\right|\right|^2 \leq 0$ and use Lemma B.6 for $(\mathcal{G}^2)^{n+1,n+1}$, on the left-hand side of (B23), such that $\frac{1}{2\pi}\left|\left|\frac{\varepsilon}{c}\mathbf{g}^{n+1}-\frac{\varepsilon}{c}\mathbf{g}^n\right|\right|^2$ gets canceled out. This yields the following inequality

$$\begin{aligned}&\frac{1}{2\Delta t}(e^{n+1}-e^n)+\frac{\varepsilon\Delta x}{4\pi c}(\tilde{\mathcal{G}}_x^3)^{n+1,n+1}+\frac{\varepsilon\Delta y}{4\pi c}(\tilde{\mathcal{G}}_y^3)^{n+1,n+1}-\frac{\Delta t}{2\pi}\left|\left|\left|\mathbf{Q}_x\right|\mathcal{D}_x^+\mathbf{g}^{n+1}\right|\right|^2\\&-\frac{\Delta t}{2\pi}\left|\left|\left|\mathbf{Q}_y\right|\mathcal{D}_y^+\mathbf{g}^{n+1}\right|\right|^2\leq -\frac{\sigma_0^t}{2\pi c}\left|\left|\mathbf{g}^{n+1}\right|\right|^2+\frac{\Delta t}{4\pi}(\tilde{\mathcal{G}}^3)^{n+1,n+1}.\end{aligned} \tag{B24}$$

For any $\phi \in \mathbb{R}^{N_q}$, since $|\Omega_v| \leq 1$, we have $\phi^\top|\mathbf{Q}_v|^\top\mathbf{M}^2|\mathbf{Q}_v|\phi \leq \phi^\top|\mathbf{Q}_v|^\top\mathbf{M}^2\phi$. Hence we obtain

$$\left|\left||\mathbf{Q}_v|\mathcal{D}_v^+\mathbf{g}^{n+1}\right|\right|^2 \leq \left(\tilde{\mathcal{G}}_v^3\right)^{n+1,n+1}. \tag{B25}$$

Combining (B25) and (B18) yields

$$\begin{aligned}\frac{1}{2\Delta t}(e^{n+1}-e^n) \quad &\leq -\frac{\sigma_0^t}{2\pi c}\left|\left|\mathbf{g}^{n+1}\right|\right|^2+\left(\frac{3\Delta t}{4\pi}-\frac{\varepsilon\Delta x}{4\pi c}\right)\left(\tilde{\mathcal{G}}_x^3\right)^{n+1,n+1}\\&+\left(\frac{3\Delta t}{4\pi}-\frac{\varepsilon\Delta y}{4\pi c}\right)\left(\tilde{\mathcal{G}}_y^3\right)^{n+1,n+1}.\end{aligned}$$

Using Lemma B.8 and expanding the sum over the quadrature, we get

$$\begin{aligned}\frac{1}{2\Delta t}(e^{n+1}-e^n) &\leq -\frac{\sigma_0^t}{2\pi c}\sum_\ell w_\ell\left[\sum_{ij}g_{\ell,i_{1/2}^+j}^2+\sum_{ij}g_{\ell,ij_{1/2}^+}^2\right]\Delta\zeta\\&+\left(\frac{3\Delta t}{4\pi}-\frac{\varepsilon\Delta x}{4\pi c}\right)\frac{4}{\Delta x^2}\sum_\ell w_\ell\left|\Omega_x^\ell\right|\left[\sum_{ij}g_{\ell,i_{1/2}^+j}^2+\sum_{ij}g_{\ell,ij_{1/2}^+}^2\right]\Delta\zeta\\&+\left(\frac{3\Delta t}{4\pi}-\frac{\varepsilon\Delta y}{4\pi c}\right)\frac{4}{\Delta y^2}\sum_\ell w_\ell\left|\Omega_y^\ell\right|\left[\sum_{ij}g_{\ell,i_{1/2}^+j}^2+\sum_{ij}g_{\ell,ij_{1/2}^+}^2\right]\Delta\zeta,\end{aligned}$$

which can be written as

$$\begin{aligned}\frac{1}{2\Delta t}(e^{n+1}-e^n) \leq &\sum_\ell w_\ell\left[\left(\frac{3\Delta t}{4\pi}-\frac{\varepsilon\Delta x}{4\pi c}\right)\frac{4\left|\Omega_x^\ell\right|}{\Delta x^2}-\frac{\sigma_0^t}{4\pi c}\right]\left[\sum_{ij}g_{\ell,i_{1/2}^+j}^2+\sum_{ij}g_{\ell,ij_{1/2}^+}^2\right]\Delta\zeta\\&+\sum_\ell w_\ell\left[\left(\frac{3\Delta t}{4\pi}-\frac{\varepsilon\Delta y}{4\pi c}\right)\frac{4\left|\Omega_y^\ell\right|}{\Delta y^2}-\frac{\sigma_0^t}{4\pi c}\right]\left[\sum_{ij}g_{\ell,i_{1/2}^+j}^2+\sum_{ij}g_{\ell,ij_{1/2}^+}^2\right]\Delta\zeta.\end{aligned}$$

Since the step size Δt satisfies the CFL condition

$$\Delta t \leq \frac{1}{3c} \min \left\{ \varepsilon \Delta x + \frac{\sigma_0^t \Delta x^2}{4\left|\Omega_x'\right|}, \varepsilon \Delta y + \frac{\sigma_0^t \Delta y^2}{4\left|\Omega_y'\right|} \right\},$$

for $\left|\Omega_x'\right|, \left|\Omega_y'\right| \neq 0$. We get $e^{n+1} \leq e^n$. ■